Chapter 5
(Results & Discussion)

5.1 PART-I: SERIES I

5.1.1 Computational studies and designing considerations

5.1.1.1 Pharmacophore modeling

The structure-based drug design approach was used to generate e-pharmacophore models using crystal structures of AChE (PDB code: 4EY7) and BACE-1 (PDB code: 2ZJM), which were selected owing to the presence of *N*-benzylpiperidine nucleus in their cocrystallized ligands. The generated e-pharmacophore models suggested the presence of two aromatic rings (R9 and R10), two hydrophobic residues (H7 and H8), and a hydrogen bond acceptor (A3) as essential features for binding of inhibitors to AChE (Figures 5.1A and 5.2A), while two aromatic rings (R14 and R15), two hydrogen bond donors (D7 and D8), and a single positive ionic group (P13) to be necessary for favored binding within BACE-1 active pocket (Figures 5.1B and 5.2B). On the basis of these pharmacophoric features, ligands from Maybridge HitFinder database (https://www.maybridge.com as accessed on June 2017) were screened using Phase module of Schrödinger Maestro 2018.1. Initial screening of total of 18930 ligands by pharmacophore model of AChE resulted into 917 hits, which were further screened by BACE-1 model to identify 206 hits.

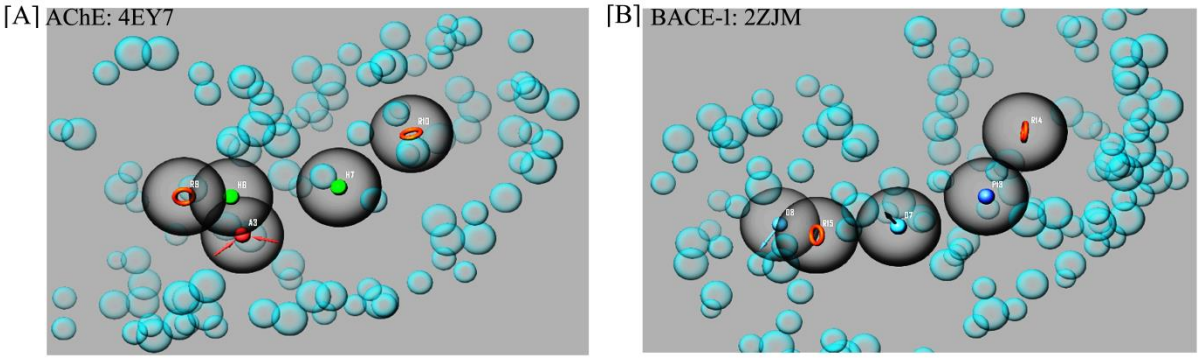

Figure 5.1. Favored binding sites in generated e-pharmacophore models. [A] AChE (PDB code: 4EY7) [B] BACE-1 (PDB code: 2ZJM).

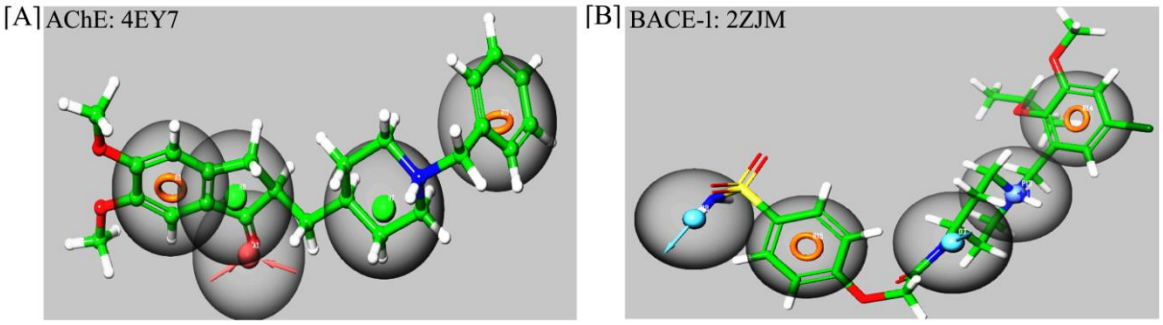

Figure 5.2. 3D Structures of cocrystallized ligands depicting numbering of favored residues. [A] AChE (PDB code: 4EY7) [B] BACE-1 (PDB code: 2ZJM).

5.1.1.2 Virtual screening and docking-post processing (DPP)

The VS workflow was employed, which comprised of three steps: HTVS, SP, and XP docking with the criteria of screening as 30% ligands in each step. The results of these protocols yielded 15 potential hits on the basis of their promising glide and dock scores on both the target structures (AChE and BACE-1).

Pose filtration was performed on identified hits using DPP function. The X-ray crystallographic structure of AChE revealed the presence of two major binding sites: PAS; and CAS. The inhibitor of AChE should be extended from PAS (Tyr72, Asp74, Tyr124, Trp286, and Tyr341) to CAS (Ser203, Glu334, and His447). BACE-1 is a membrane-bound enzyme having the presence of catalytic aspartic dyad residues (Asp32 and Asp228) at the interface of N- and C-terminus. Therefore, ligands were screened by DPP on the basis of their interactions with PAS and CAS residues of AChE and aspartate dyad of BACE-1. Only 3 common hits were identified (Figure 5.3) showing significant interactions with the active site residues of both the targets (Table 5.1). Among the identified potential hits, SEW06622 bears *N*-benzylpiperidine nucleus, while AW01119 contains 2,4-dichlorobenzyl piperazine, and PD00698 has fused pyrimido[4,5-d]pyrimidine-2,4[3H]-dione moiety, which are non-classical bioisosteric congeners of *N*-benzylpiperidine.

5.1.1.3 MM-GBSA

MM-GBSA analysis of identified hits (SEW06622, AW01119, and PD00698) was performed to ascertain the binding free energy of docked ligands into the respective proteins. The results of MM-GBSA analysis (Table 5.1) showed SEW06622 as the top hit with the minimum binding free energy of -82.86 and -52.45 kcal/mol for AChE and BACE-1, respectively.

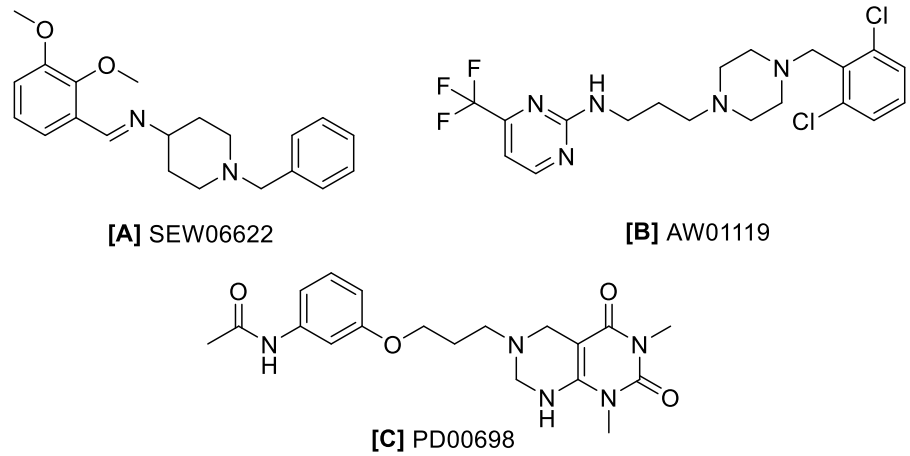

Figure 5.3. Structures of common identified hits. [A] SEW06622 [B] AW01119 [C] PD00698.

Table 5.1. Glide score, interacting residues, and MM-GBSA ΔG binding free energy of identified hits (SEW06622, AW01119, and PD00698) against AChE and BACE-1.

Comd.	Docking on AChE			ΔG binding free energy (AChE)	Docking on BACE-1		ΔG binding free energy (BACE-1)
	Glide score	Interacting residues*			Glide score	Aspartate dyad interactions*	
		PAS	CAS				
SEW06622	-19.06	Tyr72[a], Asp74[b], Tyr124[a], Trp286[a], Tyr341[a,c]	Ser203[d], His447[d]	-82.86	-7.16	Asp32[b,e], Asp228[b,e,f]	-52.45
AW01119	-15.58	Asp74[b], Tyr124[a], Trp286[a], Tyr341[a,c]	Ser203[d], His447[d]	-62.54	-8.31	Asp32[b,e,f], Asp228[b,e]	-44.22
PD00698	-15.45	Tyr72[a], Asp74[b], Tyr124[a], Trp286[a], Tyr341[a,c]	Ser203[d], His447[d]	-67.40	-7.18	Asp32[b,e,f], Asp228[b]	-41.43

*Interacting residues were observed within the distance of 4Å from ligands.
[a]hydrophobic; [b]charged; [c]π-cation; [d]polar; [e]salt-bridge; [f]H-bonding interactions.

5.1.1.4 Molecular docking study

Molecular docking studies were performed to affirm the potential noncovalent binding interactions of designed ligands on AChE and BACE-1. Initially, docking parameters and prepared grids were validated by redocking the cocrystallized ligands into respective grids of AChE and BACE-1. The superposition tool was used, which showed RMSD values within 2Å between cocrystallized and redocked ligands to confirm the suitability of docking protocols and generated grids [Kontoyianni et al. 2004] (Figures 5.4A and 5.4B). The results of docking studies confirmed that designed ligands (**S_I3j** and **S_I4j**) and hit compound SEW06622 (**S_I3a**) accommodated within the active pocket of AChE with substituted phenyl group occupied PAS, while benzylpiperidine nucleus was extended deep into CAS and formed polar interactions with Ser203 and His447. **S_I3a** elicited charged and hydrophobic interactions with Asp74 and other PAS residues (Tyr124, Trp286, and Tyr341), respectively (Figure 5.5A). While, **S_I3j** (Figure 5.6A) and **S_I4j** (Figure 5.7A) elicited similar interaction pattern at PAS, except additional π-π stacking and π-cation interactions with Tyr341 residue. At anionic subsite, benzyl portion of all compounds exhibited interactions with Trp86 (π-π stacking or π-cation) and Glu202 (charged) residues. Other active site residues of oxyanion hole and acyl binding pocket were also observed similarly in docked poses of **S_I3a**, **S_I3j**, and **S_I4j**.

The binding mode of docked ligands on BACE-1 indicated significant interactions with both the catalytic aspartate residues (Asp32 and Asp228) through either ionic salt bridge or H-bonding. **S_I3a** showed both the interactions with single —NH present in piperidine ring (Figure 5.5B), while designed series of compounds **S_I3j** (Figure 5.6B) and **S_I4j** (Figure 5.7B), showed these interactions with both —NH groups present in piperidine ring and a side chain.

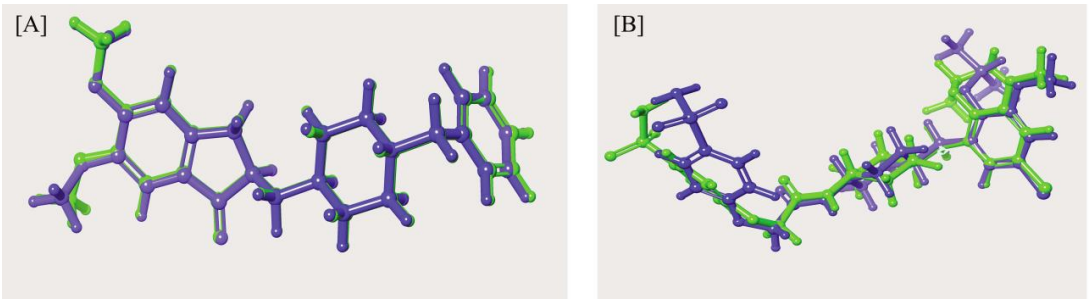

Figure 5.4. Superimpose representation. [A] Donepezil redocked (green) and cocrystallized pose (blue) on AChE (RMSD: 0.4227 Å) [B] F1M redocked (green) and cocrystallized pose (blue) on BACE-1 (RMSD: 1.9161 Å).

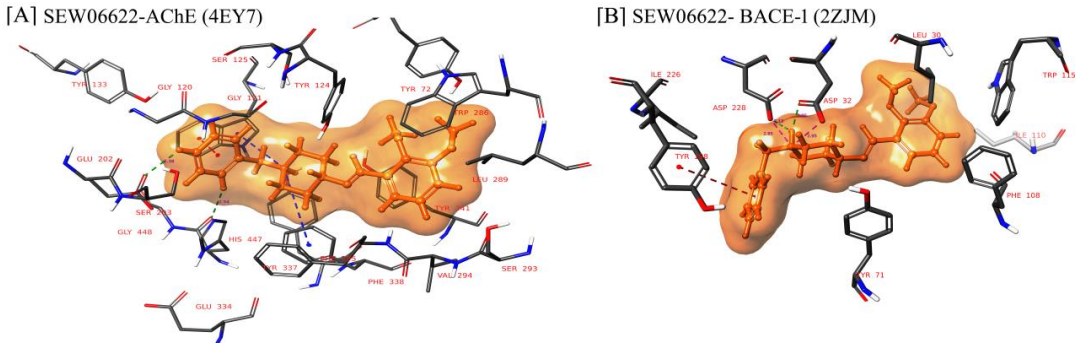

Figure 5.5. Binding pattern of SEW06622 (**S_I3a**) depicted in orange colored ligand binding surface at the active pocket. [A] AChE (4EY7) [B] BACE-1 (2ZJM).

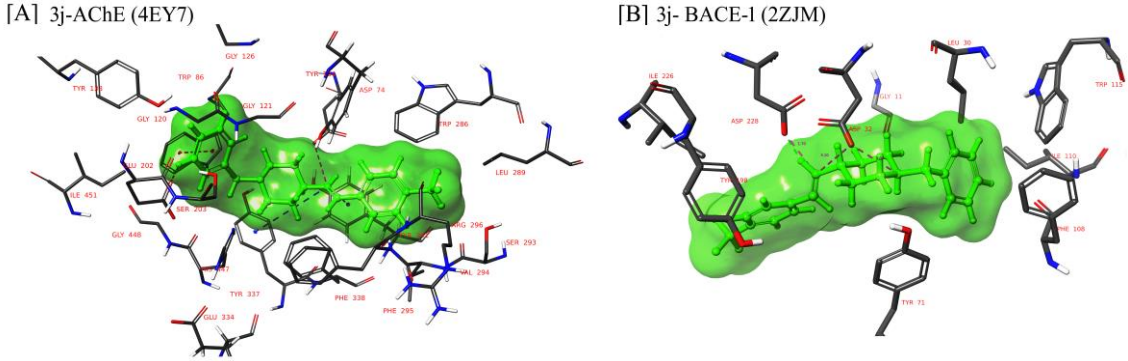

Figure 5.6. Binding pattern of **S_I3j** depicted in green colored ligand binding surface at the active pocket. [A] AChE (4EY7) [B] BACE-1 (2ZJM).

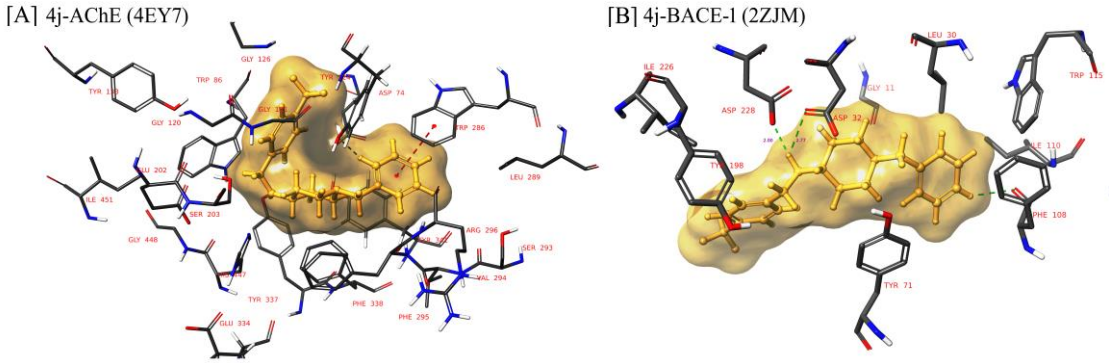

Figure 5.7. Binding pattern of **S_I4j** depicted in golden colored ligand binding surface at the active pocket. [A] AChE (4EY7) [B] BACE-1 (2ZJM).

5.1.1.5 Molecular dynamics simulations study

To evaluate the stability of docked poses, 20 ns molecular dynamics simulation runs were performed for docked complexes of SEW06622 (**S_I3a**), **S_I3j,** and **S_I4j** on both the targets AChE and BACE-1. The results of molecular dynamics studies on AChE suggested that **S_I3a** interacted significantly with PAS residues (Figures 5.8A–C). The methanimine (CH=N) functionality involved in H-bonding interaction with Tyr124 accounted for 93% interaction in selected trajectories. Other PAS residues such as Asp74 and Trp286 residues interacted through salt bridge formation and π-π stacking interactions, respectively. While Tyr72 and Tyr341 residues interacted hydrophobically with **S_I3a**. The results of dynamics simulations of designed ligands **S_I3j** (Figures 5.9A–C) and **S_I4j** (Figures 5.10A–C) on AChE exhibited prominent interactions with PAS residues compared to **S_I3a**. The imine/amine functionalities of **S_I3j** and **S_I4j** interacted with Asp74 and Tyr124 residues at PAS through H-bonding interaction. Both the ligands also interacted through π-π stacking and hydrophobic interactions with Tyr341 and Trp286 residues at PAS, while **S_I4j** additionally engaged in H-bonding interaction with Tyr341. Furthermore, these ligands also interacted with His447 at CAS through hydrophobic interaction.

The outcome of molecular dynamics simulations on BACE-1 suggested that interactions of **S_I3a** with aspartate dyad residues were unstable. **S_I3a** had formed minimal ionic interaction with Asp32 and did not interact with Asp228 throughout the simulation run (Figures 5.11A–C). Interestingly, designed ligands **S_I3j** and **S_I4j** on BACE-1 showed H-bonding with both catalytic aspartate dyad residues (Asp32 and Asp228). Compound **S_I3j** exhibited H-bonding for 10% and 51% interactions in selected trajectories with Asp32 and Asp228, respectively (Figures 5.12A–C). While **S_I4j** having reduced functionality of —NH interacted more effectively with both dyad residues (Asp32 and

Asp228) having 100% and 99% interactions, respectively (Figures 5.13A–C). Thereby, observations of molecular dynamics simulations supports our hypothesis on the improvement the inhibitory potential against both the targets: AChE and BACE-1 by the designed series of ligands.

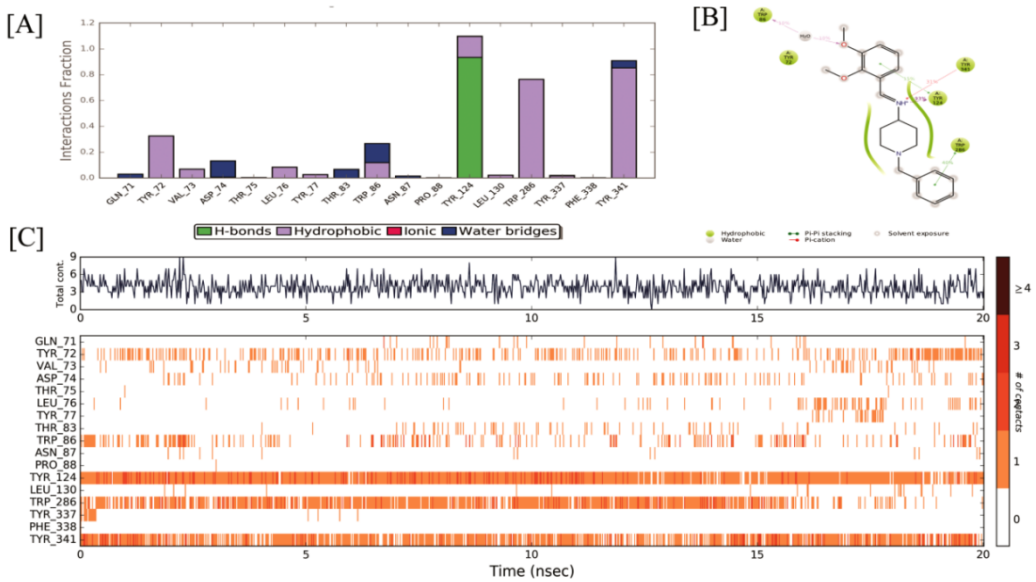

Figure 5.8. Molecular dynamics studies of SEW06622 (**S_I3a)**-AChE (4EY7) docked complex. [A] Histogram [B] Graphical representation showing percentage interactions with active site residues [C] Timeline representation showing interactions at each time frame.

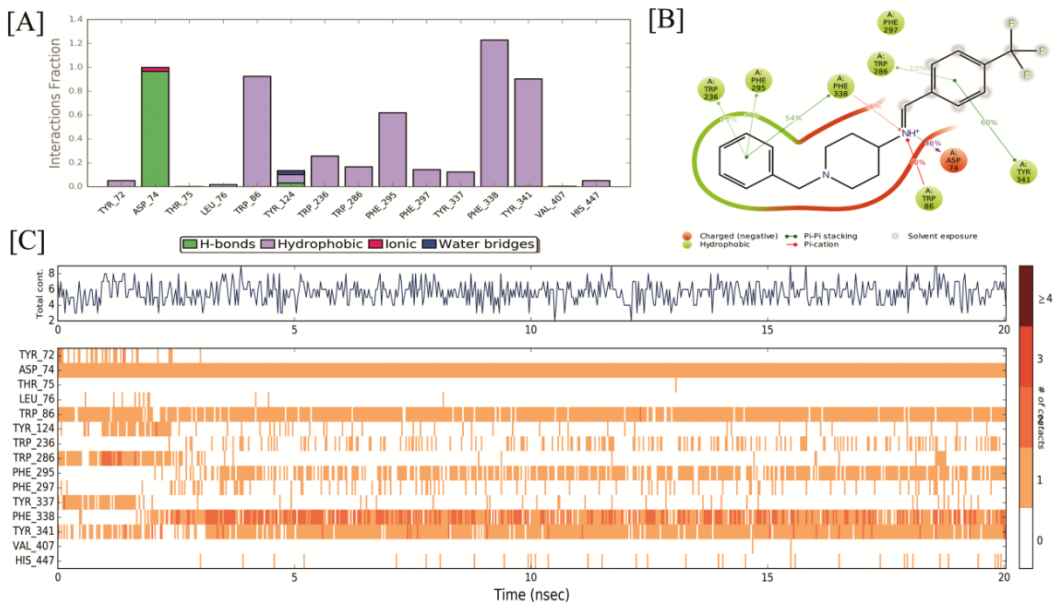

Figure 5.9. Molecular dynamics studies of **S_I3j**-AChE (4EY7) docked complex. [A] Histogram [B] Graphical representation showing percentage interactions with active site residues [C] Timeline representation showing interactions at each time frame.

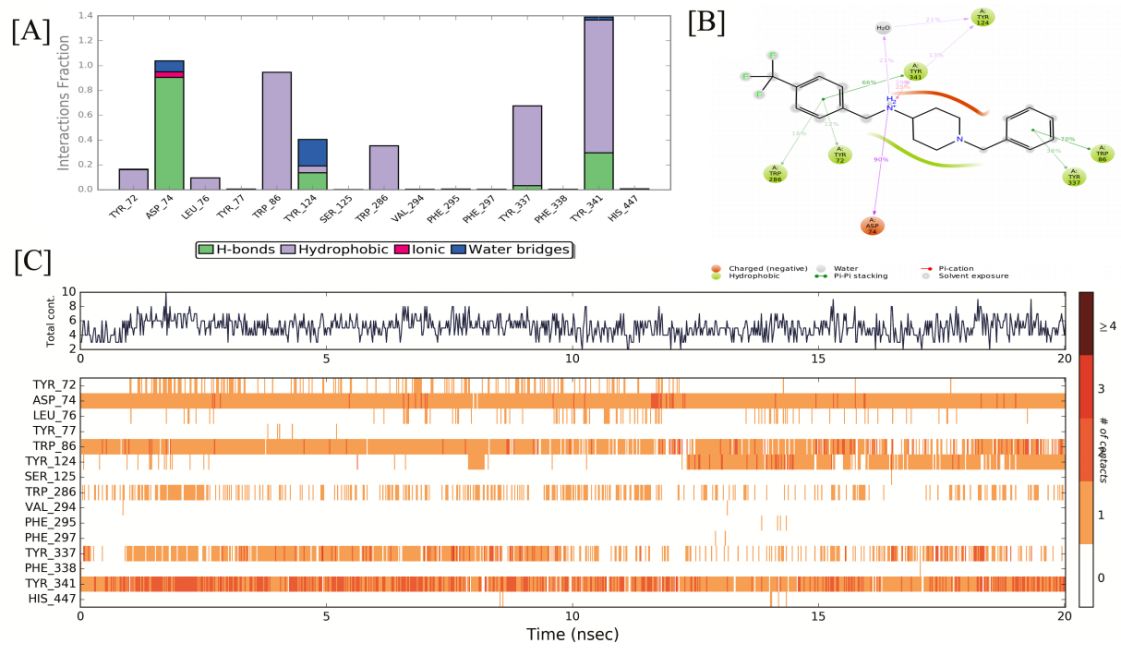

Figure 5.10. Molecular dynamics studies of **S_I4j**-AChE (4EY7) docked complex. [A] Histogram [B] Graphical representation showing percentage interactions with active site residues [C] Timeline representation showing interactions at each time frame.

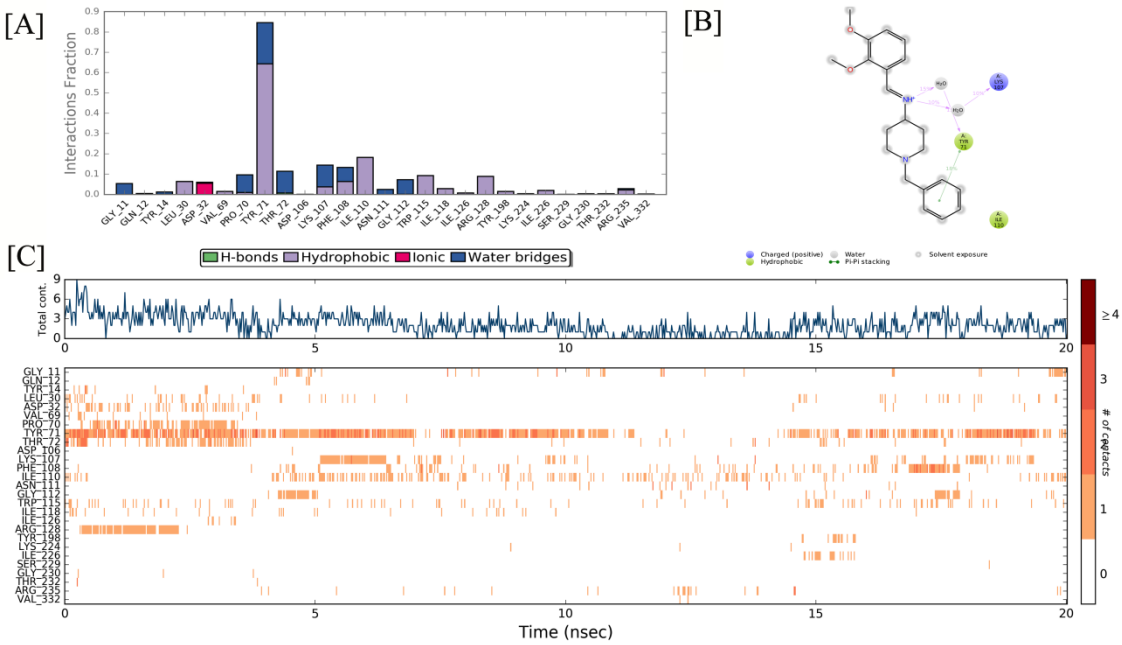

Figure 5.11. Molecular dynamics studies of SEW06622 (**S_I3a**)–BACE-1 (2ZJM) docked complex. [A] Histogram [B] Graphical representation showing percentage interactions with active site residues [C] Timeline representation showing interactions at each time frame.

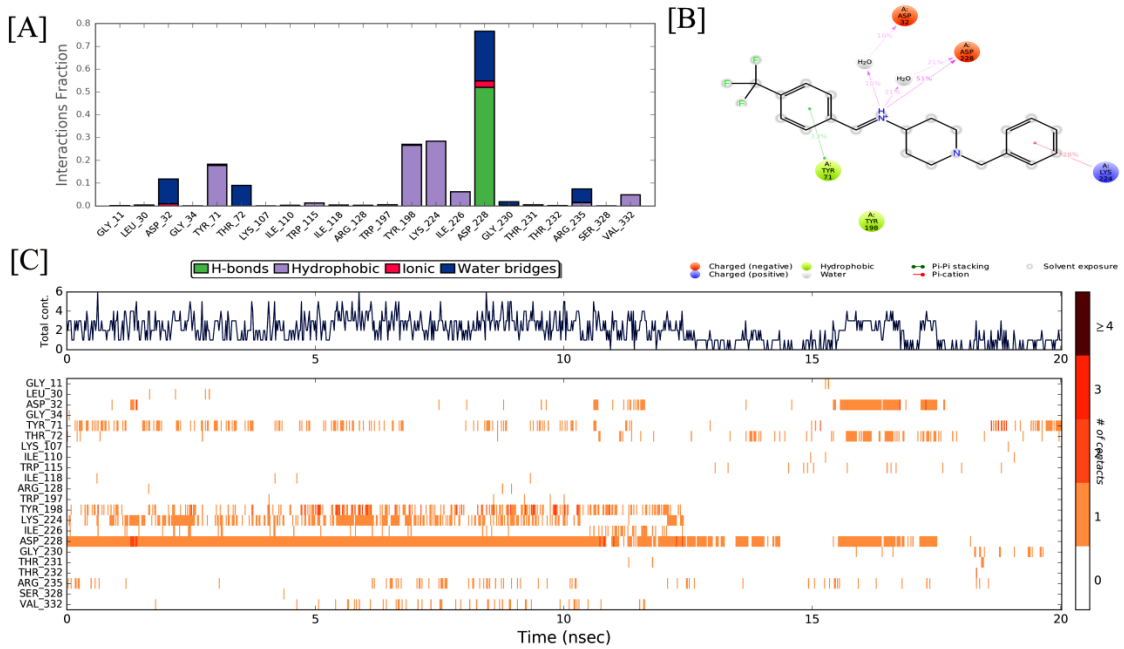

Figure 5.12. Molecular dynamics studies of **S_I3j**–BACE-1 (2ZJM) docked complex. [A] Histogram [B] Graphical representation showing percentage interactions with active site residues [C] Timeline representation showing interactions at each time frame.

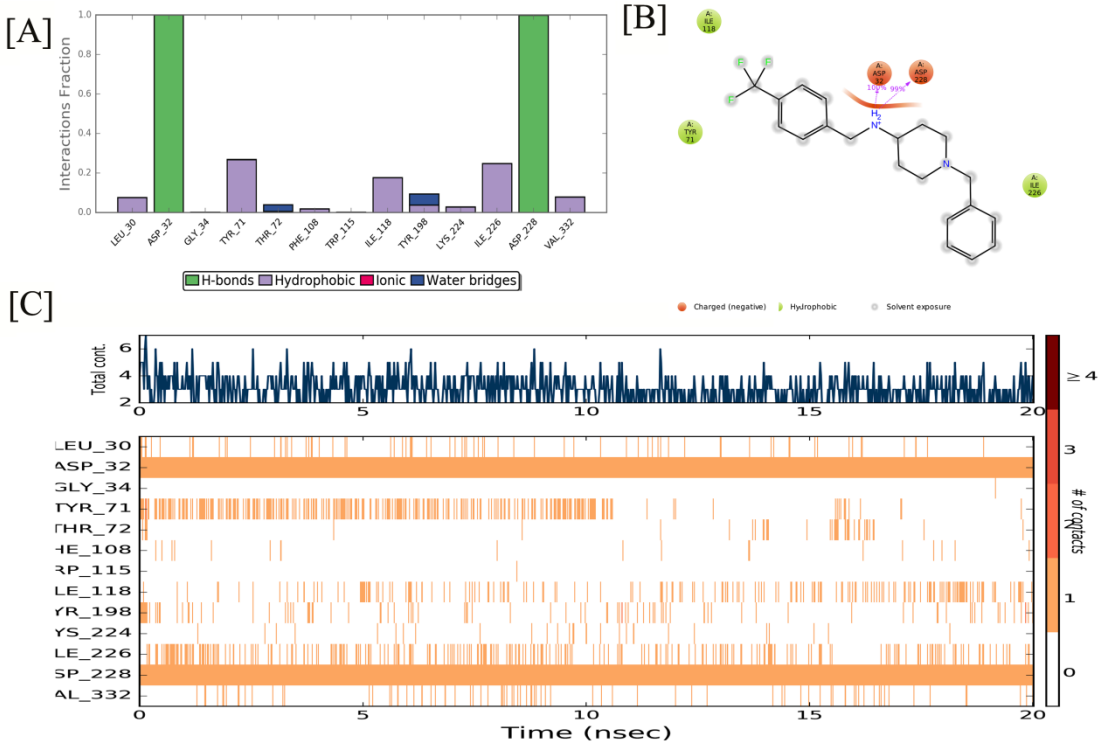

Figure 5.13. Molecular dynamics studies of **S_I4j**-BACE-1 (2ZJM) docked complex. [A] Histogram [B] Graphical representation showing percentage interactions with active site residues [C] Timeline representation showing interactions at each time frame.

5.1.2 Chemistry

5.1.2.1 Synthesis of Series I: N-Benzylpiperidine with substituted phenyl methanimines/methanamines

The series of designed compounds **S_I3a–o and S_I4a–o** were synthesized as per the Scheme 1 (Chapter 4- Experimental). Briefly, 1-benzylpiperidin-4-amine (**S_I1**) was treated with different aromatic aldehydes (**S_I2a–o**) under acidic condition (glacial acetic acid) in absolute ethanol at room temperature (4–6 h) to yield respective Schiff bases (**S_I3a–o**). FT-IR spectra of compounds **S_I3a–o** showed the appearance of a characteristic stretching band for (N=CH) in the range of 1604–1557 cm^{-1}. ^{1}H NMR spectra showed characteristic singlet peak for (N=C**H**) at δ_H = 8.66–8.27 ppm. The presence of (N=**C**H) signal at δ_C = 161.83–154.12 ppm value confirmed the formation of compounds **S_I3a–o**. The resulted compounds (**S_I3a–o**) were treated with $NaBH_4$ in dry methanol at 0–5 °C (2–4 h) to yield their reduced counterparts (**S_I4a–o**). FT-IR spectra of **S_I4a–o** showed an appearance of stretching band of —NH in the region of 3340–3204 cm^{-1}. The disappearance of sharp singlet peak of N=CH and appearance of two protons signal at δ_H = 3.99–3.3.82 ppm for NH—C**H_2** in ^{1}H NMR spectra confirmed the formation of compounds **S_I4a–o**. Also, ^{13}C NMR spectra of compounds **S_I4a–o** showed the appearance of a signal in the range of δ_C = 51.82–47.12 ppm for N—**C**H_2. The molecular weights of all synthesized compounds were confirmed by mass spectrophotometry used with electrospray ionization (ESI) source. All synthesized compounds were confirmed to have purity ≥ 95%.

5.1.2.2 Characterization of the synthesized compounds (Series I)

5.1.2.2.1 N-(1-Benzylpiperidin-4-yl)-1-phenylmethanimine (S_I3a) [Feula and Fossey 2013, Mayavel et al. 2015]

Colorless crystals (0.696 g, 2.502 mmol, 95%), mp 66–68 °C. TLC (DCM:MeOH, 95:5 v/v) R_f = 0.44. FT-IR (Alpha ATR, ν cm^{-1}): 2946, 2922 (CH aromatic), 1572 (N=CH imine). ^{1}H NMR (500 MHz, DMSO-d_6) δ_H 8.37 (s, 1H), 7.72 (dd, J = 6.4, 3.2 Hz, 2H), 7.33–7.26 (m, 7H), 7.24–7.21 (m, 1H), 3.46 (s, 2H), 3.33–3.28 (m, 1H), 2.89 (d, J = 9.8 Hz, 2H), 2.21 (t, J = 8.6 Hz, 2H), 1.87–1.82 (m, 4H). ^{13}C NMR (125 MHz, DMSO-d_6) δ_C 159.12, 142.82, 139.64, 137.82, 133.96, 128.72, 128.46, 128.07, 127.64, 126.92, 64.64, 62.77, 51.92, 31.82. LC/MS (ESI, *m/z*): 279.36 $[M + H]^+$. HPLC purity: 97.8%, retention time: 4.27 min.

5.1.2.2.2. N-(1-Benzylpiperidin-4-yl)-1-(2,3-dimethoxyphenyl)methanimine (S_I3b)

White solid (0.826 g, 2.442 mmol, 93%), mp 86–88 °C. TLC (DCM:MeOH, 95:5 v/v) R_f = 0.42. FT-IR (Alpha ATR, ν cm^{-1}): 2938, 2902 (CH aromatic), 1586 (N=CH imine). ^{1}H NMR (500 MHz, DMSO-d_6) δ_H 8.42 (s, 1H), 7.34–7.28 (m, 6H), 7.08–7.02 (m, 2H), 3.84 (s, 3H), 3.78 (s, 3H), 3.52 (s, 2H), 3.32–3.28 (m, 1H), 2.68 (d, J = 10.2 Hz, 2H), 2.32 (t, J = 9.6 Hz, 2H), 1.89–1.76 (m, 4H). ^{13}C NMR (125 MHz, DMSO-d_6) δ_C 158.67, 154.18, 148.79, 138.76, 132.17, 127.99, 127.16, 126.71, 125.41, 116.17, 115.76, 65.91, 63.76, 59.82, 57.14, 51.16, 31.61. LC/MS (ESI, *m/z*): 339.49 $[M + H]^+$. HPLC purity: 96.2%, retention time: 3.73 min.

5.1.2.2.3. N-(1-Benzylpiperidin-4-yl)-1-(3,4,5-trimethoxyphenyl)methanimine (S_I3c)

Faint yellow solid (0.857 g, 2.327 mmol, 89%), mp 97–99 °C. TLC (DCM:MeOH, 95:5 v/v) R_f = 0.47. FT-IR (Alpha ATR, ν cm^{-1}): 2941, 2908 (CH aromatic), 1594 (N=CH imine). ^{1}H NMR (500 MHz, DMSO-d_6) δ_H 8.54 (s, 1H), 7.38–7.32 (m, 5H), 7.00 (s, 2H), 3.86 (s, 6H), 3.82 (s, 3H), 3.57 (s, 2H), 3.51–3.46 (m, 1H), 2.72 (d, J = 8.6 Hz,

2H), 2.37 (t, *J* = 9.8 Hz, 2H), 1.98–1.86 (m, 4H). ^{13}C NMR (125 MHz, DMSO-d_6) δ_C 160.82, 152.64, 150.97, 139.63, 130.82, 130.61, 128.72, 127.19, 126.61, 122.73, 119.18, 66.19, 63.18, 60.71, 58.19, 51.77, 32.37. LC/MS (ESI, *m/z*): 369.67 $[M + H]^+$. HPLC purity: 98.7%, retention time: 4.20 min.

5.1.2.2.4. 2-(((1-Benzylpiperidin-4-yl)imino)methyl)phenol (S_I3d) [Fang et al. 2012]

Yellow crystals (0.662 g, 2.250 mmol, 86%), mp 74–76 °C. TLC (DCM:MeOH, 95:5 v/v) R_f = 0.36. FT-IR (Alpha ATR, *v* cm^{-1}): 3339 (phenolic OH), 2957, 2916 (CH aromatic), 1584 (N=CH imine). ^{1}H NMR (500 MHz, DMSO-d_6) δ_H 9.46 (s, 1H), 8.32 (s, 1H), 7.37 (dd, *J* = 7.6, 2.2 Hz, 1H), 7.28–7.18 (m, 5H), 7.16–7.13 (m, 1H), 6.90–6.86 (m, 1H), 6.76 (dd, *J* = 7.6, 2.3 Hz, 1H), 3.44 (s, 2H), 3.24–3.21 (m, 1H), 2.69 (d, *J* = 8.6 Hz, 2H), 2.12 (t, *J* = 8.8 Hz, 2H), 1.82–1.66 (m, 4H). ^{13}C NMR (125 MHz, DMSO-d_6) δ_C 162.14, 158.76, 137.68, 132.92, 128.17, 128.02, 127.67, 127.07, 122.19, 120.86, 117.89, 66.08, 64.09, 51.79, 32.67. LC/MS (ESI, *m/z*): 317.37 $[M + Na]^+$. HPLC purity: 96.2%, retention time: 3.72 min.

5.1.2.2.5. 4-(((1-Benzylpiperidin-4-yl)imino)methyl)phenol (S_I3e)

Off-white solid (0.689 g, 2.342 mmol, 89%), mp 81–83 °C. TLC (DCM: MeOH, 95:5 v/v) R_f = 0.36. FT-IR (Alpha ATR, *v* cm^{-1}): 3360 (phenolic OH), 2962, 2932 (CH aromatic), 1591 (N=CH imine). ^{1}H NMR (500 MHz, DMSO-d_6) δ_H 9.16 (s, 1H), 8.35 (s, 1H), 7.41 (d, *J* = 7.8 Hz, 2H), 7.30–7.20 (m, 5H), 6.96 (d, *J* = 7.5 Hz, 2H), 3.53 (s, 2H), 3.41–3.38 (m, 1H), 2.82 (d, *J* = 9.8 Hz, 2H), 2.19 (t, *J* = 9.2 Hz, 2H), 1.91–1.73 (m, 4H). ^{13}C NMR (125 MHz, DMSO-d_6) δ_C 160.72, 156.96, 141.42, 132.41, 129.21, 127.19, 127.02, 126.77, 126.23, 117.19, 65.41, 62.19, 52.19, 31.81. LC/MS (ESI, *m/z*): 317.59 $[M + Na]^+$. HPLC purity: 96.2%, retention time: 3.65 min.

5.1.2.2.6. 4-(((1-Benzylpiperidin-4-yl)imino)methyl)benzene-1,3-diol (S_I3f)

Colorless crystals (0.739 g, 2.383 mmol, 91%), mp 98–100 °C. TLC (DCM:MeOH, 95:5 v/v) R_f = 0.31. FT-IR (Alpha ATR, ν cm^{-1}): 3388 (phenolic OH), 2946, 2911 (CH aromatic), 1591 (N=CH imine). ^{1}H NMR (500 MHz, DMSO-d_6) δ_H 9.43 (s, 1H), 9.31 (s, 1H), 8.27 (s, 1H), 7.36–7.27 (m, 6H), 6.52 (dd, *J* = 8.2, 2.3 Hz, 1H), 6.31 (d, *J* = 1.9 Hz, 1H), 3.43 (s, 2H), 3.39–3.34 (m, 1H), 2.89 (d, *J* = 8.8 Hz, 2H), 2.54 (t, *J* = 9.2 Hz, 2H), 2.07–1.91 (m, 4H). ^{13}C NMR (125 MHz, DMSO-d_6) δ_C 162.68, 159.17, 158.23, 139.14, 133.69, 128.73, 128.42, 127.96, 127.09, 115.68, 111.61, 105.23, 64.09, 62.87, 51.73, 32.82. LC/MS (ESI, *m/z*): 333.74 $[M + Na]^+$. HPLC purity: 97.3%, retention time: 3.29 min.

5.1.2.2.7. N-(1-Benzylpiperidin-4-yl)-1-(m-tolyl)methanimine (S_I3g)

Yellow powder (0.690 g, 2.361 mmol, 90%), mp 82–84 °C. TLC (DCM:MeOH, 95:5 v/v) R_f = 0.49. FT-IR (Alpha ATR, ν cm^{-1}): 2929, 2898 (CH aromatic), 1602 (N=CH imine). ^{1}H NMR (500 MHz, DMSO-d_6) δ_H 8.46 (s, 1H), 7.53-7.41 (m, 2H), 7.18–6.95 (m, 7H), 3.42 (s, 2H), 3.33–3.27 (m, 1H), 2.71 (d, *J* = 9.9 Hz, 2H), 2.39 (t, *J* = 10.2 Hz, 2H), 2.36 (s, 3H), 2.01–1.81 (m, 4H). ^{13}C NMR (125 MHz, DMSO-d_6) δ_C 161.83, 139.72, 138.63, 137.18, 132.17, 129.19, 129.01, 127.63, 126.99, 65.32, 63.18, 51.47, 31.66, 22.06. LC/MS (ESI, *m/z*): 293.41 $[M + H]^+$. HPLC purity: 99.5%, retention time: 4.85 min.

5.1.2.2.8. N-(1-Benzylpiperidin-4-yl)-1-(p-tolyl)methanimine (S_I3h)

Brown crystals (0.702 g, 2.403 mmol, 91%), mp 54–56 °C. TLC (DCM:MeOH, 95:5 v/v) R_f = 0.51. FT-IR (Alpha ATR, ν cm^{-1}): 2936, 2909 (CH aromatic), 1577 (N=CH imine). ^{1}H NMR (500 MHz, DMSO-d_6) δ_H 8.34 (s, 1H), 7.48 (d, *J* = 8.2, 2H), 7.33–7.22 (m, 5H), 7.19 (d, *J* = 7.6 Hz, 2H), 3.52 (s, 2H), 3.33–3.29 (m, 1H), 2.68 (d, *J* = 9.6 Hz, 2H), 2.47 (t, *J* = 8.6 Hz, 2H), 2.35 (s, 3H), 2.02–1.78 (m, 4H). ^{13}C NMR (125 MHz,

DMSO-d_6) δ_C 161.77, 142.17, 138.23, 132.43, 129.67, 129.32, 128.47, 127.63, 126.23, 65.27, 63.82, 51.82, 32.89, 22.02. LC/MS (ESI, *m/z*): 293.33 $[M + H]^+$. HPLC purity: 97.5%, retention time: 4.64 min.

5.1.2.2.9. N-(1-Benzylpiperidin-4-yl)-1-(4-nitrophenyl)methanimine (S_I3i) [Mayavel et al. 2015]

Yellow crystals (0.816 g, 2.373 mmol, 90%), mp 84–86 °C. TLC (DCM:MeOH, 95:5 v/v) R_f = 0.43. FT-IR (Alpha ATR, ν cm^{-1}): 2942, 2917 (CH aromatic), 1596 (N=CH imine), 1515, 1338 (NO_2). ^{1}H NMR (500 MHz, DMSO-d_6) δ_H 8.56 (s, 1H), 8.30 (d, *J* = 8.5 Hz, 2H), 7.99 (d, *J* = 8.6 Hz, 2H), 7.35–7.33 (m, 4H), 7.26 (dd, *J* = 9.4, 4.3 Hz, 1H), 3.50 (s, 2H), 3.38–3.34 (m, 1H), 2.86 (d, *J* = 11.4 Hz, 2H), 2.11 (t, *J* = 10.8 Hz, 2H), 1.74–1.70 (m, 4H). ^{13}C NMR (125 MHz, DMSO-d_6) δ_C 158.28, 148.94, 142.29, 139.05, 129.36, 129.24, 128.62, 127.32, 124.37, 67.13, 62.73, 51.84, 33.61. LC/MS (ESI, *m/z*): 324.59 $[M + H]^+$. HPLC purity: 97.6%, retention time: 4.53 min.

5.1.2.2.10. N-(1-Benzylpiperidin-4-yl)-1-(4-(trifluoromethyl)phenyl)methanimine (S_I3j)

Yellow crystals (0.772 g, 2.357 mmol, 85%), mp 86–88 °C. TLC (DCM:MeOH, 95:5 v/v) R_f = 0.68. FT-IR (Alpha ATR, ν cm^{-1}): 3029, 2935 (CH aromatic), 1557 (N=CH imine), 1322 (C—F). ^{1}H NMR (500 MHz, DMSO-d_6) δ_H 8.49 (s, 1H), 7.94 (d, *J* = 8.1 Hz, 2H), 7.80 (d, *J* = 8.2 Hz, 2H), 7.35–7.30 (m, 4H), 7.26 (dd, *J* = 5.1, 3.5 Hz, 1H), 3.50 (s, 2H), 3.33–3.29 (m, 1H), 2.85 (d, *J* = 11.6 Hz, 2H), 2.10 (t, *J* = 10.0 Hz, 2H), 1.73–1.66 (m, 4H). ^{13}C NMR (125 MHz, DMSO-d_6) δ_C 158.57, 140.28, 139.03, 130.82 (q, $J_{C–F}$ = 31.8 Hz), 129.24, 128.93, 128.60, 127.30, 126.00 (q, $J_{C—F}$ = 3.6 Hz), 124.54 (q, $J_{C—F}$ = 272.3 Hz), 67.05, 62.74, 51.87, 33.64. LC/MS (ESI, *m/z*): 369.45 $[M + Na]^+$. HPLC purity: 98.8%, retention time: 5.11 min.

5.1.2.2.11. N-(1-Benzylpiperidin-4-yl)-1-(4-(trifluoromethoxy)phenyl)methanimine (S_I3k)

Colorless crystals (0.777 g, 2.145 mmol, 82%), mp 82–84 °C. TLC (DCM:MeOH, 95:5 v/v) R_f = 0.64. FT-IR (Alpha ATR, ν cm^{-1}): 2948, 2828 (CH aromatic), 1566 (N=CH imine), 1352 (C—F). ^{1}H NMR (500 MHz, DMSO-d_6) δ_H 8.39 (s, 1H), 7.88 (d, J = 9.6 Hz, 2H), 7.82 (d, J = 8.8 Hz, 2H), 7.48–7.42 (m, 5H), 3.47 (s, 2H), 3.28–3.23 (m, 1H), 2.68 (d, J = 10.8 Hz, 2H), 2.08 (t, J = 9.9 Hz, 2H), 1.67–1.48 (m, 4H). ^{13}C NMR (125 MHz, DMSO-d_6) δ_C 159.62, 151.92, 138.23, 135.82, 130.63, 129.92, 129.24, 128.93, 127.91, 126.54, 124.04, 121.88 (q, $J_{C—F}$ = 242.86), 121.37, 65.21, 63.91, 51.23, 31.69. LC/MS (ESI, *m/z*): 385.61 $[M + Na]^+$. HPLC purity: 97.5%, retention time: 6.03 min.

5.1.2.2.12. N-(1-Benzylpiperidin-4-yl)-1-(4-chlorophenyl)methanimine (S_I3l) [Mayavel et al. 2015]

Yellow crystals (0.843 g, 2.701 mmol, 89%), mp 104–106 °C. TLC (DCM:MeOH, 95:5 v/v) R_f = 0.57. FT-IR (Alpha ATR, ν cm^{-1}): 2939, 2852 (CH aromatic), 1592 (N=CH imine), 744 (C—Cl). ^{1}H NMR (500 MHz, DMSO-d_6) δ_H 8.41 (s, 1H), 7.68 (d, J = 7.8 Hz, 2H), 7.36 (d, J = 7.8 Hz, 2H), 7.22–7.11 (m, 5H), 3.59 (s, 2H), 3.33–3.26 (m, 1H), 2.78 (d, J = 10.6 Hz, 2H), 2.12 (t, J = 8.9 Hz, 2H), 1.86–1.68 (m, 4H). ^{13}C NMR (125 MHz, DMSO-d_6) δ_C 156.72, 139.69, 137.18, 135.82, 130.19, 129.71, 128.64, 127.18, 126.71, 66.19, 64.09, 51.31, 31.82. LC/MS (ESI, *m/z*): 313.43 $[M + H]^+$. HPLC purity: 95.4%, retention time: 5.41 min.

5.1.2.2.13. N-(1-Benzylpiperidin-4-yl)-1-(2,4-dichlorophenyl)methanimine (S_I3m)

White crystals (0.798 g, 2.306 mmol, 88%), mp 74–76 °C. TLC (DCM:MeOH, 95:5 v/v) R_f = 0.60. FT-IR (Alpha ATR, ν cm^{-1}): 2937, 2895 (CH aromatic), 1589 (N=CH imine), 762 (C—Cl), 734 (C—Cl). ^{1}H NMR (500 MHz, DMSO-d_6) δ_H 8.66 (s, 1H), 7.95 (d, J = 8.5 Hz, 1H), 7.68 (d, J = 1.7 Hz, 1H), 7.47 (dd, J = 8.5, 1.3 Hz, 1H), 7.35–

7.29 (m, 4H), 7.25 (dd, *J* = 5.9, 2.3 Hz, 1H), 3.48 (s, 2H), 3.44–3.38 (m, 1H), 2.83 (d, *J* = 11.4 Hz, 2H), 2.09 (t, *J* = 9.9 Hz, 2H), 1.72–1.67 (m, 4H). ^{13}C NMR (125 MHz, DMSO-d_6) δ_C 154.89, 138.87, 136.32, 135.19, 132.16, 129.84, 129.72, 129.32, 128.62, 128.31, 127.35, 67.27, 62.71, 51.74, 33.53. LC/MS (ESI, *m/z*): 347.31 $[M + H]^+$. HPLC purity: 97.2%, retention time: 7.40 min.

5.1.2.2.14. N-(1-Benzylpiperidin-4-yl)-1-(4-fluorophenyl)methanimine (S_I3n) [Mayavel et al. 2015]

Colorless crystals (0.719 g, 2.426 mmol, 92%), mp 91–93 °C. TLC (DCM:MeOH, 95:5 v/v) R_f = 0.48. FT-IR (Alpha ATR, *v* cm^{-1}): 2964, 2919 (CH aromatic), 1597 (N=CH imine), 1318 (C—F). ^{1}H NMR (500 MHz, DMSO-d_6) δ_H 8.41 (s, 1H), 7.48 (d, *J* = 7.8 Hz, 2H), 7.39 (d, *J* = 8.4 Hz, 2H), 7.32–7.26 (m, 5H), 3.61 (s, 2H), 3.37–3.33 (m, 1H), 2.91 (d, *J* = 9.6 Hz, 2H), 2.14 (t, *J* = 9.2 Hz, 2H), 1.63–1.47 (m, 4H). ^{13}C NMR (125 MHz, DMSO-d_6) δ_C 163.86 (d, J_{C-F} = 248.96 Hz), 158.64, 139.67, 133.71 (d, J_{C-F} = 2.2 Hz), 131.31 (d, J_{C-F} = 6.4 Hz), 128.78, 127.21, 126.31, 116.87 (d, J_{C-F} = 28.2 Hz), 65.83, 63.19, 51.64, 32.41. LC/MS (ESI, *m/z*): 319.54 $[M + Na]^+$. HPLC purity: 96.2%, retention time: 4.25 min.

5.1.2.2.15. N-(1-Benzylpiperidin-4-yl)-1-(2,4-difluorophenyl)methanimine (S_I3o)

Yellow crystals (0.727 g, 2.314 mmol, 88%), mp 104–106 °C. TLC (DCM:MeOH, 95:5 v/v) R_f = 0.55. FT-IR (Alpha ATR, *v* cm^{-1}): 2949, 2916 (CH aromatic), 1604 (N=CH imine), 1332 (C—F), 1316 (C—F). ^{1}H NMR (500 MHz, DMSO-d_6) δ_H 8.36 (s, 1H), 7.59–7.54 (m, 1H), 7.39–7.36 (m, 2H), 7.27–7.21 (m, 5H), 3.56 (s, 2H), 3.39–3.36 (m, 1H), 2.86 (d, *J* = 10.2 Hz, 2H), 2.11 (t, *J* = 10.8 Hz, 2H), 1.58–1.36 (m, 4H). ^{13}C NMR (125 MHz, DMSO-d_6) δ_C 165.29 (dd, J_{C-F} = 252.81, 7.8 Hz), 161.49 (dd, J_{C-F} = 258.49, 6.9 Hz), 154.12 (d, J_{C-F} = 6.8 Hz) 139.19, 133.49 (t, J_{C-F} = 7.2 Hz), 129.19, 127.69, 126.48, 120.14 (dd, J_{C-F} = 27.3, 4.2 Hz), 114.19 (dd, J_{C-F} = 28.1, 4.1 Hz),

104.92 (t, J_{C-F} = 28.2 Hz), 65.12, 63.42, 51.29, 31.67. LC/MS (ESI, *m/z*): 337.49 [M + Na]$^+$. HPLC purity: 97.5%, retention time: 4.68 min.

5.1.2.2.16. N,1-Dibenzylpiperidin-4-amine (S_I4a) [Feula and Fossey 2013]

Dark Yellow oil (0.254 g, 0.907 mmol, 84%). TLC (DCM:MeOH, 95:5 v/v) R_f = 0.30. FT-IR (Alpha ATR, ν cm^{-1}): 3218 (NH), 2942, 2790 (CH aromatic). ^{1}H NMR (500 MHz, $CDCl_3$) δ_H 7.33–7.15 (m, 10H), 3.89 (s, 2H), 3.61 (s, 2H), 2.67 (d, *J* = 9.8 Hz, 2H), 2.48–2.42 (m, 1H), 2.02 (t, *J* = 10.9 Hz, 2H), 1.89 (d, *J* = 12.2 Hz, 2H), 1.65 (s, 1H, D_2O exchangeable), 1.48–1.39 (m, 2H). ^{13}C NMR (125 MHz, $CDCl_3$) δ_C 140.68, 138.98, 128.61, 128.32, 128.01, 127.96, 128.22, 125.81, 63.82, 56.61, 52.23, 51.65, 31.69. LC/MS (ESI, *m/z*): 281.34 [M + H]$^+$. HPLC purity: 99.4%, retention time: 4.04 min.

5.1.2.2.17. 1-Benzyl-N-(2,3-dimethoxybenzyl)piperidin-4-amine (S_I4b)

Brown oil (0.237 g, 0.697 mmol, 79%). TLC (DCM:MeOH, 95:5 v/v) R_f = 0.32. FT-IR (Alpha ATR, ν cm^{-1}): 3329 (NH), 2936, 2806 (CH aromatic). ^{1}H NMR (500 MHz, $CDCl_3$) δ_H 7.29–7.11 (m, 5H), 6.93 (t, *J* = 7.8 Hz, 1H), 6.86 (dd, *J* = 7.2, 1.9 Hz, 1H), 6.69 (dd, *J* = 7.2, 2.2 Hz, 1H), 3.86 (s, 2H), 3.82 (s, 3H), 3.76 (s, 3H), 3.69 (s, 2H), 2.61 (d, *J* = 8.2 Hz, 2H), 2.54–2.49 (m, 1H), 1.99 (t, *J* = 9.8 Hz, 2H), 1.81 (d, *J* = 11.6 Hz, 2H), 1.62 (s, 1H, D_2O exchangeable), 1.44–1.31 (m, 2H). ^{13}C NMR (125 MHz, $CDCl_3$) δ_C 151.69, 146.91, 138.66, 132.33, 128.69, 127.89, 127.12, 126.43, 123.19, 120.42, 111.63, 63.93, 60.03, 58.33, 55.82, 51.65, 48.19, 32.08. LC/MS (ESI, *m/z*): 341.66 [M + H]$^+$. HPLC purity: 97.2%, retention time: 3.55 min.

5.1.2.2.18. 1-Benzyl-N-(3,4,5-trimethoxybenzyl)piperidin-4-amine (S_I4c)

Red oil (0.249 g, 0.673 mmol, 83%). TLC (DCM:MeOH, 95:5 v/v) R_f = 0.34. FT-IR (Alpha ATR, ν cm^{-1}): 3302 (NH), 2940, 2812 (CH aromatic). ^{1}H NMR (500 MHz, $CDCl_3$) δ_H 7.36–7.21 (m, 5H), 6.67 (s, 2H), 3.88 (s, 2H), 3.80 (s, 9H), 3.61 (s, 2H), 2.67

(d, *J* = 7.8 Hz, 2H), 2.51–2.46 (m, 1H), 1.94 (t, *J* = 8.2 Hz, 2H), 1.76 (d, *J* = 10.2 Hz, 2H), 1.64 (s, 1H, D_2O exchangeable), 1.39–1.28 (m, 2H). ^{13}C NMR (125 MHz, $CDCl_3$) δ_C 152.39, 147.79, 138.33, 136.56, 129.32, 128.13, 126.96, 108.81, 63.87, 60.73, 58.27, 56.18, 52.13, 51.13, 31.83. LC/MS (ESI, *m/z*): 371.81 $[M + H]^+$. HPLC purity: 95.4%, retention time: 4.11 min.

5.1.2.2.19. 2-(((1-Benzylpiperidin-4-yl)amino)methyl)phenol (S_I4d) [Chen et al. 2011]

Colorless oil (0.231 g, 0.780 mmol, 76%). TLC (DCM:MeOH, 95:5 v/v); R_f = 0.27. FT-IR (Alpha ATR, *v* cm^{-1}): 3352 (phenolic OH), 3327 (NH), 2960, 2814 (CH aromatic). ^1H NMR (500 MHz, $CDCl_3$) δ_H 9.42 (s, 1H), 7.33–7.24 (m, 5H), 7.12–7.06 (m, 2H), 6.81 (dd, *J* = 7.6, 2.2 Hz, 2H), 3.99 (s, 2H), 3.73 (s, 2H), 2.62 (d, *J* = 7.6 Hz, 2H), 2.39–2.32 (m, 1H), 1.99 (t, *J* = 8.2 Hz, 2H), 1.67 (s, 1H, D_2O exchangeable), 1.58 (d, *J* = 12.2 Hz, 2H), 1.46–1.38 (m, 2H). ^{13}C NMR (125 MHz, $CDCl_3$) δ_C 155.82, 137.69, 132.99, 129.42, 128.01, 127.65, 127.01, 120.85, 116.99, 66.03, 55.22, 51.76, 48.02, 32.46. LC/MS (ESI, *m/z*): 297.38 $[M + H]^+$. HPLC purity: 96.3%, retention time: 3.64 min.

5.1.2.2.20. 4-(((1-Benzylpiperidin-4-yl)amino)methyl)phenol (S_I4e)

Colorless oil (0.216 g, 0.729 mmol, 72%). TLC (DCM:MeOH, 95:5 v/v) R_f = 0.28. FT-IR (Alpha ATR, *v* cm^{-1}): 3365 (phenolic OH), 3316 (NH), 2955, 2782 (CH aromatic). ^1H NMR (500 MHz, $CDCl_3$) δ_H 9.15 (s, 1H), 7.33–7.23 (m, 5H), 7.12 (d, *J* = 7.2 Hz, 2H), 6.83 (d, *J* = 7.3 Hz, 2H), 3.89 (s, 2H), 3.66 (s, 2H), 2.59 (d, *J* = 7.9 Hz, 2H), 2.47–2.41 (m, 1H), 1.95 (t, *J* = 7.8 Hz, 2H), 1.74 (s, 1H, D_2O exchangeable), 1.69 (d, *J* = 11.6 Hz, 2H), 1.44–1.37 (m, 2H). ^{13}C NMR (125 MHz, $CDCl_3$) δ_C 154.68, 138.33, 130.69, 128.92, 128.69, 127.99, 126.49, 117.12, 64.05, 55.83, 51.52, 51.49, 31.98. LC/MS (ESI, *m/z*): 297.61 $[M + H]^+$. HPLC purity: 96.3%, retention time: 3.47 min.

5.1.2.2.21. 4-(((1-Benzylpiperidin-4-yl)amino)methyl)benzene-1,3-diol (S_I4f)

Colorless oil (0.212 g, 0.679 mmol, 70%). TLC (DCM:MeOH, 95:5 v/v) R_f = 0.24. FT-IR (Alpha ATR, ν cm^{-1}): 3395 (phenolic OH), 3340 (NH), 2944, 2811 (CH aromatic). ^{1}H NMR (500 MHz, $CDCl_3$) δ_H 9.35 (s, 1H), 9.28 (s, 1H), 7.38–7.29 (m, 5H), 6.96 (d, *J* = 7.4 Hz, 1H), 6.55 (dd, *J* = 8.1, 2.2 Hz, 1H), 6.32 (d, *J* = 1.9 Hz, 1H), 3.92 (s, 2H), 3.82 (s, 2H), 2.66 (d, *J* = 7.4 Hz, 2H), 2.33–2.28 (m, 1H), 1.92 (t, *J* = 9.8 Hz, 2H), 1.68 (s, 1H, D_2O exchangeable), 1.49 (d, *J* = 11.9 Hz, 2H), 1.41–1.33 (m, 2H). ^{13}C NMR (125 MHz, $CDCl_3$) δ_C 159.27, 158.23, 139.23, 131.62, 128.73, 128.41, 127.89, 126.55, 116.02, 111.61, 105.20, 64.12, 56.02, 51.23, 31.69. LC/MS (ESI, *m/z*): 313.64 $[M + H]^+$. HPLC purity: 99.2%, retention time: 3.15 min.

5.1.2.2.22. 1-Benzyl-N-(3-methylbenzyl)piperidin-4-amine (S_I4g)

Yellow oil (0.234 g, 0.795 mmol, 77%). TLC (DCM:MeOH, 95:5 v/v) R_f = 0.36. FT-IR (Alpha ATR, ν cm^{-1}): 3309 (NH), 2927, 2796 (CH aromatic). ^{1}H NMR (500 MHz, $CDCl_3$) δ_H 7.48 (t, *J* = 8.2 Hz, 1H), 7.39 (dt, *J* = 8.2, 1.9 Hz, 1H), 7.28–7.13 (m, 7H), 3.94 (s, 2H), 3.79 (s, 2H), 2.69 (d, *J* = 7.2 Hz, 2H), 2.38 (s, 3H), 2.35–2.32 (m, 1H), 1.89 (t, *J* = 8.8 Hz, 2H), 1.64 (s, 1H, D_2O exchangeable), 1.46 (d, *J* = 10.7 Hz, 2H), 1.44–1.38 (m, 2H). ^{13}C NMR (125 MHz, $CDCl_3$) δ_C 140.36, 138.21, 137.18, 129.23, 129.03, 127.68, 126.89, 124.33, 64.49, 55.22, 51.47, 32.08, 22.03. LC/MS (ESI, *m/z*): 295.71 $[M + H]^+$. HPLC purity: 97.0%, retention time: 4.79 min.

5.1.2.2.23. 1-Benzyl-N-(4-methylbenzyl)piperidin-4-amine (S_I4h) [Van Kammen et al. 2008]

Yellow oil (0.252 g, 0.857 mmol, 83%). TLC (DCM:MeOH, 95:5 v/v) R_f = 0.35. FT-IR (Alpha ATR, ν cm^{-1}): 3314 (NH), 2937 (CH aromatic), 2799 (CH aromatic); ^{1}H NMR (500 MHz, $CDCl_3$) δ_H 7.44 (d, *J* = 8.2 Hz, 1H), 7.34–7.28 (m, 6H), 7.22 (d, *J* = 7.8 Hz, 2H), 3.99 (s, 2H), 3.84 (s, 2H), 2.74 (d, *J* = 7.5 Hz, 2H), 2.42 (s, 3H), 2.38–2.34 (m,

1H), 1.86 (t, *J* = 9.6 Hz, 2H), 1.69 (s, 1H, D_2O exchangeable), 1.48 (d, *J* = 9.8 Hz, 2H), 1.46–1.40 (m, 2H). ^{13}C NMR (125 MHz, $CDCl_3$) δ_C 141.22, 138.23, 131.89, 129.82, 129.36, 128.92, 127.68, 125.23, 64.82, 56.24, 51.82, 31.89, 22.02. LC/MS (ESI, *m/z*): 295.49 $[M + H]^+$. HPLC purity: 98.3%, retention time: 4.41 min.

5.1.2.2.24. 1-Benzyl-N-(4-nitrobenzyl)piperidin-4-amine (S_I4i)

Red oil (0.239 g, 0.735 mmol, 79%). TLC (DCM:MeOH, 95:5 v/v) R_f = 0.33. FT-IR (Alpha ATR, *v* cm^{-1}): 3336 (NH), 2941, 2797 (CH aromatic), 1512 (NO_2), 1339 (NO_2). ^1H NMR (500 MHz, $CDCl_3$) δ_H 8.18 (d, *J* = 8.7 Hz, 2H), 7.52 (d, *J* = 8.6 Hz, 2H), 7.39–7.30 (m, 4H), 7.29–7.24 (m, 1H), 3.93 (s, 2H), 3.51 (s, 2H), 2.87 (d, *J* = 11.8 Hz, 2H), 2.56–2.45 (m, 1H), 2.04 (t, *J* = 10.7 Hz, 2H), 1.89 (d, *J* = 12.2 Hz, 2H), 1.75 (s, 1H, D_2O exchangeable), 1.51–1.39 (m, 2H). ^{13}C NMR (125 MHz, $CDCl_3$) δ_C 148.92, 147.13, 138.45, 129.28, 128.92, 128.67, 128.32, 127.14, 123.95, 123.73, 63.18, 54.58, 52.38, 50.23, 32.86. LC/MS (ESI, *m/z*): 326.48 $[M + H]^+$. HPLC purity: 97.3%, retention time: 4.40 min.

5.1.2.2.25. 1-Benzyl-N-(4-(trifluoromethyl)benzyl)piperidin-4-amine (S_I4j) [Boss et al. 2004]

Orange oil (0.248 g, 0.712 mmol, 82%). TLC (DCM:MeOH, 95:5 v/v) R_f = 0.58. FT-IR (Alpha ATR, *v* cm^{-1}): 3204 (NH), 2935, 2803 (CH aromatic), 1322 (C—F). ^1H NMR (500 MHz, $CDCl_3$) δ_H 7.59 (d, *J* = 7.4 Hz, 2H), 7.46 (d, *J* = 7.5 Hz, 2H), 7.33 (s, 4H), 7.28 (s, 1H), 3.89 (s, 2H), 3.52 (s, 2H), 2.87 (d, *J* = 10.6 Hz, 2H), 2.52 (s, 1H), 2.04 (t, *J* = 11.2 Hz, 2H), 1.90 (d, *J* = 11.9 Hz, 2H), 1.64 (s, 1H, D_2O exchangeable), 1.46 (dd, *J* = 21.6, 10.7 Hz, 2H). ^{13}C NMR (125 MHz, $CDCl_3$) δ_C 145.19, 138.67, 129.26 (q, J_{C-F} = 32.2 Hz), 129.13, 128.32, 128.30, 127.08, 125.41 (q, J_{C-F} = 3.8 Hz), 124.41 (q, J_{C-F} = 271.8 Hz), 63.22, 54.46, 52.45, 50.43, 32.91. LC/MS (ESI, *m/z*): 349.40 $[M + H]^+$. HPLC purity: 97.8%, retention time: 4.84 min.

5.1.2.2.26. 1-Benzyl-N-(4-(trifluoromethoxy)benzyl)piperidin-4-amine (S_I4k)

Orange oil (0.227 g, 0.623 mmol, 75%). TLC (DCM:MeOH, 95:5 v/v) R_f = 0.57. FT-IR (Alpha ATR, ν cm^{-1}): 3289 (NH), 2950, 2804 (CH aromatic), 1340 (C—F). ^{1}H NMR (500 MHz, $CDCl_3$) δ_H 7.85 (d, *J* = 9.6 Hz, 2H), 7.79 (d, *J* = 7.8 Hz, 2H), 7.32–7.18 (m, 5H), 3.90 (s, 2H), 3.76 (s, 2H), 2.59 (d, *J* = 8.2 Hz, 2H), 2.29–2.21 (m, 1H), 1.79 (t, *J* = 10.2 Hz, 2H), 1.67 (s, 1H, D_2O exchangeable), 1.55 (d, *J* = 9.2 Hz, 2H), 1.38–1.19 (m, 2H). ^{13}C NMR (125 MHz, $CDCl_3$) δ_C 152.82, 138.23, 130.09, 129.96, 129.21, 128.92, 127.91, 125.58, 123.09, 121.88 (q, J_{C-F} = 248.7), 64.09, 56.26, 51.49, 51.23, 32.96. LC/MS (ESI, *m/z*): 365.44 $[M + H]^+$. HPLC purity: 97.4%, retention time: 5.65 min.

5.1.2.2.27. 1-Benzyl-N-(4-chlorobenzyl)piperidin-4-amine (S_I4l) [Harper and Chignell 1964]

Brown oil (0.253 g, 0.805 mmol, 84%). TLC (DCM:MeOH, 95:5 v/v) R_f = 0.46. FT-IR (Alpha ATR, ν cm^{-1}): 3279 (NH), 2933, 2789 (CH aromatic), 746 (C—Cl). ^{1}H NMR (500 MHz, $CDCl_3$) δ_H 7.59 (d, *J* = 7.6 Hz, 2H), 7.33–7.26 (m, 5H), 7.17 (d, *J* = 7.6 Hz, 2H), 3.89 (s, 2H), 3.78 (s, 2H), 2.64 (d, *J* = 9.6 Hz, 2H), 2.41–2.29 (m, 1H), 1.86 (t, *J* = 11.2 Hz, 2H), 1.79 (s, 1H, D_2O exchangeable),1.58 (d, *J* = 9.6 Hz, 2H), 1.45–1.29 (m, 2H). ^{13}C NMR (125 MHz, $CDCl_3$) δ_C 139.67, 137.21, 135.86, 130.22, 129.09, 128.87, 127.88, 126.56, 64.28, 57.18, 51.31, 31.65. LC/MS (ESI, *m/z*): 315.33 $[M + H]^+$. HPLC purity: 98.4%, retention time: 5.33 min.

5.1.2.2.28. 1-Benzyl-N-(2,4-dichlorobenzyl)piperidin-4-amine (S_I4m)

Yellow oil (0.233 g, 0.669 mmol, 77%). TLC (DCM:MeOH, 95:5 v/v) R_f = 0.52. FT-IR (Alpha ATR, ν cm^{-1}): 3332 (NH), 2932, 2802 (CH aromatic), 737 (C—Cl), 697 (C—Cl). ^{1}H NMR (500 MHz, $CDCl_3$) δ_H 7.38 (s, 2H), 7.33 (d, *J* = 3.5 Hz, 4H), 7.27 (d, *J* = 7.1 Hz, 1H), 7.23 (d, *J* = 8.1 Hz, 1H), 3.87 (s, 2H), 3.51 (s, 2H), 2.87 (d, *J* = 10.8 Hz, 2H), 2.50 (t, *J* = 9.8 Hz, 1H), 2.04 (t, *J* = 11.0 Hz, 2H), 1.89 (d, *J* = 11.6 Hz, 2H), 1.67

(s, 1H, D_2O exchangeable), 1.50–1.44 (m, 2H). ^{13}C NMR (125 MHz, $CDCl_3$) δ_C 138.49, 136.79, 134.21, 133.13, 130.83, 129.23, 129.15, 128.19, 127.10, 126.97, 63.10, 54.30, 52.32, 47.70, 32.71. LC/MS (ESI, *m/z*): 349.63 $[M + H]^+$. HPLC purity: 97.5%, retention time: 6.92 min.

5.1.2.2.29. 1-Benzyl-N-(4-fluorobenzyl)piperidin-4-amine (S_I4n)

Red oil (0.241 g, 0.808 mmol, 80%). TLC (DCM:MeOH, 95:5 v/v) R_f = 0.37. FT-IR (Alpha ATR, ν cm^{-1}): 3299 (NH), 2957, 2803 (CH aromatic), 1322 (C—F). ^1H NMR (500 MHz, $CDCl_3$) δ_H 7.38 (d, J = 8.2 Hz, 2H), 7.34–7.28 (m, 5H), 7.19 (d, J = 8.2 Hz, 2H), 3.88 (s, 2H), 3.49 (s, 2H), 2.79 (d, J = 9.9 Hz, 2H), 2.49 (t, J = 10.2 Hz, 1H), 2.12 (t, J = 10.9 Hz, 2H), 1.86 (d, J = 11.6 Hz, 2H), 1.77 (s, 1H, D_2O exchangeable), 1.48–1.41 (m, 2H). ^{13}C NMR (125 MHz, $CDCl_3$) δ_C 162.60 (d, J_{C-F} = 260.8 Hz), 138.99, 135.69 (d, J_{C-F} = 2.8 Hz), 130.27 (d, J_{C-F} = 6.8 Hz), 128.69, 127.89, 126.31, 115.25 (d, J_{C-F} = 28.2 Hz), 64.23, 56.68, 51.48, 51.46, 32.39. LC/MS (ESI, *m/z*): 299.73 $[M + H]^+$. HPLC purity: 99.3%, retention time: 4.17 min.

5.1.2.2.30. 1-Benzyl-N-(2,4-difluorobenzyl)piperidin-4-amine (S_I4o)

Brown oil (0.244 g, 0.772 mmol, 81%). TLC (DCM:MeOH, 95:5 v/v) R_f = 0.42. FT-IR (Alpha ATR, ν cm^{-1}): 3292 (NH), 2946, 2806 (CH aromatic), 1331 (C—F), 1322 (C—F). ^1H NMR (500 MHz, $CDCl_3$) δ_H 7.58–7.54 (m, 1H), 7.39–7.35 (m, 2H), 7.25–7.18 (m, 5H), 3.82 (s, 2H), 3.58 (s, 2H), 2.84 (d, J = 8.6 Hz, 2H), 2.51 (t, J = 9.8 Hz, 1H), 2.19 (t, J = 9.2 Hz, 2H), 1.79 (d, J = 10.2 Hz, 2H), 1.71 (s, 1H, D_2O exchangeable), 1.46–1.42 (m, 2H). ^{13}C NMR (125 MHz, $CDCl_3$) δ_C 164.64 (dd, J_{C-F} = 262.8, 8.2 Hz), 161.82 (dd, J_{C-F} = 259.6, 8.2 Hz), 138.64, 133.41 (t, J_{C-F} = 7.3 Hz), 128.68, 127.96, 126.48, 124.68 (dd, J_{C-F} = 27.3, 4.4 Hz), 112.19 (dd, J_{C-F} = 28.2, 4.2 Hz), 103.67 (t, J_{C-F} = 28.6 Hz), 64.18, 56.49, 51.29, 47.12 (d, J_{C-F} = 7.6 Hz), 31.89. LC/MS (ESI, *m/z*): 317.33 $[M + H]^+$. HPLC purity: 99.0%, retention time: 4.59 min.

5.1.3 Biological evaluation

5.1.3.1 In vitro studies

5.1.3.1.1 Cholinesterase (AChE and BChE) inhibition by Ellman assay

The synthesized compounds **S_I3a–o and S_I4a–o** were assessed for their inhibitory potential against AChE and BChE by Ellman method using donepezil and rivastigmine as positive reference standards [Ellman et al. 1961]. Donepezil has higher selectivity for AChE, while rivastigmine selectively inhibits the BChE.

The results showed excellent to good inhibition of AChE in micromolar to submicromolar concentration range except for compounds **S_I3a, S_I3c,** and **S_I3g** (IC_{50} > 15 μM). All the tested compounds elicited moderately poor inhibitory potential against BChE. Compound **S_I4j** showed 28.2 fold AChE selective inhibition than BChE comparable to donepezil having 42.1 fold AChE selectivity. Among all the evaluated compounds, **S_I4a–o** showed slightly pronounced AChE inhibitory activity than their respective methanimine derivatives (**S_I3a–o**). The unsubstituted compounds **S_I3b** and **S_I4b** exhibited moderate AChE inhibition at micromolar levels (IC_{50}, **S_I3b:** 2.11 μM**;** **S_I4b:** 1.75 μM). The substitution of electron donating groups (—OH, —OCH_3, and —CH_3) weakened AChE inhibitory potential in compounds **S_I3a, S_I3c–h, S_I4a,** and **S_I4c–h**. The substitution of electron withdrawing groups drastically improved the inhibition against AChE. The 2,4-disubstitution with weak electron withdrawing groups (—Cl and —F) (IC_{50}, **S_I3m:** 1.34 μM; **S_I3o:** 1.33 μM**;** **S_I4m:** 0.620 μM; **S_I4o:** 0.710 μM) exhibited slightly higher inhibitory potential than their monosubstituted (4-) counterparts (IC_{50}, **S_I3l:** 1.45 μM; **S_I3n:** 2.93; **S_I4l:** 0.846 μM; **S_I4n:** 1.17 μM). The strong electron withdrawing substituted groups (—NO_2, —CF_3, and —OCF_3) showed significantly high AChE inhibitory potential in submicromolar range (IC_{50}, **S_I3i:** 0.903 μM; **S_I3j:** 0.442 μM, **S_I4i:** 0.724 μM; **S_I4j:** 0.107 μM; and **S_I4k:** 0.590 μM) exception

being compound **S_I3k,** which elicited inhibition at micromolar level (IC_{50}, **S_I3k:** 1.03 μM). The results of the AChE inhibition assay also corroborated with the outcome of docking and dynamics study with **S_I4j** being the most potent compound of the series by interacting significantly with PAS and CAS residues of AChE.

A comparative study with the previously reported similar *N*-benzylpiperidine analogs, such as substituted indoles [Andreani et al. 2001], cyclopentathiophenes [Omran et al. 2005], identified hits from the present study showed significantly higher inhibitory potential against AChE. The results are tabulated in Table 5.2.

Table 5.2. Cholinesterases (hAChE and hBChE) and hBACE-1 inhibition activity and selectivity index of compounds (Series I).

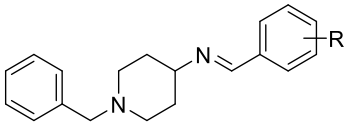

S_I3a-o

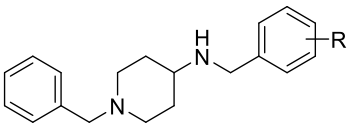

S_I4a-o

Comd.	R	IC_{50} (μM) ± SEM			hAChE SI[a]
		hAChE	hBChE	hBACE-1	
S_I3a	2,3-diOCH_3	>15 μM	>30 μM	6.27 ± 0.13	-
S_I3b	H	2.11 ± 0.06	>30 μM	3.45 ± 0.10	-
S_I3c	3,4,5-triOCH_3	>15 μM	10.9 ± 0.08	13.5 ± 0.09	-
S_I3d	2-OH	2.78 ± 0.05	16.4 ± 0.10	2.73 ± 0.07	5.9
S_I3e	4-OH	4.85 ± 0.09	>30 μM	12.2 ± 0.06	-
S_I3f	2,4-diOH	2.62 ± 0.08	19.4 ± 0.06	9.97 ± 0.11	7.4
S_I3g	3-CH_3	>15 μM	>30 μM	3.34 ± 0.07	-
S_I3h	4-CH_3	4.39 ± 0.03	>30 μM	18.7 ± 0.09	-
S_I3i	4-NO_2	0.903 ± 0.03	7.32 ± 0.07	0.726 ± 0.03	8.1
S_I3j	4-CF_3	0.442 ± 0.05	3.95 ± 0.07	0.279 ± 0.03	8.9
S_I3k	4-OCF_3	1.03 ± 0.06	5.47 ± 0.07	1.80 ± 0.06	5.3
S_I3l	4-Cl	1.45 ± 0.06	4.57 ± 0.05	1.72 ± 0.04	3.2
S_I3m	2,4-diCl	1.34 ± 0.06	5.76 ± 0.06	3.92 ± 0.10	4.3
S_I3n	4-F	2.93 ± 0.06	>30 μM	1.49 ± 0.05	-
S_I3o	2,4-diF	1.33 ± 0.03	>30 μM	3.48 ± 0.05	-
S_I4a	3,4-diOCH_3	2.17 ± 0.08	7.21 ± 0.04	5.32 ± 0.09	3.3
S_I4b	H	1.75 ± 0.07	12.1 ± 0.08	2.95 ± 0.10	6.9
S_I4c	3,4,5-triOCH_3	2.22 ± 0.06	10.6 ± 0.06	12.7 ± 0.08	4.8
S_I4d	2-OH	2.37 ± 0.06	14.3 ± 0.11	2.00 ± 0.08	6.0
S_I4e	4-OH	4.00 ± 0.07	>30 μM	9.90 ± 0.08	-
S_I4f	2,4-diOH	2.33 ± 0.07	18.5 ± 0.04	5.85 ± 0.09	8.0
S_I4g	3-CH_3	4.05 ± 0.10	>30 μM	2.59 ± 0.09	-
S_I4h	4-CH_3	3.70 ± 0.08	>30 μM	16.6 ± 0.04	-

S_I4i	4-NO_2	0.724 ± 0.04	7.80 ± 0.09	0.428 ± 0.04	10.8
S_I4j	4-CF_3	0.107 ± 0.02	3.02 ± 0.06	0.223 ± 0.02	28.2
S_I4k	4-OCF_3	0.590 ± 0.05	3.48 ± 0.06	1.35 ± 0.04	5.9
S_I4l	4-Cl	0.846 ± 0.04	4.00 ± 0.06	0.662 ± 0.06	4.7
S_I4m	2,4-diCl	0.620 ± 0.05	3.52 ± 0.09	3.04 ± 0.09	5.7
S_I4n	4-F	1.17 ± 0.08	3.89 ± 0.06	0.548 ± 0.03	3.3
S_I4o	2,4-diF	0.710 ± 0.06	3.06 ± 0.10	2.94 ± 0.03	4.3
donepezil		0.033 ± 0.01	1.39 ± 0.06	0.237 ± 0.03	42.1
rivastigmine		1.91 ± 0.06	1.10 ± 0.04	-	0.6

All the results are reported as the mean IC_{50} ± SEM (n = 3). [a] SI (Selectivity Index) = IC_{50} of hBChE/IC_{50} of hAChE.

5.1.3.1.2 Enzyme kinetics study

The enzyme kinetics study for compound **S_I4j** on hAChE was performed by Lineweaver-Burk method to establish the mechanism of enzyme inhibition [Lineweaver and Burk 1934]. The results of the Lineweaver-Burk plot (Figure 5.14) showed decreased V_{max}, while K_m remained constant with an increase in the substrate concentration. The plotted result suggested a noncompetitive type of enzyme inhibition by compound **S_I4j** on both free enzyme and the enzyme-substrate complex. The intersection points on both axes of $1/V_{max}$ and 1/[S] were found to be higher than zero, suggesting that the inhibitor was preferentially bound to free enzyme rather than enzyme-substrate complex. Further, the Dixon plot has been plotted (Figure 5.15) using three concentrations of inhibitor (0.03, 0.15, and 0.30 µM) and the outcome suggested that compound **S_I4j** has K_i = 0.10 µM.

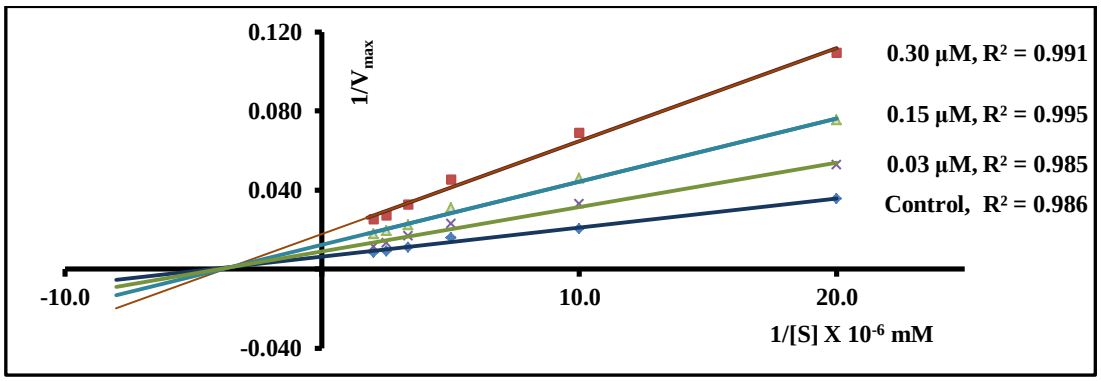

Figure 5.14. Lineweaver-Burk plot for the kinetic study of hAChE inhibition by compound **S_I4j**.

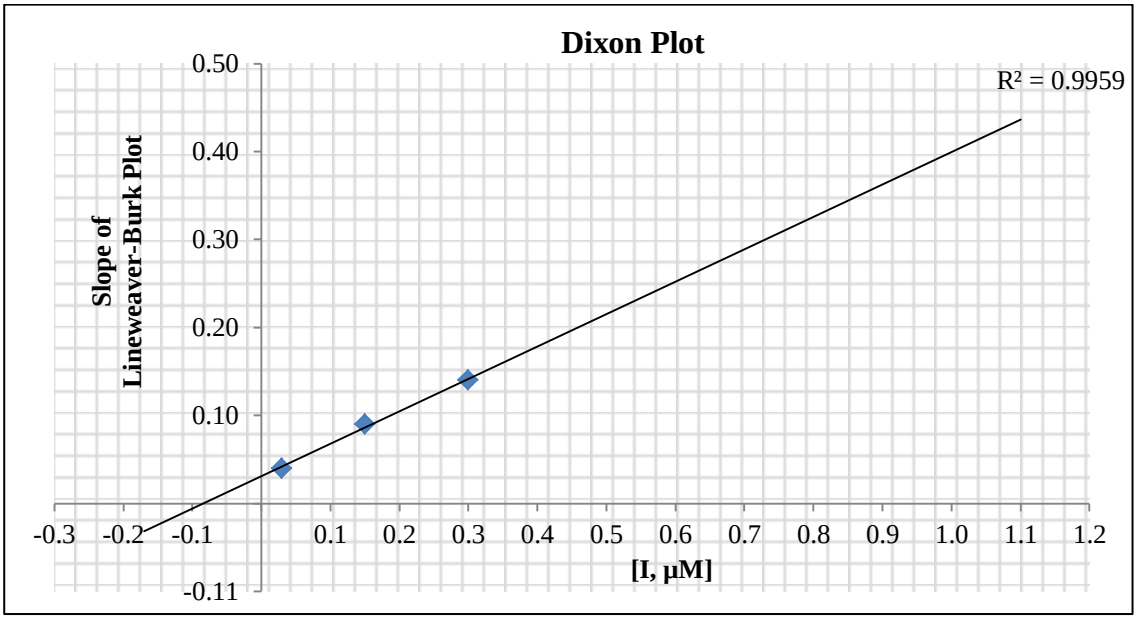

Figure 5.15. Dixon plot of compound **S_I4j** at three different concentrations (0.03, 0.15, and 0.30 µM) showing K_i value of inhibitor as the negative intersection at the x-axis.

5.1.3.1.3 BACE-1 inhibition assay

All the synthesized derivatives were evaluated for their BACE-1 inhibitory potential by FRET-based BACE-1 fluorescence assay kit (Sigma Aldrich, Catalog No. CS0010). The unsubstituted derivatives **S_I3b** and **S_I4b** showed moderate inhibition against BACE-1 (IC_{50}, **S_I3b:** 3.45 µM; **S_I4b:** 2.95 µM). However, the substitution of electron donating groups (**S_I3a, S_I3c–h**, **S_I4a,** and **S_I4c–h**) significantly reduced the BACE-1 inhibitory potential. Compounds substituted with 2-OH and 3-CH_3 electron donating groups were the exceptions and showed moderately higher inhibition potential (IC_{50}, **S_I3d:** 2.73 µM; **S_I3g:** 3.34 µM**;** **S_I4d:** 2.00 µM; **S_I4g:** 2.59 µM). These outcomes suggested that substitutions of electron donating groups were favored at *ortho* than the *para*-position. Another electron donating substitution with 3,4,5-triOCH_3 (IC_{50}, **S_I3c:** 13.5 µM**;** **S_I4c:** 12.7 µM) elicited less pronounced BACE-1 inhibition than 2,3-diOCH_3 substituted analogs (IC_{50}, **S_I3a:** 6.27 µM; **S_I4a:** 5.32 µM). The results indicated the substitution of electron donating groups at 4-position significantly declined the BACE-1 inhibitory potential of compounds. Conversely, substitution of electron withdrawing

groups (compounds **S_I3i–o** and **S_I4i–o**) drastically improved the BACE-1 inhibition. The monosubstituted 4-Cl and 4-F showed higher inhibition (IC_{50}, **S_I3l:** 1.72 μM; **S_I3n:** 1.49 μM; **S_I4l:** 0.662 μM; and **S_I4n:** 0.548 μM) compared to their 2,4-disubstituted counterparts (IC_{50}, **S_I3m:** 3.92 μM; **S_I3o:** 3.48 μM**; S_I4m:** 3.04 μM; and **S_I4o:** 2.94 μM). The potent BACE-1 inhibitors **S_I3i, S_I3j, S_I4i, S_I4j, S_I4l,** and **S_I4n** presented the IC_{50} values 0.726 μM, 0.279 μM, 0.428 μM, 0.223 μM, 0.662 μM, and 0.548 μM, respectively. The higher BACE-1 inhibitory potential in these compounds might be attributed due to their significant H-bonding interactions with the catalytic dyad residues Asp32 and Asp228 validated by the outcome of docking and dynamic simulations studies. Common compounds **S_I3i, S_I3j, S_I4i,** and **S_I4j** with significant and balanced inhibitory potential against both the target enzymes (AChE and BACE-1) were selected for further screening. The results of BACE-1 inhibition assay are tabulated in Table 5.2.

5.1.3.1.4 Propidium iodide displacement assay

The affinity of selected ligands at 10 and 50 μM concentrations for the PAS-binding was evaluated by propidium iodide displacement assay (Table 5.3). Propidium iodide is a known AChE ligand, binds specifically at PAS, and thereby, enhances its fluorescence intensity up to eight-fold [Nunes-Tavares et al. 2002]. The binding of inhibitors to PAS displaces propidium iodide and resulted into decreased fluorescence intensity. Compounds **S_I4i** and **S_I4j** exhibited higher displacement of propidium iodide (**S_I4i:** 10 μM = 23.6%, 50 μM = 33.8%; **S_I4j:** 10 μM = 27.2%, 50 μM = 37.6%) compared to donepezil (10 μM = 22.6%; 50 μM: 33.6%). Compounds **S_I3i** and **S_I3j** appeared to have considerably less capability in displacing the propidium iodide from PAS-AChE (**S_I3i:** 10 μM = 15.0%, 50 μM = 20.0%; **S_I3j:** 10 μM = 12.4%, 50 μM = 19.3%). The results of the assay were found to be in agreement with computational studies.

Table 5.3. Propidium iodide displacement and predicted BBB permeability (Series I).

Comd.	Propidium iodide displacement from AChE PAS (% inhibition)[a]		PAMPA-BBB permeability		
	At 10 μM	At 50 μM	$P_{e(exp)}$ (10^{-6} cm.s^{-1})		Permeability prediction
			Reference	Observed	
verapamil	-	-	16	18.6 ± 1.6	CNS+[b]
diazepam	-	-	16	16.9 ± 1.2	CNS+[b]
oxazepam	-	-	10	8.9 ± 1.1	CNS+[b]
progesterone	-	-	9.3	11.8 ± 1.2	CNS+[b]
chlorpromazine	-	-	6.5	7.2 ± 0.12	CNS+[b]
alprazolam	-	-	5.4	4.9 ± 0.16	CNS+[b]
lomefloxacin	-	-	1.1	1.42 ± 0.08	CNS-[c]
atenolol	-	-	0.8	0.78 ± 0.06	CNS-[c]
dopamine	-	-	0.2	0.28 ± 0.02	CNS-[c]
S_I3i	15.0 ± 1.5	20.0 ± 1.2	5.0 ± 0.2		CNS+[b]
S_I3j	12.4 ± 1.3	19.3 ± 1.4	6.2 ± 0.3		CNS+[b]
S_I4i	23.6 ± 2.5	33.8 ± 3.1	4.4 ± 0.1		CNS+[b]
S_I4j	27.2 ± 2.9	37.6 ± 3.0	6.1 ± 0.3		CNS+[b]
donepezil	22.6 ± 1.7	33.6 ± 1.7	6.9 ± 0.2		CNS+[b]

[a]Propidium iodide displacement assay was performed on AChE to test the ability of compounds to displace propidium with reference to the donepezil at 10 and 50 μM. [b]'CNS+' (prediction of high BBB permeation); P_e (10^{-6} cm.s^{-1}) > 4.4; [c]CNS-' (prediction of low BBB permeation); P_e (10^{-6} cm s^{-1}) < 1.8. All the results are reported as the mean ± SEM (n=3).

5.1.3.1.5 Parallel artificial membrane permeation assay (PAMPA-BBB)

The BBB permeability is one of the essential prerequisites to target compounds for the treatment of AD. The BBB permeability of the potent inhibitors (**S_I3i**, **S_I3j**, **S_I4i**, and **S_I4j**) on AChE and BACE-1 were assessed by PAMPA-BBB assay [Di et al. 2003]. The method involved the use of lipid-infused parallel artificial membrane through which the test compounds permeate from a donor compartment to the acceptor compartment [Ottaviani et al. 2006]. The permeability of nine commercial drugs was used as a benchmark to establish the correlation between experimental $P_{e(exp)}$ and reference permeability $P_{e(ref)}$. The CNS permeability cut-off values indicated that compounds with permeability (P_e) over 4.4×10^{-6} cm.s^{-1} suggest excellent brain penetrability, whereas with P_e less than 1.8×10^{-6} cm.s^{-1} has poor brain permeation. The permeability value in

between them was considered as uncertain. The results of assay (Table 5.3) suggested that all the tested compounds **S_I3i** (P_e = 5.0×10^{-6} cm.s^{-1}), **S_I3j** (P_e = 6.2×10^{-6} cm.s^{-1}), **S_I4i** (P_e = 4.4×10^{-6} cm.s^{-1}), and **S_I4j** (P_e = 6.1×10^{-6} cm.s^{-1}) have appreciable and high brain permeability. The higher brain permeability of compounds **S_I3j** and **S_I4j** could be attributed to the presence of highly lipophilic trifluoromethyl (4-CF_3) substituent at terminal phenyl group.

Considering the balance between inhibitory potential against both the targets (AChE and BACE-1), along with the significantly high displacement of propidium iodide from PAS-AChE, compounds **S_I4i** and **S_I4j** were chosen for further assessments.

5.1.3.1.6 Aβ aggregation (self- and AChE-induced) inhibition by thioflavin T assay

The results of propidium iodide displacement assay suggested significant binding of **S_I4i** and **S_I4j** at PAS- AChE. The AChE was also demonstrated to be involved in the promotion of Aβ aggregation by specifically binding to PAS [Inestrosa et al. 1996, Nepovimova et al. 2014]. Thus, AChEIs bound to the active site and PAS could not only result in AChE inhibition but also prevent the Aβ production and deposition. Therefore, thioflavin T based fluorometric assay was performed on compounds **S_I4i** and **S_I4j** to ascertain their PAS-AChE binding to be beneficial in preventing Aβ aggregation. The test was conducted at three different ratios of Aβ: inhibitors (10:5, 10:10, and 10:20 μM). The results were reported as % Aβ aggregation inhibition (Figures 5.16A and 5.16B) and normalized fluorescence intensity (NFI) (Figure 5.17A and 5.17B).

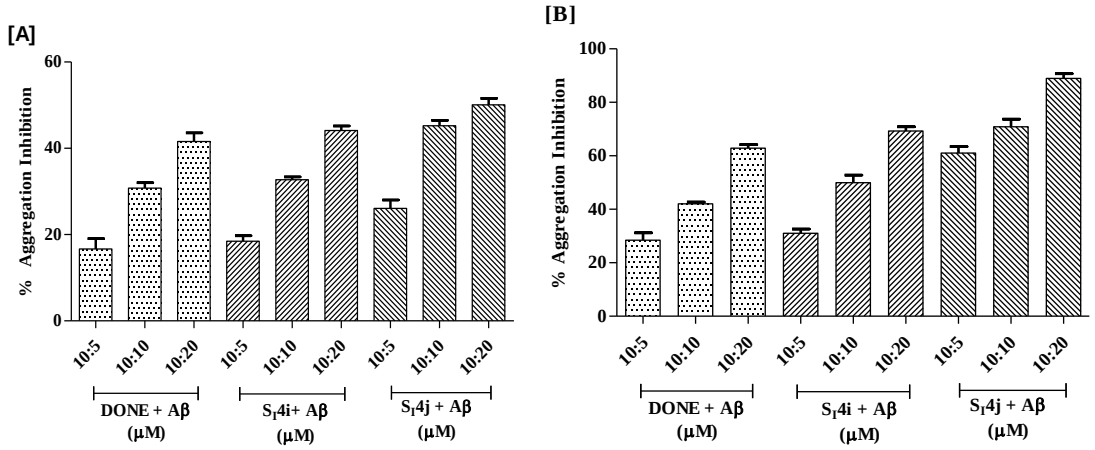

Figure 5.16. Effect of test compounds on Aβ aggregation inhibition. [A] Self-induced and [B] AChE-induced experiments. Each bar displays % Aβ aggregation as the mean ± SEM of three separate experiments. DONE = donepezil.

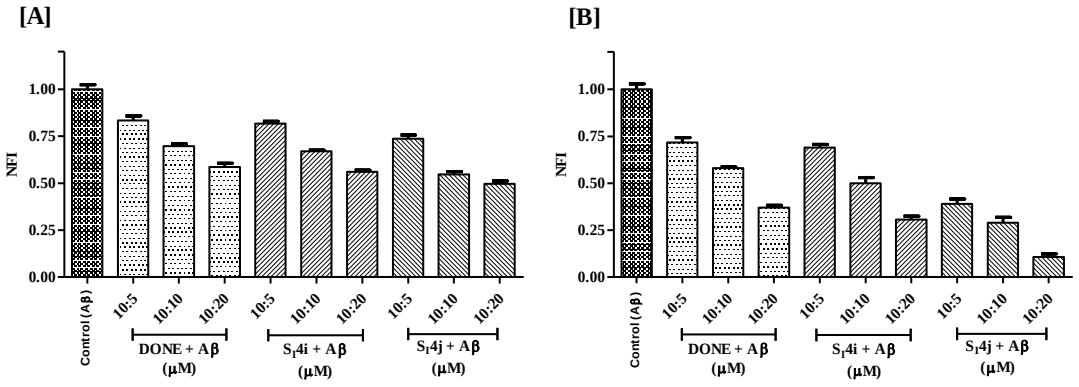

Figure 5.17. Effect of test compounds on Aβ aggregation. [A] Self-induced and [B] AChE-induced Aβ aggregation. Each bar displays the normalized fluorescence intensity (NFI) as the mean ± SEM of three separate experiments. DONE = donepezil.

Tested inhibitors showed higher anti-aggregatory property in self- (**S_I4i:** 18.5–44.1%; **S_I4j:** 26.1–50.1%) and AChE-induced (**S_I4i:** 31.0–69.3%; **S_I4j:** 61.1–89.0%) experiments compared to donepezil (Self-induced: 16.7–41.6%; AChE-induced: 28.5–62.8%). The results confirmed the PAS-AChE binding ability of these inhibitors and are in concurrence with the outcome of molecular docking and dynamics simulations.

5.1.3.1.7 AFM study

AFM experiments were conducted to visualize high-resolution images of surface topographical maps and calculate the nm size ranges of aggregates [Bruggink et al.

2012]. The changes in morphological characterization of Aβ aggregates owing to the presence or absence of inhibitor (**S_I4j**) were observed at different time intervals over 7 days of incubation period (0, 3, 5, and 7 days). Aβ aggregates, fibrils, and large oligomer formation were visually confirmed through AFM images. Further, maximum peak height and roughness index of samples were calculated to validate the inhibitory potential of compound **S_I4j**. $A\beta_{1-42}$ without inhibitor resulted into formation of large oligomers and fibrils. The AFM histogram analysis of $A\beta_{1-42}$ without inhibitor showed to increase the maximum peak height of aggregates from 23.72–226.55 nm owing to its aggregation during 7 days of the incubation period. Also, the roughness index was observed to be very high in the range of 2.33–24.36 nm. The addition of compound **S_I4j** halted the aggregation of $A\beta_{1-42}$ with the maximum peak height of aggregates was reduced drastically and observed in the range of 44.46–104.01 nm (Figure 5.18). The roughness index was also decreased remarkably to 1.70–4.40 nm in the presence of inhibitor. The results of the AFM analysis confirmed the significant inhibition of Aβ aggregation by compound **S_I4j.**

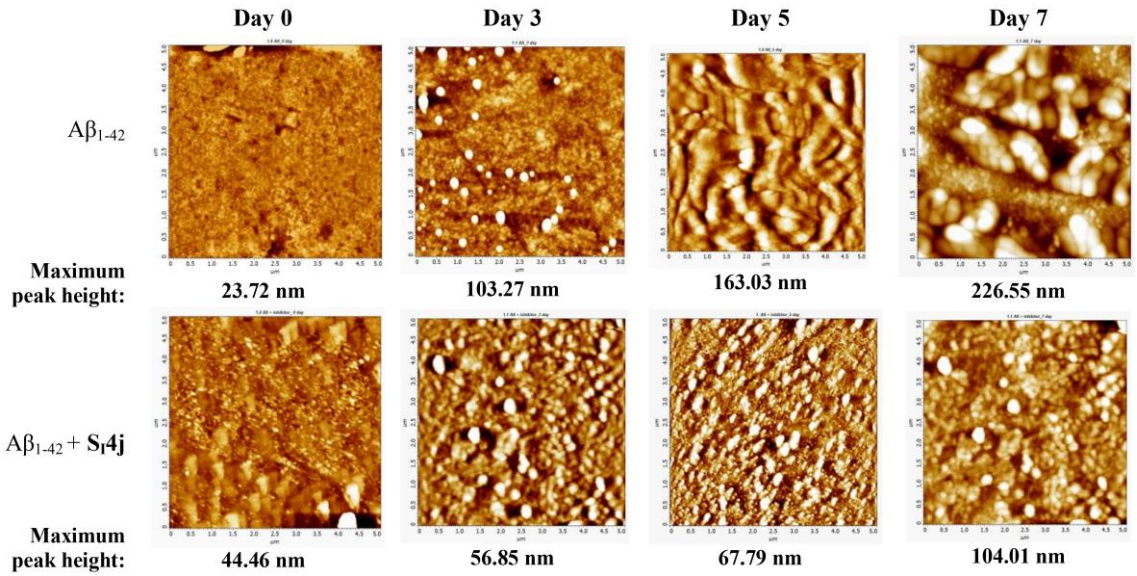

Figure 5.18. AFM images of $A\beta_{1-42}$ aggregates (10 µM) incubated with or without inhibitor (**S_I4j)** at different time intervals (0, 3, 5, and 7 days). Images were visualized at 5 × 5 µm using the Nova Px image analysis software (NT-MDT, Russia).

5.1.3.1.8 Neurotoxic liabilities against SH-SY5Y cell lines by MTT assay

The neurotoxicity liability of **S_I4i**, **S_I4j**, and donepezil was evaluated against human neuroblastoma SH-SY5Y cell lines following the MTT assay. The results suggested that compound **S_I4i** exposed to neuroblastoma cell lines SH-SY5Y exhibited nonsignificant reduction in cell viabilities up to 10 µM concentration, while **S_I4j** elicited nonsignificant reduction up to 20 µM concentration. The percentage cell viabilities at tested concentrations were observed in the range of 76.3–96.3% and 84.6–99.2% for compounds **S_I4i** and **S_I4j**, respectively (Figure 5.19).

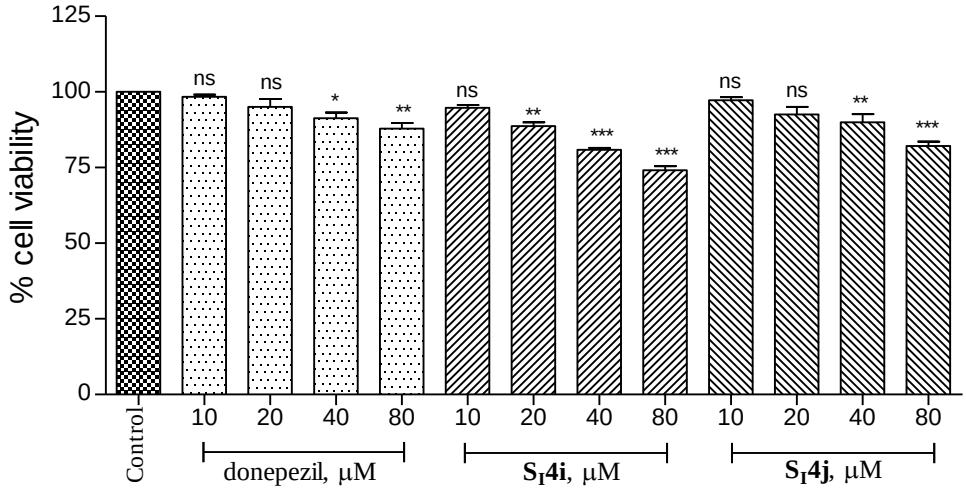

Figure 5.19. Cell viability assay on neuroblastoma SH-SY5Y cell lines with increasing concentrations of **S_I4i** and **S_I4j**. Each bar displays the mean ± SEM for three different experiments. *** $p < 0.001$, ** $p < 0.01$, * $p < 0.05$, ns nonsignificant *vs* control.

5.1.3.2 In vivo and ex vivo studies

5.1.3.2.1 Acute oral toxicity study

The acute toxicity was evaluated as per OECD guidelines 423 on healthy female Wistar rats. Compounds **S_I4i** and **S_I4j** were well tolerated and showed no sign of abnormal reactions or toxicity in the doses of 100–500 mg/kg, p.o. up to 14 days of testing. The results suggested that tested compounds possessed significant margin of safety following an oral administration.

5.1.3.2.2 Scopolamine-induced amnesia model: Y-maze test

Behavioral studies to evaluate the cognition and memory for compounds **S_I4i** and **S_I4j** were performed by the scopolamine-induced Y-maze model. Scopolamine is a gold standard drug, and its administration is the most effective way for inducing cognitive impairment due to the cholinergic deficit [Klinkenberg and Blokland 2010]. Test compounds were daily administered daily to healthy male Wistar rats at the dose of 2.5, 5, and 10 mg/kg, p.o.

On the seventh day of trial, the Y-maze test was performed to evaluate the effect of compounds (**S_I4i** and **S_I4j**), and spontaneous alternations were calculated, which is a measure of spatial working memory [Jin et al. 2014, Wolf et al. 2016]. The % spontaneous alternations was significantly reduced in the scopolamine group of animals (Figure 5.20A, $p < 0.001$) compared to the control group indicative of induction of memory and learning impairment. Donepezil (5 mg/kg) showed significantly increased spontaneous alternations (Figure 5.20A, $p < 0.001$) compared to scopolamine group. Similar to the elevated plus maze experiment, **S_I4i** (10 mg/kg) and **S_I4j** (5 and 10 mg/kg) showed the statistically nonsignificant difference in % spontaneous alternations compared to donepezil group. The total arm entries (Figure 5.20B) remained unchanged in all groups suggested that scopolamine did not hamper the locomotor activity in animals. The overall results of scopolamine-induced models advocated the potential of compounds **S_I4i** and **S_I4j** in improving spatial and immediate memory.

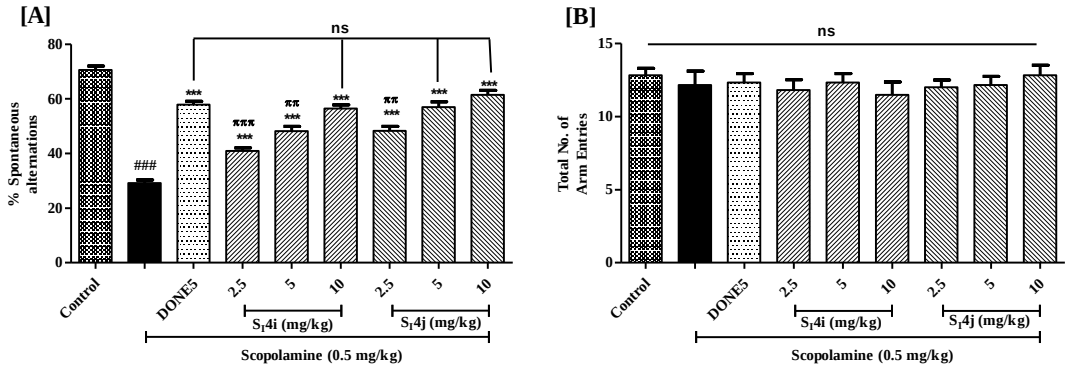

Figure 5.20. Effect of compounds **S_I4i**, **S_I4j**, and donepezil on scopolamine-induced cognition and memory improvement. [A] Spontaneous alternations (%) and [B] Total number of arm entries in the Y-maze experiment. All results are expressed as the mean ± SEM (n = 6). $^{###}p < 0.001$ *vs* control; $^{***}p < 0.001$ *vs* scopolamine; $^{\pi\pi\pi}p < 0.001$, $^{\pi\pi}p < 0.01$, $^{\pi}p < 0.05$, $^{ns}p > 0.05$ *vs* DONE5 (donepezil 5 mg/kg).

5.1.3.2.3 Ex vivo studies: AChE estimation and antioxidant activity

The effect of **S_I4i** and **S_I4j** on brain AChE level was evaluated by *ex vivo* study as per Ellman's method [Ellman et al. 1961]. The results showed a significantly higher rate (Figure 5.21A, $p < 0.001$) of substrate hydrolysis or elevated levels of AChE in the scopolamine- group of animals compared to the control group. The levels of AChE were remarkably attenuated (Figure 5.21A, $p < 0.001$) by treatment of **S_I4i** and **S_I4j** at the dose of 10 mg/kg compared to the scopolamine group. The *ex vivo* brain AChE inhibitory potential of both compounds at the tested dosage was found to be statistically nonsignificant in comparison to standard donepezil. These results also reflected the ability of compounds to permeate the BBB.

The antioxidant potential of compounds was elucidated by estimation of oxidative biochemical markers such as malonaldehyde (MDA, lipid peroxidation by-product) and superoxide dismutase (SOD, involved in dismutation of O_2^- radicals). Biochemical analysis showed that scopolamine group has significantly elevated the levels of MDA (Figure 5.21B, $p < 0.001$), while the levels of SOD (Figure 5.21C, $p < 0.001$) were considerably reduced compared to the control group. However, the treatment of **S_I4i** and

S_I4j at 10 mg/kg dose attenuated the levels of MDA (Figure 5.21B, $p < 0.001$), while significantly increasing the levels of SOD (Figure 5.21C, $p < 0.001$) compared to scopolamine group. Also, the results suggested that donepezil possesses insignificant antioxidant potential. Overall, the results of *ex vivo* studies suggested **S_I4j** to possess significant brain AChE inhibitory potential along with antioxidant property.

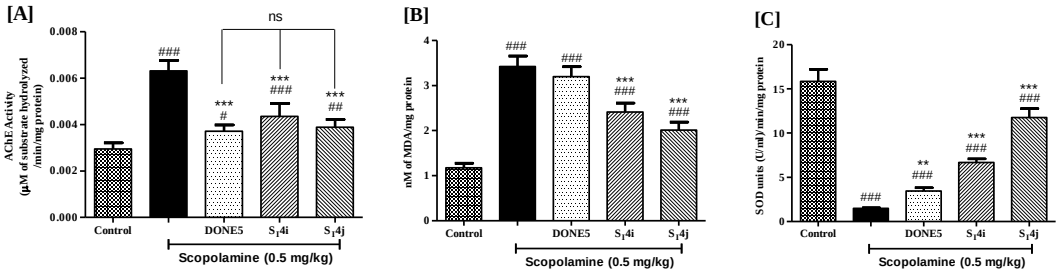

Figure 5.21. Results of *ex vivo* studies. [A] AChE activity- rate of substrate hydrolyzed [B] TBARS assay- levels of MDA [C] Superoxide dismutase assay- levels of SOD units. Values are expressed as mean ± SEM (n = 6). $^{###}p < 0.001$, $^{##}p < 0.01$, $^{#}p < 0.5$ *vs.* control; $^{***}p < 0.001$, $^{**}p < 0.01$, $^{*}p < 0.05$ *vs.* scopolamine; ^{ns}nonsignificant *vs* donepezil (DONE5).

5.1.3.2.4 Aβ-induced AD phenotypic model: Morris water maze test

The intracerebroventricular (ICV) administration of $A\beta_{1-42}$ is one of the most promising method to develop learning and memory deficits along with the AD-like phenotypic condition [Van Dam and De Deyn 2011]. Aβ is the major constituent of senile plaques in the brains of AD patients [Benedikz et al. 2009], and its deposition also augmented with the increased activity of BACE-1 [Merlini and Bellotti 2003]. The effect of most potent compound **S_I4j** was assessed in healthy Wistar rats by ICV injection of $A\beta_{1-42}$ in the hippocampal region of the brain. All the groups of animals have received the ICV $A\beta_{1-42}$ injection except the sham group. After seven days of the recovery period, rats of all groups were administered the respective treatments for nine consecutive days. During the last 5 days of treatment, the Morris water maze experiment was performed to evaluate ELT and numbers of platform crossings over the period of 90 s. The ELT was significantly prolonged (Figure 5.22A, $p < 0.001$), while the number of platform

crossings (Figure 5.22B, $p < 0.001$) progressively declined in the model group of animals owing to $A\beta_{1-42}$ administration compared to the sham group, which strongly suggested the impairment of learning and memory. The treatment with donepezil (72.5–22.5 s, $p < 0.001$) and **S_I4j** (74.5–20.3 s, $p < 0.001$) significantly decreased the ELT over the period of 5 days of trial compared to the model group (74.0–49.3 s). Also, the number of platform crossings was remarkably improved by donepezil (1.3–13.7, $p < 0.001$) and **S_I4j** (1.7–14.5, $p < 0.001$) group with definite spatial preference in correct quadrant over 5 days of trials compared to the model group (1.0–5.7). Interestingly, treatment with compound **S_I4j** demonstrated remarkable improvement in cognitive and memory functions at the tested dose.

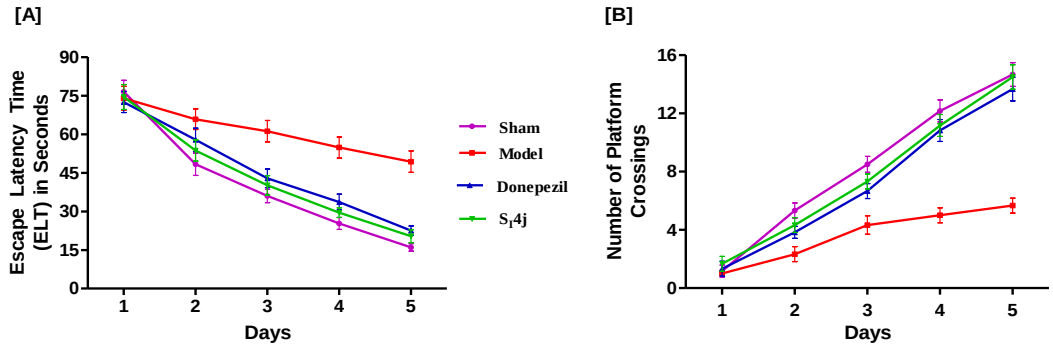

Figure 5.22. Effect of compound **S_I4j** in spatial memory improvement on ICV $A\beta_{1-42}$-induced model [A] Escape latency time (ELT) [B] Number of platform crossings in target quadrant during the last 5 days of trials by Morris water maze experiment. The values represented mean ± SEM (n = 6).

5.1.3.3 Pharmacokinetic study

Preliminary pharmacokinetic investigation of compound **S_I4j** was envisaged on healthy male Wistar rats at the dose of 10 mg/kg, p.o. The blood sampling was performed from retro-orbital plexus at several time points (See Chapter 4- Experimental Section). The parameters were calculated by following the extravascular noncompartmental model using Kinetica software (Thermo Fisher Scientific, version 5.0.11) and results are summarized in Table 5.4. The results suggested that **S_I4j** has peak plasma concentration

C_{max} = 32.8 ± 1.7 ng/mL achieved at T_{max} = 5.3 ± 1.3 h. Compound **S_I4j** has shown elimination half-life $t_{1/2}$ = 29.2 ± 2.2 h and mean residence time MRT = 45.7 ± 2.0 h. Overall, results showed significant oral absorption of test compound **S_I4j** after oral administration.

Table 5.4. Pharmacokinetic evaluation after an oral administration of **S_I4j** (10 mg/kg, p.o.)

Parameters	Effect of **S_I4j** *
C_{max} (ng/mL)	32.8 ± 1.7
T_{max} (h)	5.3 ± 1.3
$(AUC)_{0-24}$ (ng/mL*h)	633.3 ± 41.4
$t_{1/2}$ (h)	29.2 ± 2.2
MRT (h)	45.7 ± 2.0

*All values are expressed as mean ± SEM (n = 3).

5.2 PART-II: SERIES II–V

5.2.1 Chemistry

5.2.1.1 Synthesis of Series II (S_{II}9a–h) and III (S_{III}10a–h): N-Benzylpiperidine with substituted benzylidenehydrazine-1-carboxamides and substituted 5-phenyl-1,3,4-oxadiazoles tethered with an —NH linker

The target compounds **S_{II}9a–h** and **S_{III}10a–h** were synthesized following the sequential reactions mentioned in Scheme 2- Experimental Section. The carbamate intermediate **S_{II}7** was obtained in appreciable yield (85%) by the reaction of 4-amino-1-benzylpiperidine (**S_{II}5**) with phenyl chloroformate (**S_{II}6**) and pyridine in dry DCM. FT-IR spectrum showed characteristic stretching band at 1682 cm^{-1} for carbamate C=O group. ^{13}C NMR spectrum also displayed δ_C = 154.15 ppm value for **C**=O to confirm the formation compound **S_{II}7**. The **S_{II}7** was heated at reflux with hydrazine hydrate (80% v/v) in absolute EtOH to yield (77%) hydrazinecarboxamide intermediate (**S_{II}8)**, which was subsequently heated at reflux in EtOH with numerous aromatic aldehydes (variable EWG) under acidic medium to yield corresponding semicarbazones (**S_{II}9a–h)**

in appreciable yield (71–80%). FT-IR spectra of **S_{II}9a–h** displayed distinguished stretching band for (N=CH) in the range of 1602–1578 cm^{-1}. ^{1}H NMR showed characteristic singlet peak for (N=C**H**) at δ_H = 8.18–7.82 ppm. The presence of (N=**C**H) signal at δ_C = 155.94–154.92 ppm value confirmed the formation of **S_I9a–h**. Further, **S_{III}10a–c** were obtained by heating **S_{II}8** at reflux with several benzoic acids in $POCl_3$ (62–68%). Finally, **S_{III}10d–h** were prepared by oxidative cyclization of **S_{II}9d–h** using diacetoxyiodobenzene in dry DCM (65–75%). The disappearance of singlet peaks of N=C**H** and —N**H** in ^{1}H NMR spectra and appearance of signals at δ_C = 168.32–163.06 ppm and 158.05–153.67 ppm in ^{13}C NMR spectra for oxadiazole ring carbons to confirm the formation of **S_{III}10a–h**.

5.2.1.2 Characterization of the synthesized compounds (Series II and III)

5.2.1.2.1 Phenyl (1-benzylpiperidin-4-yl)carbamate (S_{II}7)

Yellow solid (1.382 g, 4.456 mmol, 85%); mp 130–132 °C; TLC (DCM:MeOH, 90:10 v/v); R_f = 0.68. FT-IR (Alpha ATR, *v* cm^{-1}): 1682 (C=O). ^{1}H NMR (500 MHz, DMSO-d_6) δ_H 8.05 (d, *J* = 7.0 Hz, 1H, —NH D_2O exchangeable), 7.64 (s, 2H), 7.46 (d, *J* = 2.9 Hz, 3H), 7.37 (t, *J* = 7.7 Hz, 2H), 7.20 (t, *J* = 7.2 Hz, 1H), 7.10 (t, *J* = 10.3 Hz, 2H), 3.89–3.76 (m, 1H), 3.62 (s, 2H), 2.82 (d, *J* = 11.8 Hz, 2H), 2.19 (t, *J* = 10.8 Hz, 2H), 1.99–1.92 (m, 2H), 1.61–1.59 (m, 2H). ^{13}C NMR (125 MHz, DMSO-d_6) δ_C 154.15, 151.40, 131.90, 130.36, 129.87, 129.74, 129.19, 125.46, 122.21, 59.23, 50.74, 46.62, 28.92.

5.2.1.2.2 Phenyl (1-benzylpiperidin-4-yl)carbamate (S_{II}8)

White solid (0.618 g, 2.489 mmol, 77%); mp 86–88 °C; TLC (DCM:MeOH, 90:10 v/v); R_f = 0.23. FT-IR (Alpha ATR, *v* cm^{-1}): 1728 (C=O). ^{1}H NMR (500 MHz, DMSO-d_6) δ_H 7.33–7.25 (m, 5H), 6.34 (s, 1H, —NH D_2O exchangeable), 6.01 (d, *J* = 8.0 Hz, 1H, —NH D_2O exchangeable), 3.70–3.63 (m, 1H), 3.51 (s, 2H), 2.83 (d, *J* = 11.5 Hz, 2H),

2.15 (t, *J* = 10.7 Hz, 2H), 1.95–1.91 (m, 2H), 1.55–1.47 (m, 2H). ^{13}C NMR (125 MHz, DMSO-d_6) δ_C 159.78, 138.37, 129.15, 128.22, 127.04, 63.10, 52.40, 46.56, 32.86.

5.2.1.2.3 2-Benzylidene-N-(1-benzylpiperidin-4-yl)hydrazine-1-carboxamide (S_{II}9a)

White solid (0.538 g, 1.599 mmol, 79%); mp 112–114 °C; TLC (DCM:MeOH, 90:10 v/v); R_f = 0.48. FT-IR (Alpha ATR, *v* cm^{-1}): 1652 (C=O), 1587 (C=N). ^{1}H NMR (500 MHz, DMSO-d_6) δ_H 10.33 (s, 1H, —NH D_2O exchangeable), 7.84 (s, 1H), 7.74–7.73 (m, 2H), 7.40–7.31 (m, 7H), 7.25–7.19 (m, 1H), 6.68 (d, *J* = 8.5 Hz, 1H, —NH D_2O exchangeable), 3.59–3.57 (m, 1H), 3.46 (s, 2H), 2.78 (d, *J* = 11.5 Hz, 2H), 2.01 (dd, *J* = 11.5, 9.9 Hz, 2H), 1.74 (d, *J* = 9.5 Hz, 2H), 1.67–1.59 (m, 2H). ^{13}C NMR (125 MHz, DMSO-d_6) δ_C 155.25, 139.89, 139.27, 135.15, 129.52, 129.13, 129.01, 128.60, 127.29, 127.12, 62.59, 52.82, 47.13, 32.55. ESI-MS (*m/z*): 337.38 $[M + H]^+$. HPLC purity: 99.2%, retention time: 3.15 min.

5.2.1.2.4 N-(1-Benzylpiperidin-4-yl)-2-(4-cyanobenzylidene)hydrazine-1-carboxamide (S_{II}9b)

Brown solid (0.549 g, 1.519 mmol, 75%); mp 138–140 °C; TLC (DCM:MeOH, 90:10 v/v); R_f = 0.52. FT-IR (Alpha ATR, *v* cm^{-1}): 1658 (C=O), 1592 (C=N). ^{1}H NMR (500 MHz, DMSO-d_6) δ_H 10.62 (s, 1H, —NH D_2O exchangeable), 7.94 (d, *J* = 8.5 Hz, 2H), 7.88 (s, 1H), 7.84 (d, *J* = 8.5 Hz, 2H), 7.34 (d, *J* = 4.1 Hz, 4H), 7.28 (d, *J* = 4.1 Hz, 1H), 6.88 (d, *J* = 8.0 Hz, 1H, —NH D_2O exchangeable), 3.60 (s, 2H), 3.47–3.43 (m, 1H), 2.86 (s, 2H), 2.12 (s, 2H), 1.74–1.68 (m, 4H). ^{13}C NMR (125 MHz, DMSO-d_6) δ_C 155.01, 139.70, 138.02, 132.90, 129.49, 128.70, 127.71, 119.34, 111.31, 62.18, 52.61, 47.04, 32.01. ESI-MS (*m/z*): 362.62 $[M + H]^+$. HPLC purity: 95.5%, retention time: 3.17 min.

5.2.1.2.5 N-(1-Benzylpiperidin-4-yl)-2-(4-nitrobenzylidene)hydrazine-1-carboxamide (S_{II}9c)

Yellow solid (0.568 g, 1.489 mmol, 74%); mp 122–124 °C; TLC (DCM:MeOH, 90:10 v/v); R_f = 0.43. FT-IR (Alpha ATR, ν cm^{-1}): 1651 (C=O), 1589 (C=N). ^{1}H NMR (500 MHz, DMSO-d_6) δ_H 10.70 (s, 1H, —NH D_2O exchangeable), 8.21 (d, J = 8.9 Hz, 2H), 8.02 (d, J = 8.9 Hz, 2H), 7.93 (s, 1H), 7.33–7.25 (m, 5H), 6.91 (d, J = 8.4 Hz, 1H, —NH D_2O exchangeable), 3.60–3.58 (m, 1H), 3.48 (s, 2H), 2.81 (d, J = 10.0 Hz, 2H), 2.02 (s, 2H), 1.74 (d, J = 9.8 Hz, 2H), 1.69–1.63 (m, 2H). ^{13}C NMR (125 MHz, DMSO-d_6) δ_C 154.92, 147.59, 141.70, 137.44, 129.15, 128.62, 127.96, 127.33, 124.21, 56.50, 52.84, 47.27, 32.44. ESI-MS (*m/z*): 382.33 $[M + H]^+$. HPLC purity: 99.8%, retention time: 2.61 min.

5.2.1.2.6 N-(1-Benzylpiperidin-4-yl)-2-(2,4-difluorobenzylidene)hydrazine-1-carboxamide (S_{II}9d)

White solid (0.602 g, 1.616 mmol, 80%); mp 102–104 °C; TLC (DCM:MeOH, 90:10 v/v); R_f = 0.56. FT-IR (Alpha ATR, ν cm^{-1}): 1672 (C=O), 1599 (C=N). ^{1}H NMR (500 MHz, DMSO-d_6) δ_H 10.52 (s, 1H, —NH D_2O exchangeable), 8.22 (dd, J = 15.6, 8.7 Hz, 1H), 8.00 (s, 1H), 7.36–7.25 (m, 6H), 7.13 (td, J = 8.6, 2.3 Hz, 1H), 6.84 (d, J = 8.2 Hz, 1H, —NH D_2O exchangeable), 3.62 (s, 3H), 2.88 (d, J = 5.6 Hz, 2H), 2.21 (s, 2H), 1.77 (d, J = 10.3 Hz, 2H), 1.73–1.68 (m, 2H). ^{13}C NMR (125 MHz, DMSO-d_6) δ_C 162.91 (dd, $J_{C–F}$ = 286.4, 12.5 Hz), 160.92 (dd, $J_{C–F}$ = 288.6, 12.4 Hz), 155.12 , 131.73 (d, $J_{C–F}$ = 2.7 Hz), 129.69, 128.64 (d, $J_{C–F}$ = 4.2 Hz), 128.56 (d, $J_{C–F}$ = 4.2 Hz), 127.83, 119.47 (dd, $J_{C–F}$ = 10.0, 3.6 Hz), 112.73 (d, $J_{C–F}$ = 3.1 Hz), 104.56 (t, $J_{C–F}$ = 25.7 Hz), 61.82, 52.38, 46.74, 31.13. ESI-MS (*m/z*): 373.36 $[M + H]^+$. HPLC purity: 96.8%, retention time: 3.36 min.

5.2.1.2.7 N-(1-Benzylpiperidin-4-yl)-2-(4-chlorobenzylidene)hydrazine-1-carboxamide (S_{II}9e)

White solid (0.576 g, 1.553 mmol, 77%); mp 116–118 °C; TLC (DCM:MeOH, 90:10 v/v); R_f = 0.62. FT-IR (Alpha ATR, ν cm^{-1}): 1669 (C=O), 1602 (C=N). ^{1}H NMR (500 MHz, DMSO-d_6) δ_H 10.41 (s, 1H, —NH D_2O exchangeable), 7.82 (s, 1H), 7.78 (d, *J* = 8.5 Hz, 2H), 7.44 (d, *J* = 8.5 Hz, 2H), 7.34–7.30 (m, 4H), 7.26–7.23 (m, 1H), 6.77 (d, *J* = 8.5 Hz, 1H, —NH D_2O exchangeable), 3.58–3.56 (m, 1H), 3.46 (d, *J* = 11.4 Hz, 2H), 2.79 (d, *J* = 11.2 Hz, 2H), 2.01 (t, *J* = 10.9 Hz, 2H), 1.72 (d, *J* = 9.7 Hz, 2H), 1.67–1.62 (m, 2H). ^{13}C NMR (125 MHz, DMSO-d_6) δ_C 155.17, 139.10, 138.57, 134.13, 133.88, 129.18, 129.04, 128.80, 128.62, 127.35, 62.51, 52.83, 47.14, 32.45. ESI-MS (*m/z*): 371.52 $[M + H]^+$. HPLC purity: 97.5%, retention time: 3.61 min.

5.2.1.2.8 N-(1-Benzylpiperidin-4-yl)-2-(2,4-dichlorobenzylidene)hydrazine-1-carboxamide (S_{II}9f)

White solid (0.592 g, 1.461 mmol, 73%); mp 98–100 °C; TLC (DCM:MeOH, 90:10 v/v); R_f = 0.72. FT-IR (Alpha ATR, ν cm^{-1}): 1657 (C=O), 1589 (C=N). ^{1}H NMR (500 MHz, DMSO-d_6) δ_H 10.65 (s, 1H, —NH D_2O exchangeable), 8.25 (d, *J* = 8.6 Hz, 1H), 8.18 (s, 1H), 7.62 (d, *J* = 2.0 Hz, 1H), 7.43 (dd, *J* = 8.6, 1.5 Hz, 1H), 7.34–7.31 (m, 4H), 7.25 (t, *J* = 6.5 Hz, 1H), 6.86 (d, *J* = 8.4 Hz, 1H, —NH D_2O exchangeable), 3.61–3.55 (m, 1H), 3.48 (s, 2H), 2.81 (d, *J* = 10.4 Hz, 2H), 2.03 (s, 2H), 1.73 (d, *J* = 10.2 Hz, 2H), 1.68–1.61 (m, 2H). ^{13}C NMR (125 MHz, DMSO-d_6) δ_C 154.94, 134.72, 134.41, 133.34, 131.44, 129.53, 129.22, 128.85, 128.63, 127.99, 127.39, 62.44, 52.79, 47.18, 32.32. ESI-MS (*m/z*): 405.30 $[M + H]^+$. HPLC purity: 96.5%, retention time: 4.65 min.

5.2.1.2.9 N-(1-Benzylpiperidin-4-yl)-2-(4-(trifluoromethyl)benzylidene)hydrazine-1-carboxamide (S_{II}9g)

White solid (0.579 g, 1.424 mmol, 71%); mp 107–109 °C; TLC (DCM:MeOH, 90:10 v/v); R_f = 0.67. FT-IR (Alpha ATR, ν cm^{-1}): 1661 (C=O), 1578 (C=N). ^{1}H NMR (500 MHz, $CDCl_3$) δ_H 10.16 (s, 1H, —NH D_2O exchangeable), 7.85 (s, 1H), 7.73 (d, J = 8.1 Hz, 2H), 7.66 (d, J = 8.1 Hz, 2H), 7.37–7.31 (m, 4H), 7.30 (d, J = 5.9 Hz, 1H), 6.12 (d, J = 8.3 Hz, 1H, —NH D_2O exchangeable), 3.88–3.82 (m, 1H), 3.59 (s, 2H), 2.91 (d, J = 10.2 Hz, 2H), 2.24 (t, J = 10.8 Hz, 2H), 2.03 (d, J = 11.1 Hz, 2H), 1.71–1.67 (m, 2H). ^{13}C NMR (125 MHz, $CDCl_3$) δ_C 155.83, 139.41, 137.91 (q, J_{C-F} = 3.8 Hz), 137.53, 131.12 (q, J_{C-F} = 32.5 Hz), 129.24, 128.31, 127.24, 126.87, 125.64 (q, J_{C-F} = 8.6 Hz), 123.96 (q, J_{C-F} = 272.2 Hz), 62.97, 52.26, 46.83, 32.64. ESI-MS (*m/z*): 405.51 $[M + H]^+$. HPLC purity: 99.9%, retention time: 4.05 min.

5.2.1.2.10 N-(1-Benzylpiperidin-4-yl)-2-(4-(trifluoromethoxy)benzylidene)hydrazine-1-carboxamide (S_{II}9h)

White solid (0.608 g, 1.446 mmol, 72%); mp 123–125 °C; TLC (DCM:MeOH, 90:10 v/v); R_f = 0.77. FT-IR (Alpha ATR, ν cm^{-1}): 1654 (C=O), 1581 (C=N). ^{1}H NMR (500 MHz, DMSO-d_6) δ_H 10.52 (s, 1H, —NH D_2O exchangeable), 7.88 (s, 2H), 7.86 (s, 1H), 7.62 (s, 2H), 7.46 (d, J = 3.1 Hz, 3H), 7.38 (d, J = 7.7 Hz, 2H), 6.99 (s, 1H, —NH D_2O exchangeable), 3.96–3.93 (m, 1H), 3.66 (s, 2H), 2.84 (d, J = 10.2 Hz, 2H), 2.28 (t, J = 10.8 Hz, 2H), 2.00 (d, J = 11.1 Hz, 2H), 1.72–1.69 (m, 2H). ^{13}C NMR (125 MHz, DMSO-d_6) δ_C 155.34, 149.07, 138.86, 134.39, 131.83, 129.23, 129.00, 121.58, 120.50 (q, J_{C-F} = 256.4 Hz), 59.48, 51.26, 45.57, 29.48. ESI-MS (*m/z*): 421.36 $[M + H]^+$. HPLC purity: 96.4%, retention time: 5.73 min.

5.2.1.2.11 N-(1-Benzylpiperidin-4-yl)-5-phenyl-1,3,4-oxadiazol-2-amine (S_{III}10a)

White solid (0.307 g, 0.918 mmol, 62%); mp 82–84 °C; TLC (DCM:MeOH, 90:10 v/v); R_f = 0.46. FT-IR (Alpha ATR, *v* cm^{-1}): 3282 (—NH), 1558 (C=N). ^1H NMR (500 MHz, $CDCl_3$) δ_H 7.88–7.84 (m, 2H), 7.59–7.55 (m, 2H), 7.42–7.38 (m, 1H), 7.25–7.19 (m, 5H), 5.12 (s, 1H, —NH D_2O exchangeable), 3.89–3.72 (m, 1H), 3.69–3.61 (m, 2H), 2.84 (d, *J* = 11.6 Hz, 2H), 2.32–2.25 (m, 2H), 2.14–2.02 (m, 2H), 1.72–1.1.64 (m, 2H). ^{13}C NMR (125 MHz, $CDCl_3$) δ_C 166.18, 155.92, 138.22, 131.64, 129.48, 129.12, 129.01, 128.64, 127.12, 127.01, 126.21, 62.82, 51.89, 50.42, 31.82. ESI-MS (*m/z*): 335.41 $[M + H]^+$. HPLC purity: 97.1%, retention time: 3.39 min.

5.2.1.2.12 4-(5-((1-Benzylpiperidin-4-yl)amino)-1,3,4-oxadiazol-2-yl)benzonitrile (S_{III}10b)

Light brown solid (0.319 g, 0.888 mmol, 64%); mp 96–98 °C; TLC (DCM:MeOH, 90:10 v/v); R_f = 0.51. FT-IR (Alpha ATR, *v* cm^{-1}): 3267 (—NH), 1564 (C=N). ^1H NMR (500 MHz, $CDCl_3$) δ_H 8.01 (d, *J* = 8.2 Hz, 1H), 7.75 (d, *J* = 8.2 Hz, 1H), 7.39–7.24 (m, 4H), 5.26 (s, 1H, —NH D_2O exchangeable), 3.80–3.72 (m, 1H), 3.66–3.55 (m, 2H), 2.93 (d, *J* = 11.6 Hz, 2H), 2.27–2.21 (m, 2H), 2.17–2.14 (m, 2H), 1.73–1.65 (m, 2H). ^{13}C NMR (125 MHz, $CDCl_3$) δ_C 163.06, 157.41, 137.55, 132.73, 129.28, 128.36, 128.28, 127.36, 126.05, 118.19, 113.77, 62.89, 51.81, 50.92, 32.10. ESI-MS (*m/z*): 360.38 $[M + H]^+$. HPLC purity: 97.9%, retention time: 3.44 min.

5.2.1.2.13 N-(1-Benzylpiperidin-4-yl)-5-(4-nitrophenyl)-1,3,4-oxadiazol-2-amine (S_{III}10c)

Beige solid (0.339 g, 0.893 mmol, 68%); mp 104–106 °C; TLC (DCM:MeOH, 90:10 v/v); R_f = 0.42. FT-IR (Alpha ATR, *v* cm^{-1}): 3268 (—NH), 1560 (C=N). ^1H NMR (500 MHz, $CDCl_3$) δ_H 8.28 (d, *J* = 7.8 Hz, 2H), 7.86 (d, *J* = 7.8 Hz, 2H), 7.38–7.24 (m, 5H), 5.28 (s, 1H, —NH D_2O exchangeable), 3.88–3.73 (m, 1H), 3.69–3.64 (m, 2H), 2.99 (d,

J = 11.8 Hz, 2H), 2.28–2.21 (m, 2H), 2.08–2.01 (m, 2H), 1.64–1.58 (m, 2H). ^{13}C NMR (125 MHz, $CDCl_3$) δ_C 168.22, 156.98, 147.42, 132.96, 128.82, 127.99, 127.56, 126.52, 124.81, 62.89, 52.89, 49.86, 31.68. ESI-MS (*m/z*): 380.29 $[M + H]^+$. HPLC purity: 99.8%, retention time: 2.93 min.

5.2.1.2.14 N-(1-Benzylpiperidin-4-yl)-5-(2,4-difluorophenyl)-1,3,4-oxadiazol-2-amine (S_{III}10d)

Light brown solid (0.325 g, 0.877 mmol, 65%); mp 77–79 °C; TLC (DCM:MeOH, 90:10 v/v); R_f = 0.54. FT-IR (Alpha ATR, *v* cm^{-1}): 3276 (—NH), 1572 (C=N). ^{1}H NMR (500 MHz, $CDCl_3$) δ_H 7.86–7.79 (m, 1H), 7.49–7.32 (m, 5H), 7.09–6.92 (m, 1H), 5.17 (s, 1H, —NH D_2O exchangeable), 3.82–3.77 (m, 1H), 3.61–3.54 (m, 2H), 2.82 (d, *J* = 11.8 Hz, 2H), 2.38–2.33 (m, 2H), 2.00–1.93 (m, 2H), 1.72–1.66 (m, 2H). ^{13}C NMR (125 MHz, $CDCl_3$) δ_C 167.08, 163.98 (dd, $J_{C–F}$ = 279.8, 11.9 Hz), 162.67 (dd, $J_{C–F}$ = 282.4, 12.2 Hz), 153.67, 133.80 (d, $J_{C–F}$ = 3.1 Hz), 129.73, 129.18 (d, $J_{C–F}$ = 3.8 Hz), 128.51 (d, $J_{C–F}$ = 3.9 Hz), 128.11, 116.76 (dd, $J_{C–F}$ = 11.2, 3.8 Hz), 113.68 (d, $J_{C–F}$ = 4.2 Hz), 105.23 (t, $J_{C–F}$ = 28.2 Hz), 62.08, 52.64, 49.52, 31.58. ESI-MS (*m/z*): 371.30 $[M + H]^+$. HPLC purity: 98.9%, retention time: 3.68 min.

5.2.1.2.15 N-(1-Benzylpiperidin-4-yl)-5-(4-chlorophenyl)-1,3,4-oxadiazol-2-amine (S_{III}10e)

White solid (0.351 g, 0.952 mmol, 71%); mp 89–91 °C; TLC (DCM:MeOH, 90:10 v/v); R_f = 0.59. FT-IR (Alpha ATR, *v* cm^{-1}): 3284 (—NH), 1579 (C=N). ^{1}H NMR (500 MHz, $CDCl_3$) δ_H 7.69 (d, *J* = 8.2 Hz, 2H), 7.48 (d, *J* = 8.2 Hz, 2H), 7.39–7.31 (m, 4H), 7.29–7.24 (m, 1H), 4.86 (s, 1H, —NH D_2O exchangeable), 3.73–3.68 (m, 1H), 3.58–3.46 (m, 2H), 2.89 (d, *J* = 11.6 Hz, 2H), 2.29–2.24 (m, 2H), 1.98–1.86 (m, 2H), 1.64–1.49 (m, 2H). ^{13}C NMR (125 MHz, $CDCl_3$) δ_C 166.92, 155.82, 140.18, 139.63, 135.13, 134.88,

129.63, 129.13, 128.93, 128.71, 126.99, 62.93, 51.86, 49.83, 31.63. ESI-MS (*m/z*): 369.40 $[M + H]^+$. HPLC purity: 98.9%, retention time: 3.88 min.

5.2.1.2.16 N-(1-Benzylpiperidin-4-yl)-5-(2,4-dichlorophenyl)-1,3,4-oxadiazol-2-amine (S_{III}10f)

White solid (0.373 g, 0.925 mmol, 75%); mp 69–71 °C; TLC (DCM:MeOH, 90:10 v/v); R_f = 0.70. FT-IR (Alpha ATR, *v* cm^{-1}): 3259 (—NH), 1555 (C=N). ^{1}H NMR (500 MHz, $CDCl_3$) δ_H 7.98 (d, *J* = 7.5 Hz, 1H), 7.49 (d, *J* = 1.8 Hz, 1H), 7.34 (dd, *J* = 8.2, 1.6 Hz, 1H), 7.39–7.29 (m, 4H), 7.26 (m, 1H), 4.81 (s, 1H, —NH D_2O exchangeable), 3.69–3.58 (m, 1H), 3.54–3.50 (m, 2H), 2.86 (d, *J* = 11.8 Hz, 2H), 2.36–2.32 (m, 2H), 1.88–1.79 (m, 2H), 1.67–1.60 (m, 2H). ^{13}C NMR (125 MHz, $CDCl_3$) δ_C 166.60, 155.19, 138.65, 135.48, 134.63, 133.19, 131.67, 129.23, 129.79, 128.67, 128.11, 127.67, 127.41, 62.47, 51.74, 49.04, 31.86. ESI-MS (*m/z*): 403.32 $[M + H]^+$. HPLC purity: 99.0%, retention time: 5.67 min.

5.2.1.2.17 N-(1-Benzylpiperidin-4-yl)-5-(4-(trifluoromethyl)phenyl)-1,3,4-oxadiazol-2-amine (S_{III}10g)

Pale yellow solid (0.333 g, 0.827 mmol, 67%); mp 90–92 °C; TLC (DCM:MeOH, 90:10 v/v); R_f = 0.66. FT-IR (Alpha ATR, *v* cm^{-1}): 3288 (—NH), 1565 (C=N). ^{1}H NMR (500 MHz, $CDCl_3$) δ_H 7.93 (d, *J* = 8.2 Hz, 2H), 7.64 (d, *J* = 8.1 Hz, 2H), 7.27–7.21 (m, 5H), 4.98 (s, 1H, —NH D_2O exchangeable), 3.64 (s, 1H), 3.51 (s, 2H), 2.82 (d, *J* = 13.6 Hz, 2H), 2.25–2.14 (m, 2H), 2.07 (d, *J* = 7.1 Hz, 2H), 1.66–1.59 (m, 2H). ^{13}C NMR (125 MHz, $CDCl_3$) δ_C 163.12, 158.05, 132.51 (q, J_{C-F} = 3.8 Hz), 132.49, 132.22, 129.52 (q, J_{C-F} = 28.6 Hz), 128.60, 127.88, 127.61, 126.20, 126.15 (q, J_{C-F} = 7.6 Hz), 125.02 (q, J_{C-F} = 269.8 Hz), 63.07, 52.01, 51.03, 32.31. ESI-MS (*m/z*): 403.35 $[M + H]^+$. HPLC purity: 98.8%, retention time: 5.25 min.

5.2.1.2.18 N-(1-Benzylpiperidin-4-yl)-5-(4-(trifluoromethoxy)phenyl)-1,3,4-oxadiazol-2-amine (S_{III}10h)

Light brown solid (0.339 g, 0.810 mmol, 68%); mp 81–83 °C; TLC (DCM:MeOH, 90:10 v/v); R_f = 0.74. FT-IR (Alpha ATR, *v* cm^{-1}): 3272 (—NH), 1569 (C=N). ^{1}H NMR (500 MHz, $CDCl_3$) δ_H 7.81 (d, *J* = 7.8 Hz, 2H), 7.62 (d, *J* = 7.8 Hz, 2H), 7.46–7.32 (m, 5H), 4.67 (s, 1H, —NH D_2O exchangeable), 3.86 (s, 1H), 3.58 (s, 2H), 2.81 (d, *J* = 14.8 Hz, 2H), 2.32–2.19 (m, 2H), 1.89 (d, J = 7.2 Hz, 2H), 1.69–1.63 (m, 2H). ^{13}C NMR (125 MHz, $CDCl_3$) δ_C 168.31, 156.19, 150.12, 138.23, 134.44, 131.92, 129.18, 129.04, 121.69, 120.18 (q, $J_{C—F}$ = 246.8 Hz), 62.89, 50.63, 49.55, 31.68. ESI-MS (*m/z*): 419.44 $[M + H]^+$. HPLC purity: 98.1%, retention time: 6.33 min.

5.2.1.3 Synthesis of Series IV (S_{IV}14a–h): N-Benzylpiperidine and substituted 5-phenyl-1,3,4-oxadiazoles tethered with the—$NHCH_2$ linker

Molecular hybrids of *N*-benzylpiperidine and substituted 5-phenyl-1,3,4-oxadiazole connected with the —$NHCH_2$ linker (**S_{IV}14a–h**) were synthesized by reaction sequence mentioned in Scheme 3- Experimental Section. In the first step, substituted benzoic acid derivatives (**S_{IV}11a–h**) were reacted with *N*-hydroxybenzotriazole (HOBT) and 1-ethyl-3-(3-dimethylaminopropyl)carbodiimide (EDC) in acetonitrile to yield benzoic acid esters, which were subsequently reacted with hydrazine hydrate (80% v/v) to obtain corresponding benzoic acid hydrazides (**S_{IV}12a–h**, yield: 79–87%). Subsequently, cyclization of compounds **S_{IV}12a–h** by heating chloroacetic acid at reflux in $POCl_3$ provided intermediates (**S_{IV}13a–h**, yield: 79–92%). ^{1}H NMR spectra of **S_{IV}13a–h** displayed two protons signal at δ_H = 5.18–4.15 ppm for C**H_2**–Cl, while ^{13}C NMR spectra showed two signals between δ_C = 165.44–162.19 ppm for oxadiazole ring carbons. Finally, the reaction of **S_{IV}13a–h** and 4-amino-1-benzylpiperidine (**S_I1**) with KI in DMF afforded the target compounds **S_{IV}14a–h** (yield: 66–81%). FT-IR spectra

showed characteristic —NH stretching band at 3292–3242 cm^{-1}. ^{1}H and ^{13}C NMR spectra displayed additional signals in aliphatic regions for piperidine protons and carbons, respectively to confirm the formation of **S_{IV}14a–h.**

5.2.1.4 Characterization of the synthesized compounds (Series IV)

5.2.1.4.1 Benzohydrazide (S_{IV}12a)

White solid (0.924 g, 6.787 mmol, 83%); mp 113–115 °C; TLC (hexane:EtOAc, 50:50 v/v); R_f = 0.18. FT-IR (Alpha ATR, *v* cm^{-1}): 3290 (—NH), 1682 (C=O). ^{1}H NMR (500 MHz, $CDCl_3$) δ_H 7.93 (s, 1H, —NH D_2O exchangeable), 7.75 (dd, *J* = 5.1, 3.4 Hz, 2H), 7.52–7.40 (m, 1H), 7.41 (dd, *J* = 10.5, 4.7 Hz, 2H) 3.87 (s, 2H, —NH_2 D_2O exchangeable). ^{13}C NMR (125 MHz, $CDCl_3$) δ_C 168.75, 132.62, 131.91, 128.71, 126.92.

5.2.1.4.2 4-Cyanobenzohydrazide (S_{IV}12b)

Beige solid (0.862 g, 5.349 mmol, 79%); mp 198–199 °C; TLC (hexane:EtOAc, 50:50 v/v); R_f = 0.16. FT-IR (Alpha ATR, *v* cm^{-1}): 3295 (—NH), 1662 (C=O). ^{1}H NMR (500 MHz, $CDCl_3$) δ_H 8.24 (s, 1H, —NH D_2O exchangeable), 7.92 (d, *J* = 7.8 Hz, 2H), 7.64 (d, *J* = 7.8 Hz, 2H), 4.04 (s, 2H, —NH_2 D_2O exchangeable). ^{13}C NMR (125 MHz, $CDCl_3$) δ_C 166.82, 135.82, 132.41, 128.76, 128.21, 119.08, 113.64.

5.2.1.4.3 4-Nitrobenzohydrazide (S_{IV}12c)

Pale yellow solid (0.889 g, 4.908 mmol, 82%); mp 212–214 °C; TLC (hexane:EtOAc, 50:50 v/v); R_f = 0.19. FT-IR (Alpha ATR, *v* cm^{-1}): 3308 (—NH), 1692 (C=O). ^{1}H NMR (500 MHz, DMSO-d_6) δ_H 10.13 (s, 1H, —NH D_2O exchangeable), 8.30 (d, *J* = 8.9 Hz, 2H), 8.04 (d, *J* = 8.9 Hz, 2H), 4.66 (s, 2H, —NH_2 D_2O exchangeable). ^{13}C NMR (125 MHz, DMSO-d_6) δ_C 163.93, 148.94, 139.04, 130.68, 129.06, 128.47, 123.94, 123.87, 123.59.

5.2.1.4.4 2,4-Difluorobenzohydrazide (S_{IV}12d)

White solid (0.867 g, 5.037 mmol, 80%); mp 138–140 °C; TLC (hexane:EtOAc, 50:50 v/v); R_f = 0.22. FT-IR (Alpha ATR, ν cm^{-1}): 3278 (—NH), 1661 (C=O). ^{1}H NMR (500 MHz, DMSO-d_6) δ_H 9.41 (s, 1H, —NH D_2O exchangeable), 7.83–7.79 (m, 1H), 7.22–7.14 (m, 2H), 4.39 (s, 2H, —NH_2 D_2O exchangeable). ^{13}C NMR (125 MHz, DMSO-d_6) δ_C 166.42 (dd, J_{C-F} = 271.9, 10.8 Hz), 162.82 (d, J_{C-F} = 11.2 Hz), 161.92 (dd, J_{C-F} = 272.6, 10.8 Hz), 132.69 (t, J_{C-F} = 7.8 Hz), 119.28 (dd, J_{C-F} = 27.6, 3.2 Hz), 114.92 (dd, J_{C-F} = 28.2, 3.8 Hz), 105.42 (t, J_{C-F} = 26.9 Hz).

5.2.1.4.5 4-Chlorobenzohydrazide (S_{IV}12e)

White solid (0.923 g, 5.410 mmol, 85%); mp 160–162 °C; TLC (hexane:EtOAc, 50:50 v/v); R_f = 0.21. FT-IR (Alpha ATR, ν cm^{-1}): 3281 (—NH), 1669 (C=O). ^{1}H NMR (500 MHz, DMSO-d_6) δ_H 9.86 (s, 1H, —NH D_2O exchangeable), 7.83 (d, J = 8.4 Hz, 2H), 7.52 (d, J = 8.4 Hz, 2H), 4.52 (s, 2H, —NH_2 D_2O exchangeable). ^{13}C NMR (125 MHz, DMSO-d_6) δ_C 165.25, 136.33, 132.51, 129.32, 128.87.

5.2.1.4.6 2,4-Dichlorobenzohydrazide (S_{IV}12f)

White solid (0.899 g, 4.385 mmol, 84%); mp 204–206 °C; TLC (hexane:EtOAc, 50:50 v/v); R_f = 24. FT-IR (Alpha ATR, ν cm^{-1}): 3287 (—NH), 1677 (C=O). ^{1}H NMR (500 MHz, DMSO-d_6) δ_H 9.62 (s, 1H, —NH D_2O exchangeable), 7.68 (d, J = 1.9 Hz, 1H), 7.48 (dd, J = 8.2, 2.0 Hz, 1H), 7.41 (d, J = 8.2 Hz, 1H), 4.52 (s, 2H, —NH_2 D_2O exchangeable). ^{13}C NMR (125 MHz, DMSO-d_6) δ_C 165.23, 135.10, 134.98, 132.07, 130.99, 130.12, 129.64, 127.74.

5.2.1.4.7 4-(Trifluoromethyl)benzohydrazide (S_{IV}12g)

White solid (0.886 g, 4.340 mmol, 83%); mp 122–124 °C; TLC (hexane:EtOAc, 50:50 v/v); R_f = 0.23. FT-IR (Alpha ATR, ν cm^{-1}): 3298 (—NH), 1668 (C=O). ^{1}H NMR (500 MHz, $CDCl_3$) δ_H 7.96 (s, 1H, —NH D_2O exchangeable), 7.89 (d, J = 8.1 Hz, 2H), 7.71

(d, *J* = 8.1 Hz, 2H), 3.97 (s, 2H, —NH_2 D_2O exchangeable). ^{13}C NMR (125 MHz, $CDCl_3$) δ_C 167.41, 135.86, 133.64 (q, *J* = 32.8 Hz), 127.43, 125.78 (q, *J* = 3.6 Hz), 123.55 (q, *J* = 272.6 Hz).

5.2.1.4.8 4-(Trifluoromethoxy)benzohydrazide (S_{IV}12h)

White solid (0.934 g, 4.243 mmol, 87%); mp 116–118 °C; TLC (hexane:EtOAc, 50:50 v/v); R_f = 0.23. FT-IR (Alpha ATR, *v* cm^{-1}): 3296 (—NH), 1678 (C=O). ^1H NMR (500 MHz, $CDCl_3$) δ_H 8.38 (s, 1H, —NH D_2O exchangeable), 7.88 (d, *J* = 8.4 Hz, 2H), 7.79 (d, *J* = 8.4 Hz, 2H), 4.22 (s, 2H, —NH_2 D_2O exchangeable). ^{13}C NMR (125 MHz, $CDCl_3$) δ_C 167.41, 148.68, 131.82, 128.71, 126.94, 122.18 (q, J_{C-F} = 268.2 Hz).

5.2.1.4.9 2-(Chloromethyl)-5-phenyl-1,3,4-oxadiazole (S_{IV}13a)

White solid (0.568 g, 2.919 mmol, 79%); mp 119–121 °C; TLC (DCM:MeOH 90:10 v/v); R_f = 0.82. FT-IR (Alpha ATR, *v* cm^{-1}): 1614 (C=N). ^1H NMR (500 MHz, $CDCl_3$) δ_H 8.15 (dd, *J* = 7.6, 1.3 Hz, 2H), 7.58–7.54 (m, 3H), 4.15 (s, 2H). ^{13}C NMR (125 MHz, $CDCl_3$) δ_C 164.66, 163.98 131.92, 129.16, 127.03, 123.71, 31.63.

5.2.1.4.10 4-(5-(Chloromethyl)-1,3,4-oxadiazol-2-yl)benzonitrile (S_{IV}13b)

Brown solid (0.592 g, 2.695 mmol, 87%); mp 125–127 °C; TLC (DCM:MeOH 90:10 v/v); R_f = 0.78. FT-IR (Alpha ATR, *v* cm^{-1}): 1622 (C=N). ^1H NMR (500 MHz, $CDCl_3$) δ_H 7.98 (d, *J* = 7.4 Hz, 2H), 7.68 (d, *J* = 7.4 Hz, 2H), 4.32 (s, 2H). ^{13}C NMR (125 MHz, $CDCl_3$) δ_C 164.38, 163.19, 134.91, 133.46, 129.94, 128.52, 118.86, 112.64, 32.25.

5.2.1.4.11 2-(Chloromethyl)-5-(4-nitrophenyl)-1,3,4-oxadiazole (S_{IV}13c)

Pale yellow solid (0.586 g, 2.446 mmol, 89%); mp 117–119 °C; TLC (DCM:MeOH 90:10 v/v); R_f = 0.81. FT-IR (Alpha ATR, *v* cm^{-1}): 1609 (C=N). ^1H NMR (500 MHz, DMSO-d_6) δ_H 8.26 (d, *J* = 9.2 Hz, 2H), 7.82 (d, *J* = 9.4 Hz, 2H), 4.28 (s, 2H). ^{13}C NMR (125 MHz, DMSO-d_6) δ_C 164.28, 162.19, 148.69, 138.94, 131.04, 129.19, 128.57, 123.64, 123.21, 123.02, 33.07.

5.2.1.4.12 2-(Chloromethyl)-5-(2,4-difluorophenyl)-1,3,4-oxadiazole (S_{IV}13d)

White solid (0.541 g, 2.346 mmol, 81%); mp 98–100 °C; TLC (DCM:MeOH 90:10 v/v); R_f = 0.81. FT-IR (Alpha ATR, ν cm^{-1}): 1612 (C=N). ^{1}H NMR (500 MHz, DMSO-d_6) δ_H 7.83–7.79 (m, 1H), 7.22–7.14 (m, 2H), 4.17 (s, 2H). ^{13}C NMR (125 MHz, DMSO-d_6) δ_C 164.98 (dd, J_{C-F} = 268.9, 9.2 Hz), 163.42 (dd, J_{C-F} = 268.8, 9.2 Hz), 162.61, 161.22 (d, J_{C-F} = 9.2 Hz), 133.22 (t, J_{C-F} = 8.1 Hz), 119.22 (dd, J_{C-F} = 28.2, 2.8 Hz), 113.61 (dd, J_{C-F} = 27.9, 3.2 Hz), 106.31 (t, J_{C-F} = 28.2 Hz), 33.24.

5.2.1.4.13 2-(Chloromethyl)-5-(4-chlorophenyl)-1,3,4-oxadiazole (S_{IV}13e)

White solid (0.588 g, 2.567 mmol, 88%); mp 83–85 °C; TLC (DCM:MeOH 90:10 v/v); R_f = 0.82. FT-IR (Alpha ATR, ν cm^{-1}): 1621 (C=N). ^{1}H NMR (500 MHz, $CDCl_3$) δ_H 8.01 (d, J = 8.6 Hz, 2H), 7.50 (d, J = 8.6 Hz, 2H), 4.77 (s, 2H). ^{13}C NMR (125 MHz, $CDCl_3$) δ_C 165.44, 162.51, 138.80, 129.79, 128.59, 121.96, 33.16.

5.2.1.4.14 2-(Chloromethyl)-5-(2,4-dichlorophenyl)-1,3,4-oxadiazole (S_{IV}13f)

White solid (0.549 g, 2.083 mmol, 85%); mp 112–113 °C; TLC (DCM:MeOH 90:10 v/v); R_f = 0.88. FT-IR (Alpha ATR, ν cm^{-1}): 1625 (C=N). ^{1}H NMR (500 MHz, DMSO-d_6) δ_H 8.01 (d, J = 8.5 Hz, 1H), 7.95 (d, J = 2.1 Hz, 1H), 7.69 (dd, J = 8.5, 2.1 Hz, 1H), 5.17 (s, 2H). ^{13}C NMR (125 MHz, DMSO-d_6) δ_C 163.88, 162.96, 138.01, 133.48, 133.03, 131.30, 128.80, 121.61, 33.56.

5.2.1.4.15 2-(Chloromethyl)-5-(4-(trifluoromethyl)phenyl)-1,3,4-oxadiazole (S_{IV}13g)

White solid (0.591 g, 2.250 mmol, 92%); mp 206–208 °C; TLC (DCM:MeOH 90:10 v/v); R_f = 0.85. FT-IR (Alpha ATR, ν cm^{-1}): 1602 (C=N). ^{1}H NMR (500 MHz, DMSO-d_6) δ_H 8.23 (d, J = 8.1 Hz, 2H), 7.99 (d, J = 8.3 Hz, 2H), 5.18 (s, 2H). ^{13}C NMR (125 MHz, DMSO-d_6) δ_C 163.95, 163.53, 131.90 (q, J = 32.1 Hz), 126.67, 126.53 (q, J = 3.7 Hz), 123.68 (q, J = 272.5 Hz), 33.18.

5.2.1.4.16 2-(Chloromethyl)-5-(4-(trifluoromethoxy)phenyl)-1,3,4-oxadiazole (S_{IV}13h)

White solid (0.518 g, 1.859 mmol, 82%); mp 94–96 °C; TLC (DCM:MeOH 90:10 v/v); R_f = 0.84. FT-IR (Alpha ATR, ν cm^{-1}): 1598 (C=N). ^{1}H NMR (500 MHz, DMSO-d_6) δ_H 8.26 (d, J = 9.2 Hz, 2H), 7.92 (d, J = 9.4 Hz, 2H), 5.12 (s, 2H). ^{13}C NMR (125 MHz, DMSO-d_6) δ_C 164.68, 164.02, 150.82, 132.04, 129.62, 126.84, 121.97 (q, J_{C-F} = 268.2 Hz), 32.98.

5.2.1.4.17 1-Benzyl-N-((5-phenyl-1,3,4-oxadiazol-2-yl)methyl)piperidin-4-amine (S_{IV}14a)

White solid (0.591 g, 1.696 mmol, 66%); mp 104–106 °C; TLC (DCM:MeOH 90:10 v/v); R_f = 0.42. FT-IR (Alpha ATR, ν cm^{-1}): 3262 (—NH), 1602 (C=N). ^{1}H NMR (500 MHz, $CDCl_3$) δ_H 8.08–8.06 (m, 2H), 7.57–7.51 (m, 3H), 7.33–7.26 (m, 5H), 4.15 (s, 2H), 3.51 (s, 2H), 2.87 (d, J = 11.7 Hz, 2H), 2.61 (ddd, J = 14.1, 10.1, 3.8 Hz, 1H), 2.05 (t, J = 11.0 Hz, 2H), 1.90 (d, J = 12.3 Hz, 2H), 1.85 (s, 1H, —NH D_2O exchangeable), 1.52–1.44 (m, 2H). ^{13}C NMR (125 MHz, $CDCl_3$) δ_C 165.52, 165.11, 138.35, 131.77, 129.14, 129.06, 128.21, 127.01, 126.93, 123.82, 63.02, 54.11, 52.05, 40.97, 32.34. ESI-MS (*m/z*): 349.40 $[M + H]^+$. HPLC purity: 99.9%, retention time: 3.21 min.

5.2.1.4.18 4-(5-(((1-Benzylpiperidin-4-yl)amino)methyl)-1,3,4-oxadiazol-2-yl)benzonitrile (S_{IV}14b)

Beige solid (0.608 g, 1.628 mmol, 72%); mp 118–120 °C; TLC (DCM:MeOH 90:10 v/v); R_f = 0.48. FT-IR (Alpha ATR, ν cm^{-1}): 3248 (—NH), 1612 (C=N). ^{1}H NMR (500 MHz, $CDCl_3$) δ_H 7.86 (d, J = 7.8 Hz, 2H), 7.62 (d, J = 7.8 Hz, 2H), 7.32–7.25 (m, 5H), 4.23 (s, 2H), 3.56 (s, 2H), 2.89 (d, J = 11.2 Hz, 2H), 2.71–2.68 (m, 1H), 2.06 (t, J = 9.8 Hz, 2H), 1.88 (d, J = 9.2 Hz, 2H), 1.85 (s, 1H, —NH D_2O exchangeable), 1.54–1.44 (m, 2H). ^{13}C NMR (125 MHz, $CDCl_3$) δ_C 166.41, 165.32, 139.02, 131.64, 131.01, 129.22, 129.01, 128.64, 127.81, 127.08, 126.94, 126.09, 123.18, 119.03, 113.11, 63.01, 54.81,

52.19, 40.99, 32.26. ESI-MS (*m/z*): 374.67 $[M + H]^+$. HPLC purity: 99.5%, retention time: 3.32 min.

5.2.1.4.19 1-Benzyl-N-((5-(4-nitrophenyl)-1,3,4-oxadiazol-2-yl)methyl)piperidin-4-amine (S_{IV}14c)

Yellow solid (0.613 g, 1.558 mmol, 75%); mp 88–90 °C; TLC (DCM:MeOH 90:10 v/v); R_f = 0.36. FT-IR (Alpha ATR, *v* cm^{-1}): 3260 (—NH), 1628 (C=N). ^1H NMR (500 MHz, $CDCl_3$) δ_H 8.42 (d, *J* = 8.8 Hz, 2H), 7.96 (d, *J* = 8.8 Hz, 2H), 7.42–7.37 (m, 5H), 4.18 (s, 2H), 3.60 (s, 2H), 2.86 (d, *J* = 10.6 Hz, 2H), 2.66–2.63 (m, 1H), 2.02 (t, *J* = 9.6 Hz, 2H), 1.82 (d, *J* = 10.2 Hz, 2H), 1.88 (s, 1H, —NH D_2O exchangeable), 1.59–1.53 (m, 2H). ^{13}C NMR (125 MHz, $CDCl_3$) δ_C 165.98, 164.64, 149.01, 138.94, 132.08, 131.92, 129.56, 129.01, 128.72, 127.98, 126.12, 125.64, 125.04, 123.62, 62.82, 53.96, 52.01, 40.86, 32.19. ESI-MS (*m/z*): 394.56 $[M + H]^+$. HPLC purity: 99.1%, retention time: 2.87 min.

5.2.1.4.20 1-Benzyl-N-((5-(2,4-difluorophenyl)-1,3,4-oxadiazol-2-yl)methyl)piperidin-4-amine (S_{IV}14d)

Pale yellow solid (0.628 g, 1.634 mmol, 75%); mp 68–70 °C; TLC (DCM:MeOH 90:10 v/v); R_f = 0.51. FT-IR (Alpha ATR, *v* cm^{-1}): 3258 (—NH), 1610 (C=N). ^1H NMR (500 MHz, $CDCl_3$) δ_H 7.89–7.82 (m, 1H), 7.68–7.62 (m, 2H), 7.36–7.24 (m, 5H), 4.14 (s, 2H), 3.58 (s, 2H), 2.84 (d, *J* = 10.8 Hz, 2H), 2.61–2.56 (m, 1H), 2.09 (t, *J* = 9.8 Hz, 2H), 1.85 (d, *J* = 8.6 Hz, 2H), 1.84 (s, 1H, —NH D_2O exchangeable), 1.63–1.58 (m, 2H). ^{13}C NMR (125 MHz, $CDCl_3$) δ_C 166.84, 164.89 (dd, J_{C-F} = 258.6, 10.8 Hz), 162.12 (dd, J_{C-F} = 256.9, 11.2 Hz), 158.43 (d, J_{C-F} = 11.6 Hz), 139.06, 133.14 (t, J_{C-F} = 8.1 Hz), 129.11, 127.27, 125.08, 117.61 (dd, J_{C-F} = 29.4, 3.2 Hz), 114.12 (dd, J_{C-F} = 28.9, 3.2 Hz), 105.61 (t, J_{C-F} = 29.3 Hz), 63.08, 54.09, 52.61, 40.79, 32.11. ESI-MS (*m/z*): 385.31 $[M + H]^+$. HPLC purity: 99.6%, retention time: 3.57 min.

5.2.1.4.21 1-Benzyl-N-((5-(4-chlorophenyl)-1,3,4-oxadiazol-2-yl)methyl)piperidin-4-amine (S_{IV}14e)

Brown solid (0.579 g, 1.512 mmol, 69%); mp 74–76 °C; TLC (DCM:MeOH 90:10 v/v); R_f = 0.55. FT-IR (Alpha ATR, ν cm^{-1}): 3264 (—NH), 1608 (C=N). ^{1}H NMR (500 MHz, $CDCl_3$) δ_H 7.82 (d, *J* = 9.2 Hz, 2H), 7.46 (d, *J* = 9.2 Hz, 2H), 7.32–7.21 (m, 5H), 4.08 (s, 2H), 3.66 (s, 2H), 2.81 (d, *J* = 9.6 Hz, 2H), 2.69–2.63 (m, 1H), 2.13 (t, *J* = 10.2 Hz, 2H), 1.87 (d, *J* = 9.1 Hz, 2H), 1.81 (s, 1H, —NH D_2O exchangeable), 1.59–1.51 (m, 2H). ^{13}C NMR (125 MHz, $CDCl_3$) δ_C 166.84, 163.69, 139.08, 138.71, 132.64, 129.92, 129.14, 128.52, 127.64, 127.01, 125.29, 63.22, 54.24, 52.19, 40.61, 32.29. ESI-MS (*m/z*): 383.40 $[M + H]^+$. HPLC purity: 98.4%, retention time: 3.65 min.

5.2.1.4.22 1-Benzyl-N-((5-(2,4-dichlorophenyl)-1,3,4-oxadiazol-2-yl)methyl)piperidin-4-amine (S_{IV}14f)

Brown solid (0.643 g, 1.541 mmol, 81%); mp 108–110 °C; TLC (DCM:MeOH 90:10 v/v); R_f = 0.64. FT-IR (Alpha ATR, ν cm^{-1}): 3278 (—NH), 1619 (C=N). ^{1}H NMR (500 MHz, $CDCl_3$) δ_H 7.98 (d, *J* = 8.5 Hz, 1H), 7.91 (d, *J* = 2.0 Hz, 1H), 7.67 (dd, *J* = 8.5, 2.0 Hz, 1H), 7.33–7.21 (m, 5H), 4.01 (s, 2H), 3.42 (s, 2H), 2.72 (d, *J* = 11.0 Hz, 2H), 2.58–2.50 (m, 1H), 1.93 (t, *J* = 10.2 Hz, 2H), 1.81 (s, 1H, —NH D_2O exchangeable), 1.76 (d, *J* = 11.5 Hz, 2H), 1.31–1.24 (m, 2H). ^{13}C NMR (125 MHz, $CDCl_3$) δ_C 167.21, 161.98, 140.69, 137.53, 133.28, 132.83, 129.27, 128.69, 128.60, 127.35, 123.63, 123.18, 62.55, 53.90, 52.05, 40.59, 31.99. ESI-MS (*m/z*): 417.52 $[M + H]^+$. HPLC purity: 95.2%, retention time: 6.27 min.

5.2.1.4.23 1-Benzyl-N-((5-(4-(trifluoromethyl)phenyl)-1,3,4-oxadiazol-2-yl)methyl)piperidin-4-amine (S_{IV}14g)

White solid (0.631 g, 1.515 mmol, 80%); mp 126–128 °C; TLC (DCM:MeOH 90:10 v/v); R_f = 0.62. FT-IR (Alpha ATR, ν cm^{-1}): 3242 (—NH), 1624 (C=N). ^{1}H NMR (500

MHz, $CDCl_3$) δ_H 7.96 (d, *J* = 9.2 Hz, 2H), 7.89 (d, *J* = 9.2 Hz, 2H), 7.53–7.37 (m, 5H), 4.18 (s, 2H), 3.95 (s, 2H), 2.88 (d, *J* = 8.9 Hz, 2H), 2.52–2.48 (m, 1H), 2.08 (t, *J* = 10.2 Hz, 2H), 1.92 (s, 1H, —NH D_2O exchangeable), 1.71 (d, *J* = 10.6 Hz, 2H), 1.42–1.37 (m, 2H). ^{13}C NMR (125 MHz, $CDCl_3$) δ_C 168.27, 164.86, 139.87, 133.64, 132.19 (q, *J* = 8.2 Hz), 131.64 (q, *J* = 28.8 Hz), 126.91, 126.78 (q, *J* = 4.2 Hz), 123.41 (q, *J* = 268.6 Hz), 63.04, 53.64, 52.08, 40.12, 32.14. ESI-MS (*m/z*): 417.36 $[M + H]^+$. HPLC purity: 97.8%, retention time: 4.49 min.

5.2.1.4.24 1-Benzyl-N-((5-(4-(trifluoromethoxy)phenyl)-1,3,4-oxadiazol-2-yl)methyl)piperidin-4-amine (S_{IV}14h)

Pale yellow solid (0.609 g, 1.408 mmol, 78%); mp 79–81 °C; TLC (DCM:MeOH 90:10 v/v); R_f = 0.69. FT-IR (Alpha ATR, *v* cm^{-1}): 3292 (—NH), 1600 (C=N). ^1H NMR (500 MHz, $CDCl_3$) δ_H 7.99 (d, *J* = 8.6 Hz, 2H), 7.81 (d, *J* = 8.6 Hz, 2H), 7.39–7.21 (m, 5H), 4.10 (s, 2H), 3.89 (s, 2H), 2.77 (d, *J* = 8.2 Hz, 2H), 2.49–2.46 (m, 1H), 2.13 (t, *J* = 9.2 Hz, 2H), 1.84 (s, 1H, —NH D_2O exchangeable), 1.69 (d, *J* = 11.2 Hz, 2H), 1.58–1.49 (m, 2H). ^{13}C NMR (125 MHz, $CDCl_3$) δ_C 168.13, 163.49, 150.64, 138.69, 132.18, 131.69, 129.62, 127.62, 126.84, 125.98, 121.97 (q, J_{C-F} = 258.9 Hz), 63.17, 53.19, 52.01, 40.64, 32.24. ESI-MS (*m/z*): 433.28 $[M + H]^+$. HPLC purity: 99.2%, retention time: 5. 90 min.

5.2.1.5 Synthesis of Series V (S_V17a–h): N-Benzylpiperidine and substituted 5-phenyl-1,3,4-oxadiazoles tethered without linker

The synthetic route for compounds **S_V17a–h** (directly linked molecular hybrids of *N*-benzylpiperidine and substituted 5-phenyl-1,3,4-oxadiazoles) is mentioned in Scheme 4-Experimental Section. As shown, compounds **S_{IV}12a–h** (from Scheme 2) and *N*-benzylpiperidine-4-carboxaldehyde (**S_V15**) were heated at reflux in EtOH under the acidic condition to yield corresponding imines (**S_V16a–h**), which were subsequently

reacted with chloramine T to obtain target compounds **S_V17a–h** in appreciable yields (65–75%). FT-IR spectra showed characteristic stretching bands at 3029–2988 cm_{-1} and 1627–1609 cm^{-1} for C—H and C=N groups, respectively. 13C NMR spectra displayed signals of oxadiazole ring carbons at δ_C = 169.44–168.62 ppm and 164.92–163.54 ppm to confirm the formation of compounds **S_V17a–h.**

5.2.1.6 Characterization of the synthesized compounds (Series V)

5.2.1.6.1 2-(1-Benzylpiperidin-4-yl)-5-phenyl-1,3,4-oxadiazole (S_V17a)

White solid (0.768 g, 2.404 mmol, 65%); mp 121–123 °C; TLC (DCM:MeOH 90:10 v/v); R_f = 0.56. FT-IR (Alpha ATR, *v* cm^{-1}): 3019 (CH), 1621 (C=N). ^{1}H NMR (500 MHz, $CDCl_3$) δ_H 8.05 (dd, *J* = 8.0, 1.6 Hz, 2H), 7.55–7.50 (m, 3H), 7.38–7.28 (m, 5H), 3.58 (s, 2H), 3.06–3.02 (m, 1H), 3.00 (d, *J* = 11.6 Hz, 2H), 2.20 (t, *J* = 10.9 Hz, 2H), 2.13 (d, *J* = 10.6 Hz, 2H), 2.08–2.00 (m, 2H). ^{13}C NMR (125 MHz, $CDCl_3$) δ_C 169.10, 164.63, 131.56, 129.16, 129.02, 128.30, 127.15, 126.80, 124.08, 63.26, 52.75, 33.51, 29.72, 29.45. ESI-MS (*m/z*): 320.30 $[M + H]^+$. HPLC purity: 97.8%, retention time: 3.84 min.

5.2.1.6.2 4-(5-(1-Benzylpiperidin-4-yl)-1,3,4-oxadiazol-2-yl)benzonitrile (S_V17b)

Beige solid (0.719 g, 2.088 mmol, 67%); mp 152–154 °C; TLC (DCM:MeOH 90:10 v/v); R_f = 0.61. FT-IR (Alpha ATR, *v* cm^{-1}): 3027 (CH), 1627 (C=N). ^{1}H NMR (500 MHz, $CDCl_3$) δ_H 7.92 (d, *J* = 8.2 Hz, 2H), 7.58 (d, *J* = 8.2 Hz, 2H), 7.38–7.30 (m, 5H), 3.57 (s, 2H), 3.08–3.00 (m, 1H), 2.88 (d, *J* = 11.6 Hz, 2H), 2.19 (t, *J* = 10.9 Hz, 2H), 2.09 (d, *J* = 10.6 Hz, 2H), 2.03–1.96 (m, 2H). ^{13}C NMR (125 MHz, $CDCl_3$) δ_C 168.62, 164.91, 139.19, 131.92, 131.09, 129.04, 128.19, 127.64, 127.00, 126.58, 126.01, 119.16, 113.19, 63.28, 52.69, 33.54, 29.69, 29.44. ESI-MS (*m/z*): 345.58 $[M + H]^+$. HPLC purity: 96.1%, retention time: 4.00 min.

5.2.1.6.3 2-(1-Benzylpiperidin-4-yl)-5-(4-nitrophenyl)-1,3,4-oxadiazole (S_V17c)

Yellow solid (0.678 g, 1.861 mmol, 67%); mp 161–163 °C; TLC (DCM:MeOH 90:10 v/v); R_f = 0.51. FT-IR (Alpha ATR, ν cm^{-1}): 2988 (CH), 1609 (C=N). ^{1}H NMR (500 MHz, $CDCl_3$) δ_H 8.38 (d, *J* = 9.2 Hz, 2H), 8.09 (d, *J* = 9.2 Hz, 2H), 7.38–7.29 (m, 5H), 3.54 (s, 2H), 3.14–3.08 (m, 1H), 2.94 (d, *J* = 11.6 Hz, 2H), 2.24 (t, *J* = 10.9 Hz, 2H), 2.13 (d, *J* = 10.6 Hz, 2H), 2.08–2.00 (m, 2H). ^{13}C NMR (125 MHz, $CDCl_3$) δ_C 169.04, 164.92, 149.19, 138.99, 132.18, 131.64, 129.19, 129.00, 128.67, 127.11, 126.27, 125.54, 125.01, 123.58, 63.29, 52.73, 33.53, 29.68, 29.42. ESI-MS (*m/z*): 365.29 $[M + H]^+$. HPLC purity: 99.9%, retention time: 3.09 min.

5.2.1.6.4 2-(1-Benzylpiperidin-4-yl)-5-(2,4-difluorophenyl)-1,3,4-oxadiazole (S_V17d)

Pale yellow solid (0.779 g, 2.192 mmol, 75%); mp 106–108 °C; TLC (DCM:MeOH 90:10 v/v); R_f = 0.64. FT-IR (Alpha ATR, ν cm^{-1}): 3016 (CH), 1622 (C=N). ^{1}H NMR (500 MHz, $CDCl_3$) δ_H 7.85–7.79 (m, 1H), 7.64–7.56 (m, 2H), 7.39–7.28 (m, 5H), 3.59 (s, 2H), 3.16–3.13 (m, 1H), 2.89 (d, *J* = 10.8 Hz, 2H), 2.25 (t, *J* = 8.6 Hz, 2H), 2.11 (d, *J* = 9.6 Hz, 2H), 2.10–2.03 (m, 2H). ^{13}C NMR (125 MHz, $CDCl_3$) δ_C 168.67, 164.92 (dd, J_{C-F} = 280.8, 9.6 Hz), 163.54 (dd, J_{C-F} = 278.6, 9.6 Hz), 156.81 (d, J_{C-F} = 11.8 Hz), 139.12, 133.57 (t, J_{C-F} = 9.8 Hz), 129.21, 127.84, 125.13, 117.92 (dd, J_{C-F} = 28.7, 2.8 Hz), 113.99 (dd, J_{C-F} = 28.8, 2.9 Hz), 105.55 (t, J_{C-F} = 28.2 Hz), 63.48, 52.91, 33.64, 29.79, 29.64. ESI-MS (*m/z*): 356.42 $[M + H]^+$. HPLC purity: 96.3%, retention time: 4.72 min.

5.2.1.6.5 2-(1-Benzylpiperidin-4-yl)-5-(4-chlorophenyl)-1,3,4-oxadiazole (S_V17e)

White solid (0.745 g, 2.105 mmol, 72%); mp 135–137 °C; TLC (DCM:MeOH 90:10 v/v); R_f = 0.68. FT-IR (Alpha ATR, ν cm^{-1}): 3029 (CH), 1624 (C=N). ^{1}H NMR (500 MHz, $CDCl_3$) δ_H 7.96 (d, *J* = 8.6 Hz, 2H), 7.47 (d, *J* = 8.6 Hz, 2H), 7.34–7.31 (m, 4H), 7.29–7.26 (m, 1H), 3.55 (s, 2H), 3.01–2.96 (m, 3H), 2.17 (t, *J* = 10.9 Hz, 2H), 2.11–2.08

(m, 2H), 2.04–1.97 (m, 2H). ^{13}C NMR (125 MHz, $CDCl_3$) δ_C 169.30, 163.84, 138.14, 137.80, 129.41, 129.13, 128.29, 128.08, 127.14, 122.57, 63.24, 52.73, 33.53, 29.71, 29.48. ESI-MS (*m/z*): 354.67 $[M + H]^+$. HPLC purity: 98.7%, retention time: 5.29 min.

5.2.1.6.6 2-(1-Benzylpiperidin-4-yl)-5-(2,4-dichlorophenyl)-1,3,4-oxadiazole (S_V17f)

White solid (0.641 g, 1.651 mmol, 68%); mp 182–184 °C; TLC (DCM:MeOH 90:10 v/v); R_f = 0.79. FT-IR (Alpha ATR, ν cm^{-1}): 3022 (CH), 1619 (C=N). ^{1}H NMR (500 MHz, $CDCl_3$) δ_H 8.06 (d, *J* = 9.8 Hz, 1H), 7.94 (d, *J* = 1.8 Hz, 1H), 7.72 (dd, *J* = 9.2, 2.2 Hz, 1H), 7.36–7.25 (m, 5H), 3.59 (s, 2H), 3.09–3.02 (m, 3H), 2.24 (t, *J* = 9.8 Hz, 2H), 2.18–2.14 (m, 2H), 2.11–2.04 (m, 2H). ^{13}C NMR (125 MHz, $CDCl_3$) δ_C 169.02, 163.54, 139.68, 137.12, 133.54, 132.51, 129.67, 128.12, 128.01, 127.64, 123.51, 123.01, 63.00, 52.51, 33.41, 29.08, 28.94. ESI-MS (*m/z*): 388.46 $[M + H]^+$. HPLC purity: 98.1%, retention time: 7.49 min.

5.2.1.6.7 2-(1-Benzylpiperidin-4-yl)-5-(4-(trifluoromethyl)phenyl)-1,3,4-oxadiazole (S_V17g)

White solid (0.622 g, 1.606 mmol, 66%); mp 125–127 °C; TLC (DCM:MeOH 90:10 v/v); R_f = 0.69. FT-IR (Alpha ATR, ν cm^{-1}): 3002 (CH), 1612 (C=N). ^{1}H NMR (500 MHz, $CDCl_3$) δ_H 8.17 (d, *J* = 8.9 Hz, 2H), 7.92 (d, *J* = 8.9 Hz, 2H), 7.38–7.30 (m, 5H), 3.53 (s, 2H), 3.14–3.08 (m, 3H), 2.29 (t, *J* = 9.8 Hz, 2H), 2.22–2.18 (m, 2H), 2.15–2.09 (m, 2H). ^{13}C NMR (125 MHz, $CDCl_3$) δ_C 168.98, 163.57, 139.57, 133.29, 132.54 (q, *J* = 7.8 Hz), 131.48 (q, *J* = 29.0 Hz), 126.54, 126.02 (q, *J* = 2.9 Hz), 122.94 (q, *J* = 282.1 Hz), 62.97, 52.72, 32.55, 28.69, 28.47. ESI-MS (*m/z*): 388.39 $[M + H]^+$. HPLC purity: 98.9%, retention time: 5.23 min.

5.2.1.6.8 2-(1-Benzylpiperidin-4-yl)-5-(4-(trifluoromethoxy)phenyl)-1,3,4-oxadiazole (S_V17h)

Pale yellow solid (0.610 g, 1.512 mmol, 67%); mp 118–120 °C; TLC (DCM:MeOH 90:10 v/v); R_f = 0.78. FT-IR (Alpha ATR, *v* cm^{-1}): 3017 (CH), 1618 (C=N). ^{1}H NMR (500 MHz, $CDCl_3$) δ_H 8.28 (d, *J* = 9.2 Hz, 2H), 8.01 (d, *J* = 9.2 Hz, 2H), 7.36–7.25 (m, 5H), 3.69 (s, 2H), 3.24–3.17 (m, 3H), 2.28 (t, *J* = 8.8 Hz, 2H), 2.18–2.11 (m, 2H), 2.06–1.99 (m, 2H). ^{13}C NMR (125 MHz, $CDCl_3$) δ_C 169.44, 163.97, 150.48, 137.99, 132.44, 131.82, 129.54, 127.49, 126.61, 125.99, 121.61 (q, J_{C-F} = 282.6 Hz), 63.14, 53.19, 33.00, 28.89, 28.64. ESI-MS (*m/z*): 404.39 $[M + H]^+$. HPLC purity: 97.1%, retention time: 7.65 min.

5.2.2 Biological evaluation

5.2.2.1 In vitro studies

5.2.2.1.1 Cholinesterase (AChE and BChE) inhibition by Ellman assay

The target compounds from Series II-V (**S_{II}9a–h, S_{III}10a–h, S_{IV}14a–h and S_V17a–h)** were designed to investigate the inhibitory potential, selectivity profile, and preliminary SAR studies against hAChE (from human erythrocytes) and hBChE (from human serum). Donepezil and rivastigmine were used as positive reference standards. The results of enzyme assays are summarized in Table 5.5.

The *N*-benzylpiperidine was retained as a core nucleus, as studies suggested that modification of the benzyl ring leads to a significant reduction in ChE inhibition activity [Costanzo et al. 2016, Kryger et al. 1999]. The SAR studies were envisaged by modifications of the X-spacer and substitution of variable EWGs at the terminal phenyl group. The majority of compounds from Series II (**S_{II}9a–h**) exhibited lower inhibitory activity against hAChE in the micromolar range. Among compounds from Series II, **S_{II}9h** with strong EWG and 4–OCF_3 showed maximum hAChE inhibitory potential

(IC_{50}: 1.05 µM). The concomitant modification of open-chain methylene hydrazide with the cyclic oxadiazole nucleus increased the ChE inhibitory potential to several fold in compounds from Series III, IV, and V. Among the Series III (**S_{III}10a–h),** compounds with an —NH linker presented optimum inhibitory potency compared to compounds with an —$NHCH_2$ linker (Series IV, **S_{IV}14a–h**) and directly linked congeners (Series V, **S_V17a–h**). So, the order of hAChE inhibitory potency was observed as —NH (Series III) > —$NHCH_2$ (Series IV) > directly linked (Series V), with the exception being **S_V17e** (IC_{50}: 0.098 µM), which showed better hAChE inhibitory activity than their respective counterparts (IC_{50}, **S_{III}10e**: 0.828 µM; and **S_{IV}14e**: 1.64 µM). The spacer group (—NH) and oxadiazole hybrids might have formed additional π-cation interactions with PAS-hAChE to increase the anti-hAChE activity. Also, the —NH spacer may be responsible for providing optimum conformational flexibility to the terminal phenyl group and *N*-benzylpiperidine nucleus for their effective interactions with the PAS and CAS residues of AChE, respectively.

To optimize the interaction of compounds with PAS-hAChE, variable EWGs were substituted at the terminal phenyl region. Among all the tested compounds, the unsubstituted derivatives showed moderately poor hAChE inhibitory potential in the micromolar range (IC_{50}, **S_{II}9a**: > 5 µM; **S_{III}10a**: 1.32 µM; **S_{IV}14a**: 1.70 µM; **S_V17a**: > 5 µM). The introduction of EWGs drastically increased the hAChE inhibitory potency several fold. Among the Series III (**S_{III}10a–h)** and **IV** (**S_{IV}14a–h**), substitution with 4–CN (IC_{50}, **S_{III}10b**: 0.783 µM; **S_{IV}14b**: 1.050 µM) and 4–Cl (IC_{50}, **S_{III}10e**: 0.828 µM; **S_{IV}14e**: 1.640 µM) groups resulted in moderately active compounds with inhibitory potential in the micromolar to submicromolar range. The substitution with 4-NO_2, a strong EWG, has proven to produce a slightly more potent hAChE inhibitor (IC_{50}, **S_{III}10c**: 0.149 µM; **S_{IV}14c**: 0.222 µM). Interestingly, disubstitution at positions 2 and 4

with —Cl functionality showed remarkable hAChE inhibitory activity in two-digit nanomolar concentration range (IC_{50}, **S_{III}10f**: 0.075 µM; **S_{IV}14f**: 0.086 µM) and exhibited 10–20 fold higher activity compared to their monosubstituted counterparts **S_{III}10e** and **S_{IV}14e**, respectively. Further, substitution with highly lipophilic and strong EWGs, 4–CF_3 (IC_{50}, **S_{III}10g**: 0.055 µM; **S_{IV}14g**: 0.144 µM) and 4–OCF_3 (IC_{50}, **S_{III}10h**: 0.096 µM; **S_{IV}14h**: 0.119 µM) produced an excellent inhibitor of hAChE. The presence of halogen functional groups (F, Cl, CF_3, and OCF_3) was demonstrated to be indispensable for hAChE inhibitory activity.

Compounds from Series V (**S_V17a–h**) with directly linked 5-phenyl-1,3,4-oxadiazoles and *N*-benzylpiperidine hybrids also showed moderate hAChE inhibition. The disubstitution was found to be unfavorable in Series V compared to Series III and IV with 2,4–diF (IC_{50}, **S_V17d**: 3.49 µM) and 2,4–diCl (IC_{50}, **S_V17f**: 3.26 µM) functionalities exhibited poor anti-hAChE activity. The substitution at the para position with 4–NO_2 (IC_{50}, **S_V17c**: 0.235 µM), 4–CF_3 (IC_{50}, **S_V17g**: 0.207 µM), and 4–OCF_3 (IC_{50}, **S_V17h**: 0.162 µM) groups enhanced the hAChE inhibitory activity up to a three-digit nanomolar concentration. Compound **S_V17e** bearing a 4–Cl substitution was a most pronounced inhibitor of Series V with IC_{50} = 0.098 µM. Overall, **S_{III}10f**, **S_{III}10g**, **S_{III}10h**, **S_{IV}14f**, and **S_V17e** were found to be the potent hAChE inhibitors with two-digit nanomolar IC_{50} values comparable to that of donepezil (IC_{50}: 0.046 µM). These compounds also complement our design concept with the IC_{50} values in two-digit nanomolar concentrations compared to the most potent compound from Series I (IC_{50}, **SI4j:** 0.107 µM).

In addition to the hAChE, clinical evidence has suggested that BChE also plays a significant role in the regulation of ACh and maintaining normal cholinergic functions in AD [Greig et al. 2001, Kumar et al. 2018, Lane et al. 2006]. The activity of BChE

was observed to be elevated during AD [Perry et al. 1978]. Therefore, dual inhibition of AChE and BChE can be considered a potential therapeutic advantage in advanced and late phase AD [Blesa et al. 2006, Bullock and Lane 2007, Kandiah et al. 2017]. All the tested compounds exhibited comparatively lower hBChE inhibition than hAChE except compound **S_V17e**, which has more selectivity toward hBChE. Compounds from Series II (**S_{II}9a–h**) were not found to be active against hBChE (IC_{50} > 10 µM). The order of activity against hBChE was increased by lengthening the chain of the linker, i.e., Series IV > Series III > Series V, which can be ascribed to the larger catalytic gorge of hBChE to occupy the lengthy molecule. Compound **S_V17e** from Series V was an exception, which demonstrated higher hBChE inhibition (IC_{50}: 0.418 µM) as compared to its counterparts from Series III (IC50, **S_{III}10e**: 4.28 µM) and IV (IC50, **S_{IV}14e**: 1.49 µM). Apart from **S_V17e**, compounds with 2,4–diCl, 4–CF_3, and 4–OCF_3 substitutions in Series III (IC50, **S_{III}10f**: 0.336 µM; **S_{III}10g**: 0.186 µM; **S_{III}10h:** 0.796 µM) and Series IV (IC50, **S_{IV}14f**: 0.143 µM; **S_{IV}14g**: 0.220 µM; **S_{IV}14h**: 0.751 µM) were observed to be potent hBChE inhibitors with IC_{50} in the three-digit nanomolar range.

Table 5.5. Cholinesterases (hAChE and hBChE) and hBACE-1 inhibition activity and selectivity index of compounds (Series II-V).

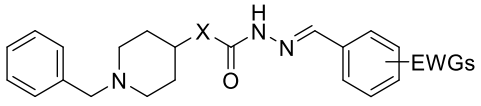

Series II (S_{II}9a-h)

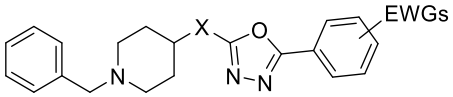

Series III (S_{III}10a-h); Series IV (S_{IV}14a-h); Series V (S_V17a-h)

Comd.	EWG	X-Group	IC_{50} (µM) ± SEM			hAChE SI[a]
			hAChE	hBChE	hBACE-1	
S_{II}9a	-H	NH	>5	>10	nd	--
S_{II}9b	4-CN	NH	>5	>10	nd	--
S_{II}9c	4-NO_2	NH	1.56 ± 0.068	>10	5.07 ± 0.169	--
S_{II}9d	2,4-diF	NH	2.03 ± 0.034	>10	8.10 ± 0.143	--
S_{II}9e	4-Cl	NH	4.20 ± 0.044	>10	>10	--
S_{II}9f	2,4-diCl	NH	2.10 ± 0.085	>10	4.97 ± 0.253	--

S_{II}9g	4-CF_3	NH	1.78 ± 0.062	>10	1.36 ± 0.108	--
S_{II}9h	4-OCF_3	NH	1.05 ± 0.040	>10	1.37 ± 0.080	--
S_{III}10a	-H	NH	1.32 ± 0.029	>10	7.33 ± 0.091	--
S_{III}10b	4-CN	NH	0.783 ± 0.044	>10	6.17 ± 0.105	--
S_{III}10c	4-NO_2	NH	0.149 ± 0.009	1.69 ± 0.078	2.35 ± 0.054	11.3
S_{III}10d	2,4-diF	NH	0.264 ± 0.017	2.68 ± 0.117	3.93 ± 0.046	10.2
S_{III}10e	4-Cl	NH	0.828 ± 0.054	4.28 ± 0.081	4.06 ± 0.213	5.2
S_{III}10f	2,4-diCl	NH	0.075 ± 0.003	0.336 ± 0.018	0.236 ± 0.007	4.5
S_{III}10g	4-CF_3	NH	0.055 ± 0.003	0.186 ± 0.005	0.146 ± 0.012	3.4
S_{III}10h	4-OCF_3	NH	0.096 ± 0.005	0.796 ± 0.036	1.34 ± 0.051	8.3
S_{IV}14a	-H	$NHCH_2$	1.70 ± 0.092	>10	4.92 ± 0.116	--
S_{IV}14b	4-CN	$NHCH_2$	1.05 ± 0.029	>10	1.94 ± 0.111	--
S_{IV}14c	4-NO_2	$NHCH_2$	0.222 ± 0.014	1.00 ± 0.028	1.39 ± 0.066	4.5
S_{IV}14d	2,4-diF	$NHCH_2$	0.356 ± 0.035	1.25 ± 0.059	1.36 ± 0.084	3.5
S_{IV}14e	4-Cl	$NHCH_2$	1.64 ± 0.104	1.49 ± 0.065	0.296 ± 0.006	0.90
S_{IV}14f	2,4-diCl	$NHCH_2$	0.086 ± 0.007	0.143 ± 0.004	0.114 ± 0.004	1.7
S_{IV}14g	4-CF_3	$NHCH_2$	0.144 ± 0.007	0.220 ± 0.003	0.186 ± 0.006	1.5
S_{IV}14h	4-OCF_3	$NHCH_2$	0.119 ± 0.008	0.751 ± 0.012	0.931 ± 0.037	6.3
S_V17a	-H	--*	>5	>10	nd	--
S_V17b	4-CN	--*	1.37 ± 0.125	9.09 ± 0.272	7.51 ± 0.178	6.6
S_V17c	4-NO_2	--*	0.235 ± 0.015	5.71 ± 0.075	7.44 ± 0.197	24.3
S_V17d	2,4-diF	--*	3.49 ± 0.134	7.13 ± 0.099	>10	2.0
S_V17e	4-Cl	--*	0.098 ± 0.005	0.418 ± 0.006	0.690 ± 0.056	4.3
S_V17f	2,4-diCl	--*	3.26 ± 0.059	6.83 ± 0.081	8.87 ± 0.369	2.1
S_V17g	4-CF_3	--*	0.207 ± 0.006	1.20 ± 0.059	1.83 ± 0.100	5.8
S_V17h	4-OCF_3	--*	0.162 ± 0.004	4.23 ± 0.126	5.94 ± 0.148	26.1
	donepezil		0.046 ± 0.003	1.94 ± 0.093	0.220 ± 0.006	42.2
	rivastigmine		2.58 ± 0.032	1.07 ± 0.054	nd	0.41

[a]The assays were performed on hAChE, hBChE, and hBACE-1. Data are expressed as the mean IC_{50} ± SEM of three separate experiments (n = 3); [b]selectivity ratio = IC_{50} of hBChE/hAChE; [*]compounds **S_V17a–h** have directly linked *N*-benzylpiperidine and substituted 5-phenyl-1,3,4-oxadiazoles without X-spacer group; nd = not determined.

5.2.2.1.2 Enzyme kinetics study

To gain insight into the mechanism of inhibition for the most potent inhibitor **S_{III}10g**, enzyme kinetics study was performed against hAChE and hBChE. The type of inhibition was elucidated by a Lineweaver-Burk double reciprocal plot between the initial velocities of the substrate (y-axis) at increasing concentrations (x-axis;

acetylthiocholine iodide, ATCI for hAChE; butyrylthiocholine iodide, BTCI for hBChE). The plots revealed decreased V_{max}, while K_m increased with increasing concentration of **S_{III}10g**, the trend being attributed to the mixed-type of inhibition for hAChE and hBChE (Figures 5.23A and 5.23B). The Dixon plots were constructed between the Lineweaver-Burk slope and the inhibitor concentration (Figures 5.24A and 5.24B). The intersection point at the x-axis of the plot was considered as the dissociation constant K_i for the inhibitor, which was estimated to be 0.026 µM and 0.115 µM for hAChE and hBChE, respectively.

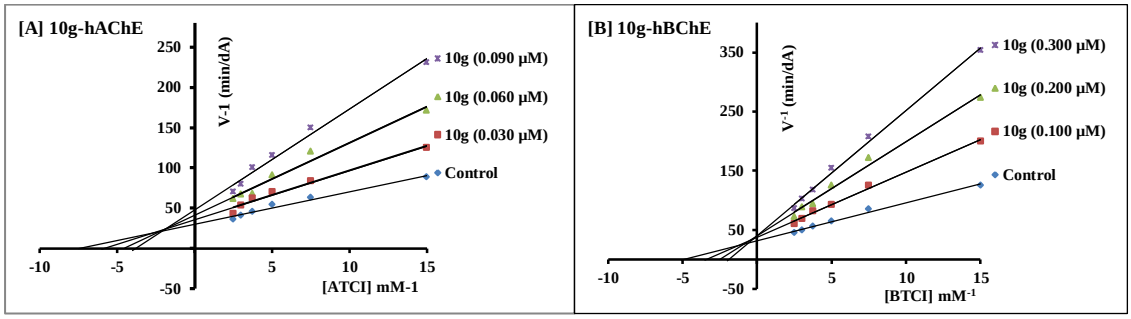

Figure 5.23. Lineweaver-Burk double reciprocal plot showing the mechanism of enzyme inhibition by compound **S_{III}10g** [A] hAChE inhibition with acetylthiocholine iodide (ATCI) as substrate; [B] hBChE inhibition with butyrylthiocholine iodide (BTCI) as substrate.

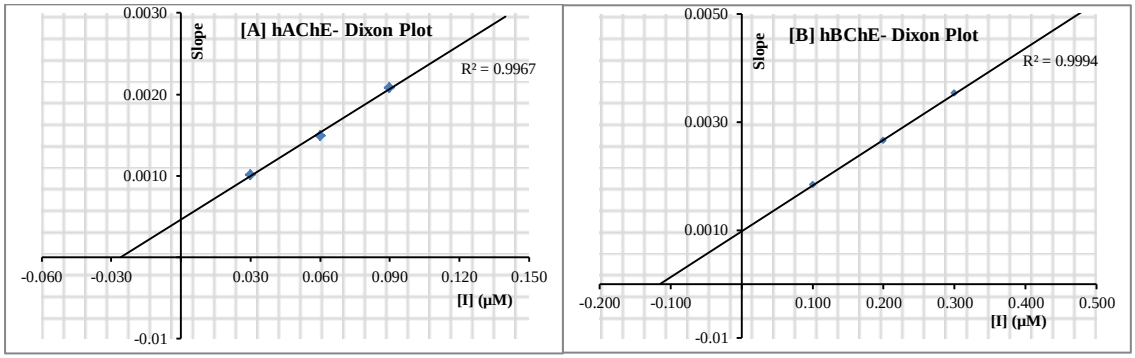

Figure 5.24. The Dixon plots of compound **S_{III}10g** between Lineweaver-Burk double reciprocal slope and inhibitor concentrations. [A] Dissociation constant Ki = 0.026 µM for hAChE and [B] Dissociation constant K_i = 0.115 µM for hBChE.

5.2.2.1.3 BACE-1 inhibition assay

The FRET-based fluorometric assay was performed to determine the hBACE-1 inhibitory potential of synthesized compounds (Series II-V) using donepezil as a

reference standard. The results of hBACE-1 inhibition assay are summarized in Table 5.5. The length of linkers in the designed series was varied with an aim to improve the interaction with aspartate dyad (Asp32 and Asp228) of hBACE-1.

The modification of the linker chain length from an —NH (Series III) to an —$NHCH_2$ (Series IV) has quite a significant influence on the hBACE-1 inhibitory potential as compounds from Series IV showed remarkably higher activity compared to Series II, III, and V, with the exception being compound **S_{III}10g** (IC_{50}: 0.146 μM), which showed slightly higher inhibitory potential than its counterpart from Series IV (IC_{50}, **S_{IV}14g**, 0.186 μM). Most of the compounds (**S_{III}10b**, **S_{III}10c**, **S_{III}10d**, **S_{III}10e**, **S_{III}10h**, **S_{IV}14c**, **S_{IV}14d**, **S_V17c**, **S_{III}17e**, and **S_V17h**) were found to be a good inhibitor of hAChE, but unfortunately, devoid of activity against hBACE-1 (IC_{50} > 1 μM). Conversely, compound **S_{IV}14e** displayed excellent hBACE-1 inhibition (IC_{50}: 0.296 μM), but remarkably decreased anti-hAChE activity (IC_{50} > 1 μM). Apart from **S_{III}10g**, **S_{IV}14e**, and **S_{IV}14g**, four more compounds **S_{III}10f** (IC_{50}: 0.236 μM), **S_{IV}14f** (IC_{50}: 0.114 μM), **S_{IV}14h** (IC_{50}: 0.931 μM), and **S_V17e** (IC_{50}: 0.690 μM) displayed significant hBACE-1 inhibition with IC_{50} in a three-digit nanomolar range. It is also worth noticing that compounds with dual (hAChE and hBChE) inhibitory potential were also good candidates to provide activity against hBACE-1 and common compounds (**S_{III}10f**, **S_{III}10g**, **S_{IV}14f**, **S_{IV}14g**, **S_{IV}14h**, and **S_V17e**) were selected as MTDLs by the same virtue to be investigated further.

5.2.2.1.4 Propidium iodide displacement assay

To affirm our hypothesis that designed ligands would bind effectively with PAS-AChE, PI displacement assay was conducted for the selected MTDLs using the method described by Taylor et al [Taylor et al. 1974]. PI is the known ligand, selectively binding to PAS-AChE and displaying increased fluorescence intensity up to 8–10 folds

[Chalupova et al. 2019, Taylor and Lappi 1975]. The decreased fluorescence intensity can be estimated as the percentage PI displacement from PAS-hAChE due to the presence of inhibitor at 10 µM and 50 µM concentrations. Donepezil was used as the reference standard. Among the tested compounds, **S_{III}10f**, **S_{IV}14h**, and **S_V17e** have considerably lower PI displacement (< 25%), while **S_{IV}14g** (10 µM: 17.79%, 50 µM: 27.37%) exhibited slightly higher PI displacement from PAS-hAChE. The results demonstrated the remarkable PI displacement capability of **S_{III}10g** (10 µM: 32.41%, 50 µM: 55.81%) and **S_{IV}14f** (10 µM: 27.70%, 50 µM: 51.42%) compared to donepezil (10 µM: 23.23%, 50 µM: 32.58%). The results of PI displacement assay are summarized in Table 5.6.

5.2.2.1.5 Parallel artificial membrane permeation assay (PAMPA-BBB)

The penetrability through the BBB is the major concern for the development of drugs to treat AD. To explore the permeability characteristics of selected compounds (**S_{III}10f**, **S_{III}10g**, **S_{IV}14f**, **S_{IV}14g**, **S_{IV}14h**, and **S_V17e**), PAMPA-BBB assay was performed following the method already reported [Di et al. 2003]. The assay is based on passive diffusion of compounds from the donor to the acceptor compartment through a parallel artificial membrane made up of porcine brain lipid. The experimental ($P_{e(exp)}$) and reference ($P_{e(ref)}$) permeability values of nine commercial drugs were compared for assay validation (Table 5.3). The results of the PAMPA-BBB assay demonstrated the excellent brain permeability (CNS+) for all the tested compounds **S_{III}10f**, **S_{III}10g**, **S_{IV}14f**, **S_{IV}14g**, and **S_{IV}14h**, with the exception being **S_V17e**, which showed uncertain brain permeability (CNS±). The significant brain permeability may be attributed to the presence of lipophilic functional groups (2,4-diCl, 4–CF_3, and 4–OCF_3) at the terminal phenyl group of compounds. The results of PAMPA-BBB assay are summarized in Table 5.6.

Considering the balanced multifunctional enzyme inhibitory potential (dual ChE and hBACE-1), significant displacement of PI from PAS-hAChE, and excellent brain permeability characteristics, compounds **S_{III}10g** and **S_{IV}14f** were selected for further pharmacological investigations.

Table 5.6. Propidium iodide displacement and predicted BBB permeability (Series II-V).

Comd.	Propidium iodide displacement from AChE PAS (% inhibition)[a]		PAMPA-BBB permeability	
	At 10 μM	At 50 μM	$P_{e(exp)}$ (10^{-6} cm.s^{-1})	Permeability prediction
S_{III}10f	14.54 ± 0.56	19.01 ± 1.14	7.1 ± 0.30	CNS+[b]
S_{III}10g	32.41 ± 1.81	55.81 ± 2.15	6.9 ± 0.22	CNS+[b]
S_{IV}14f	27.70 ± 1.41	51.42 ± 1.69	5.9 ± 0.18	CNS+[b]
S_{IV}14g	17.79 ± 1.17	27.37 ± 1.83	5.3 ± 0.24	CNS+[b]
S_{IV}14h	12.27 ± 1.00	18.28 ± 1.42	6.2 ± 0.29	CNS+[b]
S_{V}17e	13.24 ± 1.44	22.50 ± 2.00	3.9 ± 0.32	CNS±[c]
donepezil	23.23 ± 1.31	32.58 ± 1.94	6.7 ± 0.18	CNS+[b]

[a]The PI assay was conducted to investigate the ability of compounds to displace PI from PAS-AChE at 10 μM and 50 μM; [b]'CNS+' (prediction of excellent brain permeability with Pe > 4.4 × 10^{-6} cm s^{-1}); [c]'CNS±' (prediction of uncertain brain permeability with P_e between 4.4 to 1.8 × 10^{-6} cm s^{-1}). Data are expressed as the mean ± SEM of three separate experiments (n = 3).

5.2.2.1.6 Aβ aggregation (self- and AChE-induced) inhibition by thioflavin T assay

The deposition and aggregation of Aβ can be considered as a major detrimental factor in AD [Sadigh-Eteghad et al. 2015]. The results of PI displacement assay signified the remarkable binding capability of compounds **S_{III}10g** and **S_{IV}14f** with PAS-hAChE, and it is a known fact that PAS binding of the inhibitor will not only result in AChE inhibition but also have a significant role in prevention of Aβ aggregation [Inestrosa et al. 1996]. Moreover, compounds **S_{III}10g** and **S_{IV}14f** were also observed to be potential inhibitors of hBACE-1, an enzyme responsible for cleavage of the amyloid precursor protein into Aβ [Yan and Vassar 2014]. All these outcomes have prompted us to determine the anti-Aβ aggregation activity of these compounds**,** using thioflavin T assay in self– and hAChE–induced experiments. The tests were performed at three varied concentration ratios of Aβ and inhibitor (10:5 μM, 10:10 μM, and 10:20 μM,

respectively) and the results were reported as % inhibition of Aβ aggregation (Figures 5.25A and 5.25B) and NFI (Figures 5.26A and 5.26B). The results demonstrated the concentration-dependent inhibition of Aβ aggregation with the maximum activity being observed at 20 μM inhibitor concentration (Aβ:inhibitor, 10:20 μM). A slightly higher Aβ inhibition for compound **S_{IV}14f** (self-induced: 14.66–49.19; hAChE-induced: 33.73–78.65%) than donepezil (self-induced: 16.96–38.46%; hAChE-induced: 24.17–60.55%) was observed, while compound **S_{III}10g** displayed remarkable anti-Aβ aggregatory activity in self– (17.83–56.03%) and hAChE-induced (45.60–89.92%) experiments. The observed results were in accordance with the assays of hAChE, hBChE, hBACE-1, and PI displacement.

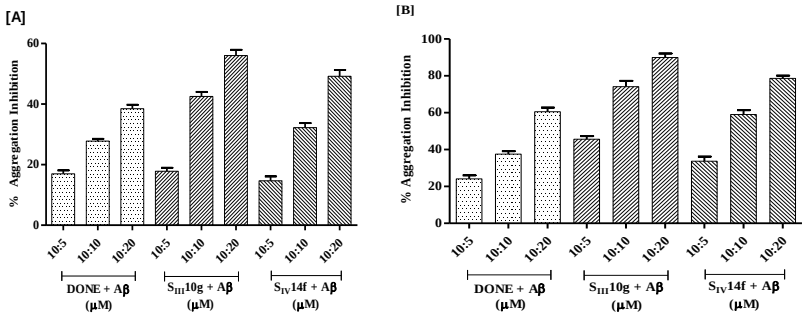

Figure 5.25. Effect of test compounds on Aβ aggregation inhibition. [A] Self-induced and [B] AChE-induced experiments. Each bar displays % Aβ aggregation as the mean ± SEM of three separate experiments. DONE = donepezil.

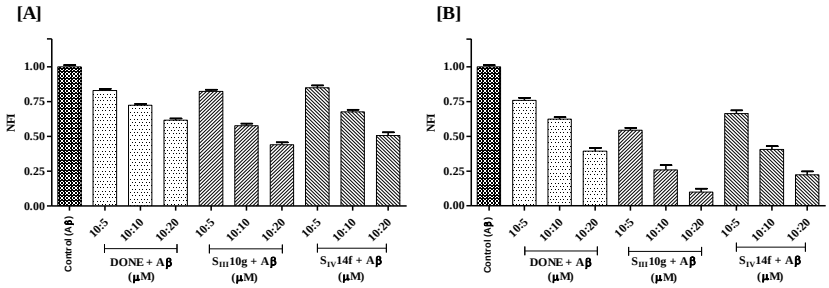

Figure 5.26. Effect of test compounds on Aβ aggregation. [A] Self-induced and [B] AChE-induced Aβ aggregation. Each bar displays the normalized fluorescence intensity (NFI) as the mean ± SEM of three separate experiments. DONE = donepezil.

Similar *N*-benzylpiperidine molecular hybrids, such as indolylpropargylamines [Bolea et al. 2011], 2-aminopyridine-3,5-dicarbonitriles [Samadi et al. 2012], ferulic acid-based

hybrids [Benchekroun et al. 2015], diarylthiazoles [Shidore et al. 2016], etc. were reported previously. But none of those ligands were as potent as our identified multitargeted hits.

5.2.2.1.7 AFM study

The AFM analysis was performed to validate the Aβ-inhibitory potential of compound **S_{III}10g** by visualizing the surface topographical maps for the samples of Aβ (10 μM) in the presence or absence of inhibitor (Figure 5.27). The morphological changes of Aβ aggregates in the presence or absence of inhibitors over different incubation time points (0, 4, 7, and 10 days) exhibited a positive correlation with its aggregation phenomenon, i.e., the formation of Aβ aggregates, oligomers, or fibrils.

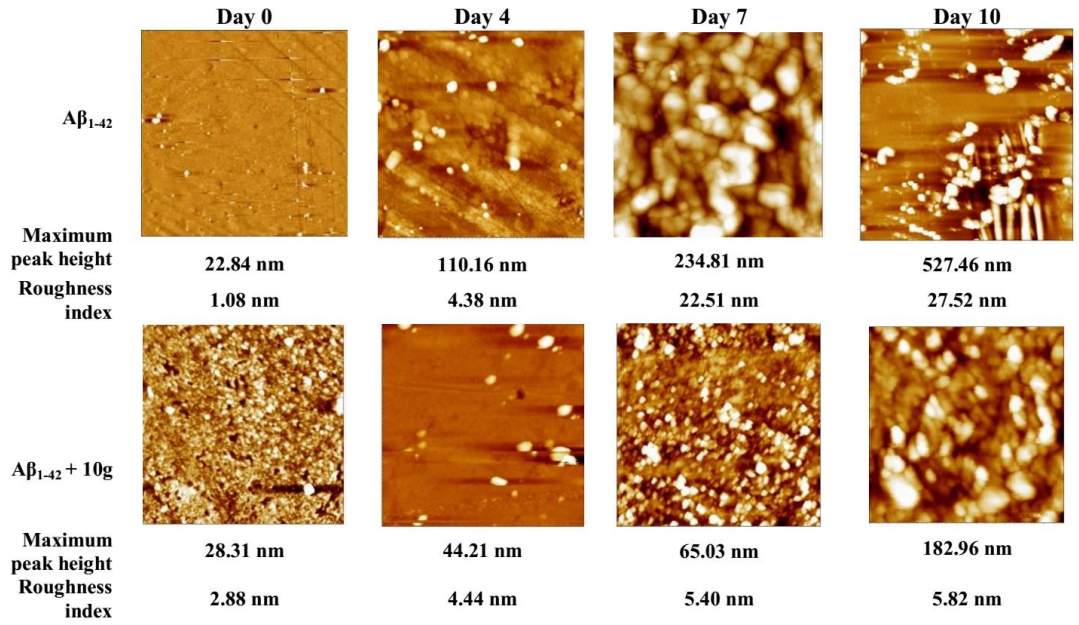

Figure 5.27. AFM images of $Aβ_{1-42}$ aggregates (10 μM) incubated with or without inhibitor (**S_{III}10g)** at different time intervals (on days 0, 4, 7, and 10). Images were visualized at 5 × 5 μm using the Nova Px image analysis software (NT-MDT, Russia).

The estimation of maximum peak height and roughness index provided the actual size of the deposited aggregates. The results revealed the formation of larger aggregates and oligomers for the samples of Aβ with the exponential rise in maximum peak height (22.84–527.46 nm) and roughness index (1.08–27.52 nm) throughout the 10 day incubation. The presence of inhibitor (**S_{III}10g**) displayed remarkable cessation in oligomer formation and deposition of Aβ aggregates, which was ascertained by several

fold reduction in maximum peak height (28.31–182.96 nm) and roughness index (2.88–5.82 nm) over a 10 day incubation period.

5.2.2.1.8 Neurotoxic liabilities against SH-SY5Y cell lines by MTT assay

To ascertain the neurotoxic liability of compounds **S_{III}10g** and **S_{IV}14f**, cell viability assay based on MTT was performed on neuroblastoma SH-SY5Y cell lines. The cell viability was determined at concentrations of 10, 20, 40, and 80 µM of test compounds with parallels to the standard drug donepezil. The outcome of the assay demonstrated a nonsignificant reduction in cell viabilities toward neuroblastoma cell lines by both compounds (**S_{III}10g** and **S_{IV}14f**) up to the maximum tested concentration of 80 µM (Figure 5.28). Therefore, compounds **S_{III}10g** and **S_{IV}14f** can be considered for further preclinical investigations.

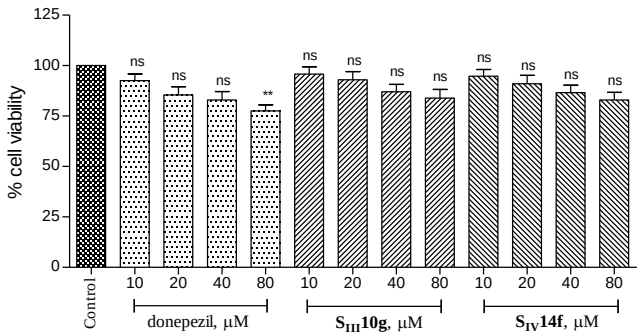

Figure 5.28. Cell viability assay on neuroblastoma SH-SY5Y cell lines with increasing concentrations of **S_{III}10g** and **S_{IV}14f**. Each bar displays the mean ± SEM for three different experiments. $^{**}p < 0.01$, ^{ns}nonsignificant *vs* control.

5.2.2.2 In vivo and ex vivo studies

5.2.2.2.1 Acute oral toxicity study

The acute toxicity study was accomplished to evaluate the safety profile of compounds **S_{III}10g** and **S_{IV}14f** in female Wistar rats following oral administration. The results demonstrated no toxic or abnormal reactions on animals after administration of compounds in graduated doses of 677, 1333, and 2000 mg/kg, p.o. Overall results suggested that both compounds can be well tolerated up to the maximum dose of 2000 mg/kg.

5.2.2.2.2 Scopolamine-induced amnesia model: Y-maze test

The *in vivo* efficacy of compounds **S_{III}10g** and **S_{IV}14f** to improve learning and memory was evaluated by scopolamine-induced Y-maze test in healthy male Wistar rats. Scopolamine is the most commonly used drug for inducing cognitive impairment from a cholinergic deficit [Klinkenberg and Blokland 2010]. Donepezil was used as a standard (5 mg/kg, p.o.) and compounds were evaluated at a dose range of 2.5, 5, and 10 mg/kg, p.o.

The respective group of rats was administered with test compounds and donepezil for seven consecutive days. The treatment on the seventh day was followed with an administration of scopolamine hydrobromide (0.5 mg/kg, i.p.) to induce the cognitive impairment and the Y-maze test was conducted to measure the spontaneous alternations and total arm entries. The increased % spontaneous alternation was considered as a score of improvement in cognitive deficit.

The cognitive deficit was induced by administration of scopolamine affirmed by a significant reduction in % spontaneous alternation (Figure 5.29A, $^{###}p < 0.001$) compared to the control. The treatment with donepezil displayed significantly higher (Figure 5.29A, $^{***}p < 0.001$) % spontaneous alternations compared to scopolamine. Further, the treatment with test compounds **S_{III}10g** and **S_{IV}14f** demonstrated an improvement in the scopolamine-induced cognitive deficit in a dose-dependent manner with maximum activity at 10 mg/kg. The treatment with **S_{III}10g** and **S_{IV}14f** showed significantly higher % spontaneous alternations (Figure 5.29A, $^{***}p < 0.001$) compared to scopolamine, with the exception being compound **S_{IV}14f** at the dose of 2.5 mg/kg (Figure 5.29A, $^{**}p < 0.01$). Interestingly, compounds **S_{III}10g** (5 and 10 mg/kg) and **S_{IV}14f** (10 mg/kg) demonstrated a statistically nonsignificant difference in % spontaneous alternation (Figure 5.29A, ns) than donepezil. Moreover, similar total arm

entries of all the groups (Figure 5.29B, ns) ascertained that scopolamine did not impede the locomotive behavior in animals during the experiment.

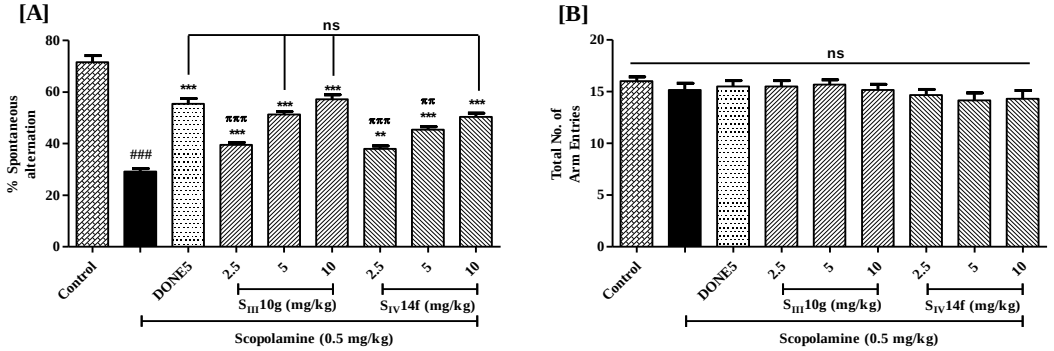

Figure 5.29. Effect of compounds **S_{III}10g**, **S_{IV}14f**, and donepezil on scopolamine-induced cognition and memory improvement. [A] Spontaneous alternations (%) and [B] Total number of arm entries in the Y-maze experiment. All results are expressed as the mean ± SEM (n = 6). $^{###}p < 0.001$ *vs* control; $^{***}p < 0.001$ *vs* scopolamine; $^{\pi\pi\pi}p < 0.001$, $^{\pi\pi}p < 0.01$, $^{\pi}p < 0.05$, $^{ns}p > 0.05$ *vs* DONE5 (donepezil 5 mg/kg).

5.2.2.2.3 Ex vivo studies: AChE estimation and antioxidant activity

Immediately after Y-maze test, the rats of the respective groups were decapitated; the brain hippocampus region was isolated and homogenized. The *ex vivo* studies were performed to estimate the AChE levels and oxidative stress biomarkers, in hippocampal homogenates by the treatment of donepezil (5 mg/kg), **S_{III}10g** (10 mg/kg) and **S_{IV}14f** (10 mg/kg).

The *ex vivo* study was performed to determine brain AChE levels following the Ellman colorimetric assay [Ellman et al. 1961] and the results demonstrated that scopolamine significantly elevated AChE activity (Figure 5.30A, $^{###}p < 0.001$) by means of extensive substrate hydrolysis compared to the healthy control, while treatment with compounds **S_{III}10g**, **S_{IV}14f**, and donepezil showed remarkable attenuation of AChE activity (Figure 5.30A, $^{***}p < 0.001$) compared to scopolamine. Interestingly, compound **S_{III}10g** and donepezil showed a nonsignificant difference (Figure 5.30A, ns) in AChE

activity. Overall, the results of *ex vivo* studies were observed in agreement with *in vitro* hAChE assay.

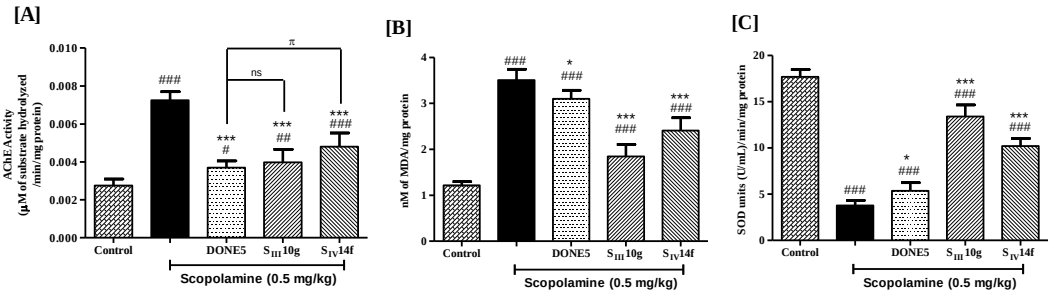

Figure 5.30. Results of *ex vivo* studies. [A] AChE activity- rate of substrate hydrolyzed [B] TBARS assay- levels of MDA [C] Superoxide dismutase assay- levels of SOD units. Data are expressed as the mean ± SEM (n = 6). $^{###}p < 0.001$, $^{##}p < 0.01$, $^{#}p < 0.05$ *vs* control; $^{***}p < 0.001$, $^{*}p < 0.05$ *vs* scopolamine; $^{\pi}p < 0.05$, ^{ns}nonsignificant *vs* DONE5 (donepezil 5 mg/kg).

Scopolamine is responsible for the induction of oxidative stress by altering the levels of several biochemical markers, such as MDA and SOD [Fan et al. 2005, Sakurai et al. 1998]. Therefore, to evaluate the antioxidant potential of compounds **S_{III}10g** and **S_{IV}14f**, oxidative stress biomarkers, such as MDA and SOD were estimated. The MDA is an important oxidative stress biomarker formed as a byproduct of the lipid peroxidation reaction [Placer et al. 1966]. Whereas SOD specifically catalyzes the dismutation reactions to convert superoxide (O_2^-) radicals into free oxygen (O_2) [McCord and Fridovich 1969]. The results suggested the induction of oxidative stress with scopolamine administration due to significant elevation of MDA (Figure 5.30B, $^{###}p < 0.001$), and substantial attenuation of SOD (Figure 5.30C, $^{###}p < 0.001$) compared to the control. The treatment with compound **S_{III}10g** and **S_{IV}14f** showed remarkable attenuation in the MDA level (Figure 5.30B, $^{***}p < 0.001$), while the SOD activity was increased significantly (Figure 5.30C, $^{***}p < 0.001$) compared to scopolamine. Also, the results signified the nonantioxidant potential of donepezil. The investigations also demonstrated the slightly higher antioxidant potential of compound **S_{III}10g** than **S_{IV}14f**.

5.2.2.2.4 Aβ-induced AD phenotypic model: Morris water maze test

The Aβ aggregation and deposition is one of the most crucial pathophysiological mechanisms involved in AD, and its production also increased with BACE-1 activity. Thereby, the effect of the candidate with highest potential, **S_{III}10g**, in ameliorating Aβ-induced cognitive deficit was evaluated by Morris water maze test. The AD-like phenotypic condition was produced by ICV injection of Aβ (4 μM, 5 μL) in the hippocampal brain region of rats through stereotaxic surgery. All the groups were administered Aβ, except for the sham group of animals. The treatments of **S_{III}10g** and donepezil were given to the corresponding group of animals for nine consecutive days, while rats from the model (Aβ) group were given vehicle only. The Morris water maze test was conducted during the last 5 days of treatment and escape latency time (ELT, i.e., time to find the hidden platform), and the total platform crossovers were calculated for 90 s. The cognitive impairment induced by Aβ administration affirmed a significant prolongation of ELT (Figure 5.31A), while the total platform crossovers were considerably reduced (Figure 5.31B) in the model group of animals compared to the control over 5 days. The treatment with **S_{III}10g** drastically reduced ELT (Figure 5.31A), while total platform crossovers were increased significantly (Figure 5.31B) compared to the model group of animals. Moreover, the results also demonstrated a slightly better effect of **S_{III}10g** in ameliorating cognitive deficit than donepezil. The overall results of behavioral studies suggested a remarkable profile of compound **S_{III}10g** at the tested dosage in improving learning and memory impairment.

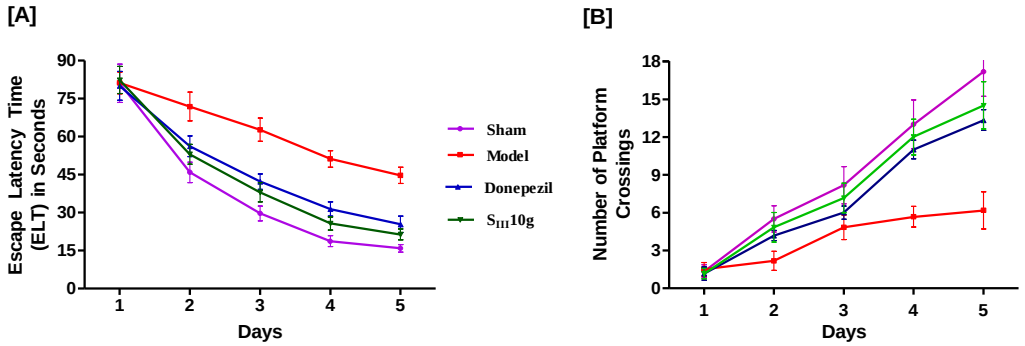

Figure 5.31. Effect of compound **S_{III}10g** in spatial memory improvement on ICV $A\beta_{1-42}$-induced model [A] Escape latency time (ELT) [B] Number of platform crossings in target quadrant during the last 5 days of trials by Morris water maze experiment. The values represented mean ± SEM (n = 10).

5.2.2.2.5 Western Blot Analysis

The elevation of Aβ and BACE-1 are the key pathophysiological hallmarks of AD. Thereby, at the end of the Morris water maze experiment, Aβ and BACE-1 expression levels were estimated in hippocampal tissue samples of all the experimental groups by Western blot analysis. A significant elevation Aβ ($^{***}p < 0.001$, Figures 5.32A and 5.32B) and BACE-1 ($^{***}p < 0.001$, Figures 5.32A and 5.32C) levels was observed in the Aβ treated (model) group of animals compared to the control. The results demonstrated significant attenuation of Aβ ($^{**}p < 0.01$, Figures 5.32A and 5.32B) and BACE-1 ($^{**}p < 0.01$, Figures 5.32A and 5.32C) expression levels and were in accordance to *in vitro* assays. Moreover, the results also signified the nonsignificant difference between **S_{III}10g** and donepezil in attenuating the expression levels of Aβ and BACE-1.

5.2.2.2.6 Immunohistochemical Analysis.

The expression levels of Aβ and BACE-1 in rat hippocampal region were further examined by immunofluorescence staining. The results demonstrated elevated levels of Aβ ($^{***}p < 0.001$, Figures 5.32D (a4) and 5.32E) and BACE-1 ($^{***}p < 0.001$, Figures 5.32D (b4) and 5.32F) expressions in the model group of animals compared to the sham group (Figures 5.32D (a1, b1), 5.32E and 5.32F). The treatment with **S_{III}10g**

significantly declined the expression levels of both target proteins, Aβ ($^{**}p < 0.01$, Figures 5.32D (a3) and 5.32E) and BACE-1 ($^{**}p < 0.01$, Figures 5.32D (b3) and 5.32F) compared to the model group of animals. Moreover, the results of compound **S_{III}10g** mediated expression levels were observed to be nonsignificant (ns) compared to donepezil (Figures 5.32D (a2, b2), 5.32E and 5.32F).

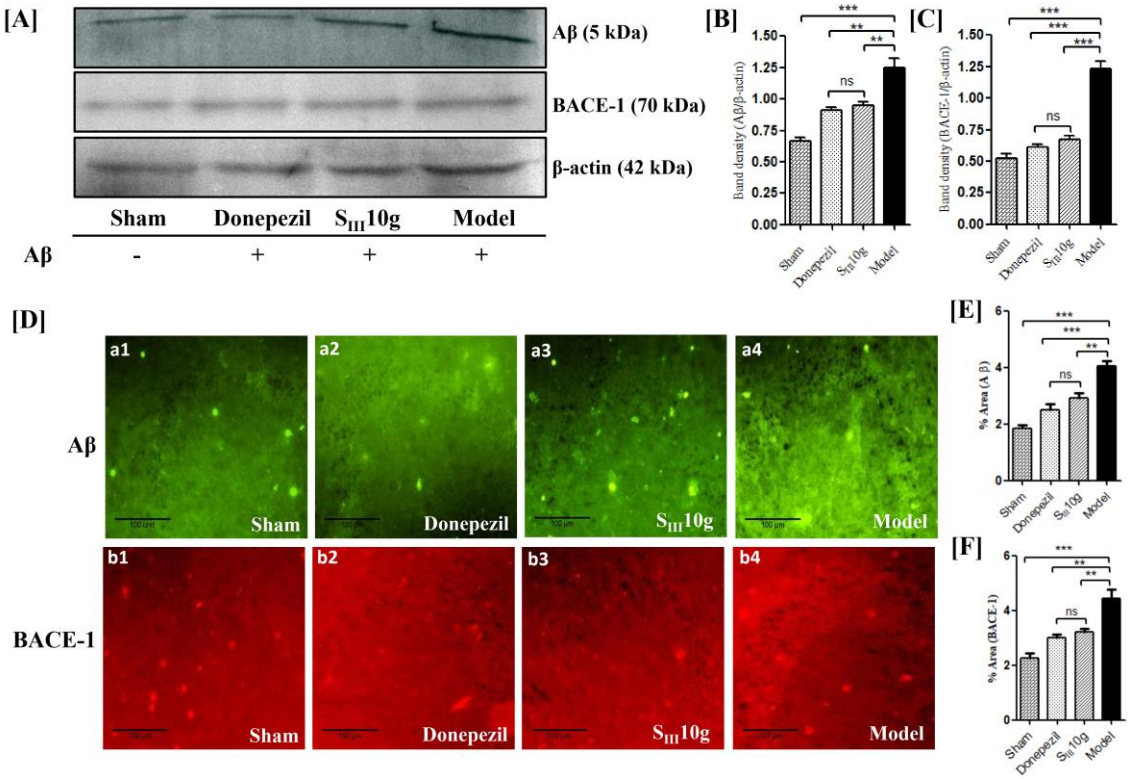

Figure 5.32. Effect of **S_{III}10g** on *in vivo* expression of Aβ and BACE-1 levels in the hippocampal region of the rat brain. [A] Representative bands in the Western blot analysis [B] densitometric quantification showing attenuated levels of Aβ and [C] BACE-1, which were elevated with ICV administration of Aβ; [D] Immunostaining showing attenuated levels of Aβ and BACE-expression by **S_{III}10g** at 10× magnification after staining; [E, F] Quantification analysis of immunostains showing changes in burden (% area) of Aβ and BACE-1 levels, respectively. Data are expressed as the mean ± SEM (n = 5). $^{***}p < 0.001$, $^{**}p < 0.01$ *vs* model group; ^{ns}nonsignificant *vs* donepezil.

5.2.2.3 Pharmacokinetic studies

The pharmacokinetic profiling of lead candidate **S_{III}10g** was performed in healthy male Wistar rats at the dose of 10 mg/kg, p.o. The blood samples were collected at several time points (Chapter 4- Experimental) from retro-orbital plexus, and several pharmacokinetic parameters such as C_{max}, T_{max}, AUC, $t_{1/2}$, and MRT were calculated by

the extravascular noncompartment model using Kinetica 5.0 (Thermo Scientific Kinetica, USA). The maximum concentration (C_{max} = 245.9 ng/mL) of compound **S_{III}10g** in blood was attained at time T_{max} = 5.33 h after an oral administration. The elimination half-life $t_{1/2}$ = 45.59 h, mean residence time MRT = 67.39 h, $(AUC)_{0-24}$ = 1524 ng/mL*h, and $(AUC)_{0-24}$ = 4926 ng/mL*h, were indicative of significant oral absorption and excellent bioavailability of compound **S_{III}10g** following an oral administration. As the T_{max} was achieved at 5.33 h, plasma-drug concentration was remained in therapeutic range for significant period, and further eliminated to half at 45.59 h ($t_{1/2}$). It is the time at which the maximal plasma-drug C_{max} reduced to half or the time at which half of the active drug eliminated from the body. The results of the pharmacokinetic experiment are summarized in Table 5.7.

Table 5.7. Pharmacokinetic evaluation after an oral administration of **S_{III}10g** (10 mg/kg, p.o.)

Parameters	Effect of **S_{III}10g** *
C_{max} (ng/mL)	245.9 ± 8.54
T_{max} (h)	5.33 ± 1.33
$(AUC)_{0-8}$ (ng/mL*h)	1524 ± 10
$(AUC)_{0-24}$ (ng/mL*h)	4926 ± 159
$t_{1/2}$ (h)	45.59 ± 0.995
MRT (h)	67.39 ± 2.013

*All values are expressed as mean ± SEM (n = 3).

5.2.3 Computational studies

5.2.3.1 Molecular docking study

To gain insight into the noncovalent interactions of compounds **S_{III}10g** and **S_{IV}14f** within the active site residues of AChE and BACE-1, molecular docking studies were undertaken using Schrödinger Glide Program. Initially, prepared protein grids were validated by extracting and redocking the cocrystallized ligands, i.e., donepezil and F1M for AChE (4EY7) and BACE-1 (2ZJM), respectively (Figures 5.4A and 5.4B). The ligands **S_{III}10g** and **S_{IV}14f** were docked using Glide XP module, and the results were visualized using XP visualizer tool.

The results of docking on AChE revealed that both compounds **S_{III}10g** and **S_{IV}14f** interacted effectively with residues of PAS and extended into the deep gorge of CAS. At PAS, **S_{III}10g** interacted hydrophobically with Tyr72, Tyr124, and Tyr341 residues and its terminal phenyl group formed a face-to-face π-π stacking interaction with Trp286 (Figure 5.33A). In compound **S_{IV}14f,** the terminal phenyl group interacted with Tyr124 and Trp286 hydrophobically, while, the —$NHCH_2$ linker formed π-cation interaction with Tyr341 (Figure 5.33B). The 1,3,4-oxadiazole linker extended the ligands deep into the gorge through interactions at oxyanion hole (Gly120 and Gly121) and the acyl binding pocket (ABP, Phe297). At the anionic subsite, *N*-benzyl nuclei of both **S_{III}10g** and **S_{IV}14f** stacked with Trp86 and Glu202 *via* π-π and electrostatic interactions, respectively. Moreover, *N*-benzylpiperidine formed polar interactions with Ser203 and His447 at CAS. Overall, results suggested that the —NH linker in **S_{III}10g** provided optimum flexibility to the terminal phenyl group to interact more effectively with PAS residues than **S_{IV}14f** with the —$NHCH_2$ linker. These outcomes were consistent with the *in vitro* assay, which suggested the slightly higher inhibitory potential of compound **S_{III}10g** (IC_{50}: 0.055 μM) compared to **S_{IV}14f** (IC_{50}: 0.086 μM).

Additionally, the binding mode interaction of compounds **S_{III}10g** and **S_{IV}14f** were observed on BACE-1 (2ZJM), and the results are presented in Figures 5.34A and 5.34B. The N-atom of the piperidine nucleus in **S_{III}10g** contacted Asp32 through the salt bridge, while forming electrostatic interactions with Asp228. However, the —$NHCH_2$ linker in **S_{IV}14f** is responsible for salt bridge formation with catalytic dyad (Asp32 and Asp228) and additional H-bonding with Asp32. Compound **S_{IV}14f** displayed better interaction profile with catalytic dyad residues than **S_{III}10g** and the observed results are in agreement with *in vitro* BACE-1 inhibition assay (IC_{50}, **S_{IV}14f:** 0.114 μM; **S_{III}10g:** = 0.143 μM).

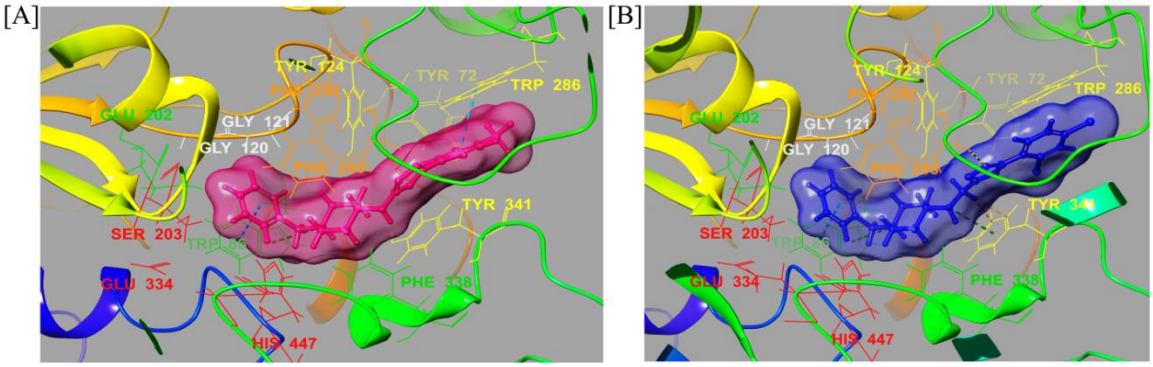

Figure 5.33. Docking poses of ligands in the active site of AChE (4EY7) [A] **S_{III}10g** and [B] **S_{IV}14f** are shown as pink and blue ligand-bound surfaces, respectively. The peripheral anionic site (PAS) residues are indicated as yellow (Tyr72, Tyr124, Trp286, and Tyr341), catalytic active site (CAS) as red (Ser203, His447, and Glu334), anionic subsite as green (Trp86, Glu202, and Phe338), acyl binding pocket (ABP) as orange (Phe295 and Phe297), and oxyanion hole as white (Gly120 and Gly121). Blue and green dotted lines denoted for π-π stacking and π-cation interactions, respectively.

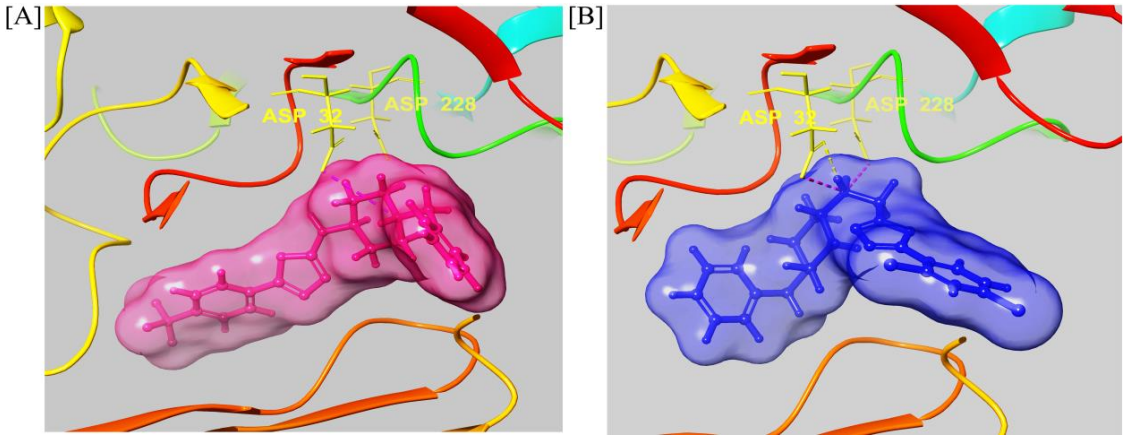

Figure 5.34. Docking poses of ligands in the active site of BACE-1 (2ZJM) [A] **S_{III}10g** and [B] **S_{IV}14f** are shown as pink and blue ligand-bound surfaces, respectively. Aspartate dyad (Asp32 and Asp228) residues are showing as yellow. The pink and yellow dotted lines are denoting salt bridges and H-bonding, respectively.

5.2.3.2 Molecular dynamics simulations study

The molecular dynamics simulation studies were performed to affirm the stability of docked complexes of **S_{III}10g** and **S_{IV}14f** on both the targets, i.e., AChE and BACE-1. The RMSD values for each simulation run were calculated to measure the stability of the protein-ligand positions relative to protein backbone structure, and the results suggested that conformational changes in all the docked complexes were well within the acceptable limit of 1–3 Å (Figures 5.35A–5.38A) during the simulation run of 100 ns.

The ligand-protein interactions were visualized by histograms (Figures 5.35B–5.38B), timeline (Figures 5.35C–5.38C), and 2D-graphical representations (Figures 5.39A–D).

At PAS-hAChE, the results showed that the terminal phenyl groups of compounds **S_{III}10g** and **S_{IV}14f** interacted through a face-to-face π-π stacking with Trp286 for 93% and 47% of total simulation runs, respectively. The Tyr341 residue also formed a similar face-to-face π-π stacking interaction with oxadiazole nucleus of **S_{III}10g** (68%), and terminal phenyl group of **S_{IV}14f** (38%). The —$NHCH_2$ linker of compound **S_{IV}14f** interacted via H-bonding with residues Tyr341 (38%) and Asp74 (86%). The —NH linker of compound **S_{III}10g** exhibited an H-bonding interaction with Tyr124 (90%), while an N-piperidine atom formed a salt bridge with Asp74 (36%). At CAS, the contact between the *N*-benzyl nucleus of **S_{IV}14f** and His447 remained stable by forming π-π stacking interactions (56%) (Figures 5.39A and 5.39B).

The docked pose analysis of compounds **S_{III}10g** and **S_{IV}14f** on BACE-1 displayed stable and significant interactions with catalytic dyads (Asp32 and Asp228). In compound **S_{III}10g**, the N-atom of the piperidine nucleus and the —NH linker contacted through H-bonding with Asp32 (98%) and Asp228 (98%), respectively. While in compound **S_{IV}14f**, the —$NHCH_2$ linker was responsible for H-bonding interactions with BACE-1 aspartate dyad (Asp32, 109% and Asp228, 22%) (Figures 5.39C and 5.39D).

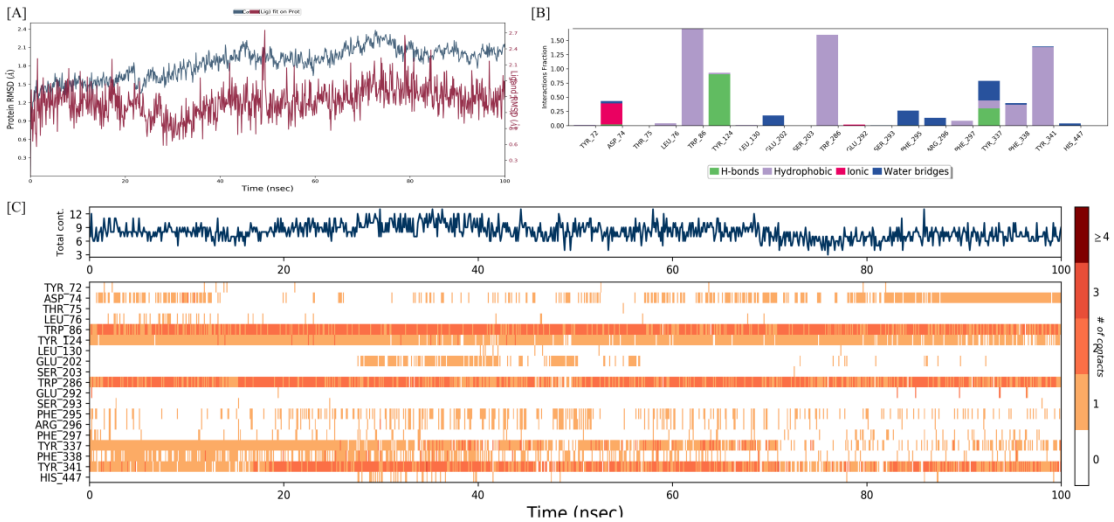

Figure 5.35. Results of molecular dynamics simulation run of 100 ns for **S_{III}10g**-AChE (4EY7) docked complex [A] Ligand-protein RMSD relative to protein backbone structure [B] Histogram showing interaction fractions and [C] Time-line graphical representation showing interaction with individual residues in each trajectory frame.

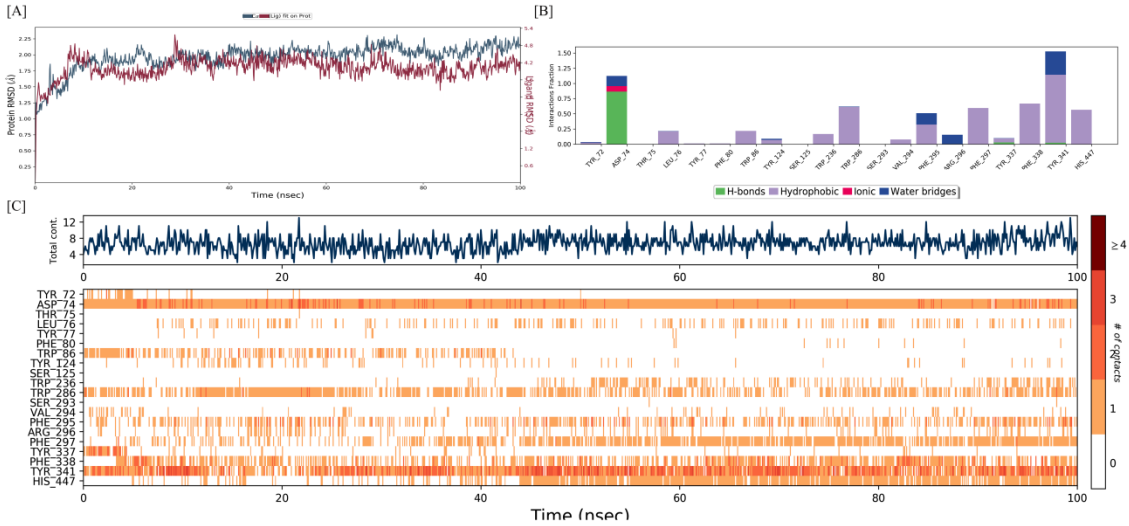

Figure 5.36. Results of molecular dynamics simulation run of 100 ns for **S_{IV}14f**-AChE (4EY7) docked complex [A] Ligand-protein RMSD relative to protein backbone structure [B] Histogram showing interaction fractions and [C] Time-line graphical representation showing interaction with individual residues in each trajectory frame.

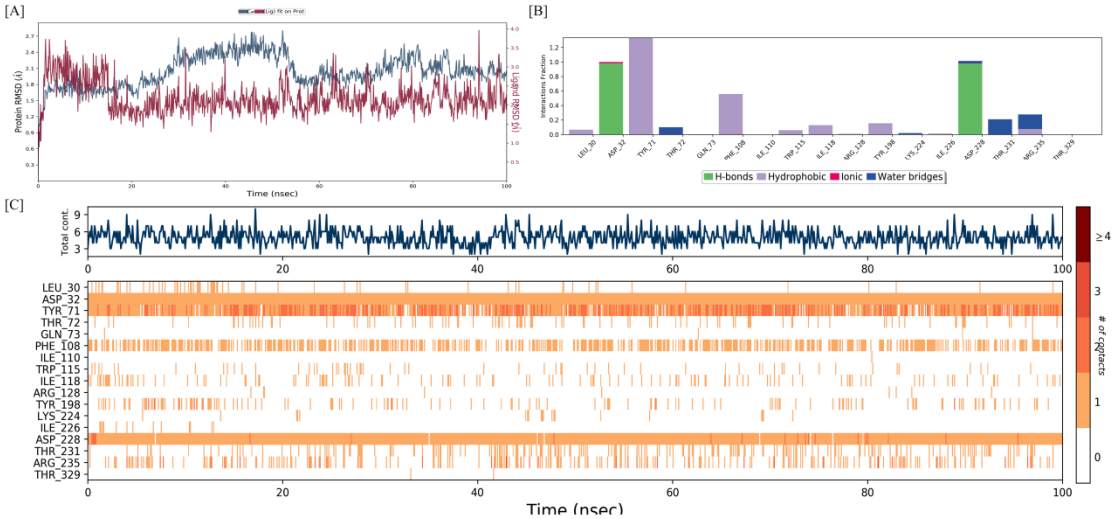

Figure 5.37. Results of molecular dynamics simulation run of 100 ns for **S_{III}10g**-BACE-1 (2ZJM) docked complex [A] Ligand-protein RMSD relative to protein backbone structure [B] Histogram showing interaction fractions and [C] Time-line graphical representation showing interaction with individual residues in each trajectory frame.

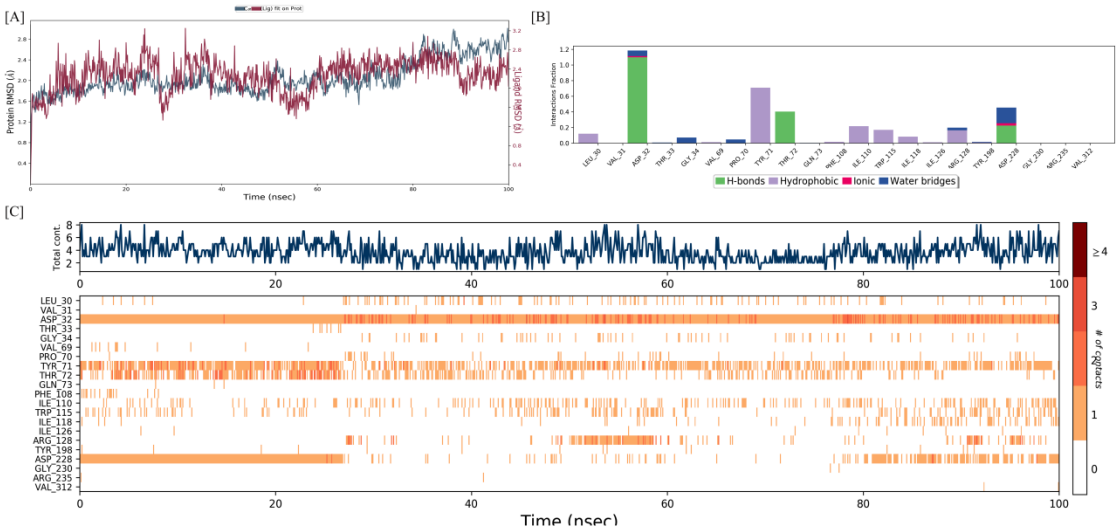

Figure 5.38. Results of molecular dynamics simulation run of 100 ns for **S_{IV}14f**-BACE-1 (2ZJM) docked complex [A] Ligand-protein RMSD relative to protein backbone structure [B] Histogram showing interaction fractions and [C] Time-line graphical representation showing interaction with individual residues in each trajectory frame.

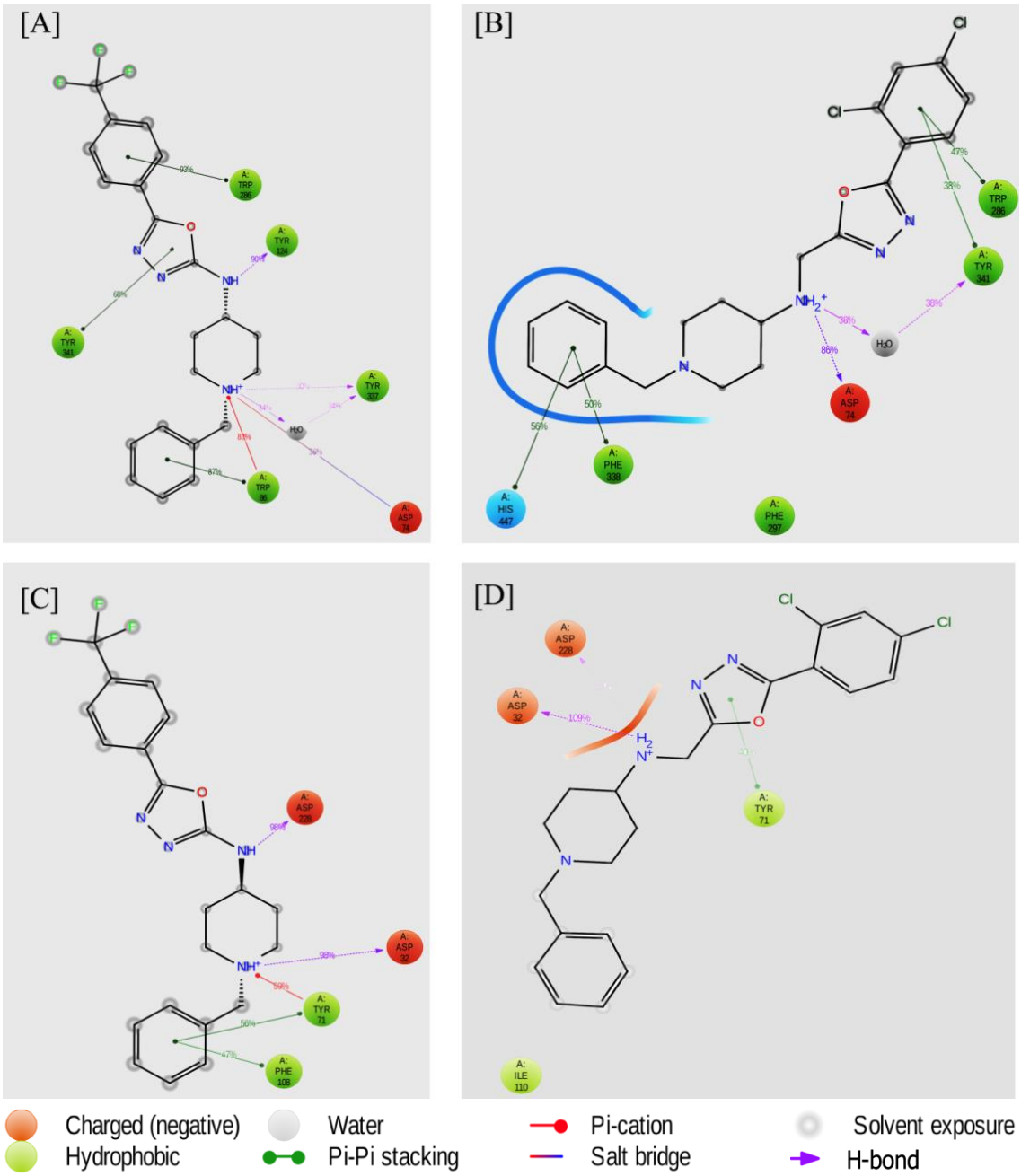

Figure 5.39. 2D graphical representation of active site interactions in 100 ns molecular dynamics simulations runs [A] **S_{III}10g**-AChE [B] **S_{IV}14f**-AChE [C] **S_{III}10g**-BACE-1 and [D] **S_{IV}14f**-BACE-1.